Aus dem Institut für Cell und Neurobiologie
der Medizinischen Fakultät Charité – Universitätsmedizin Berlin

DISSERTATION

NeuroD Family Transcription Factors Regulate Corpus Callosum Formation and Cell Differentiation during Cerebral Cortical Development

zur Erlangung des akademischen Grades
Doctor of Philosophy (PhD)
Im Rahmen des
International Graduate Program Medical Neurosciences

vorgelegt der Medizinischen Fakultät
Charité – Universitätsmedizin Berlin

von

Kuo Yan

aus: Jinan, China

Datum der Promotion: 5. Juni 2016

Table of Contents

Abstract:

Corpus callosum formation is severely defective in NeuroD2/6 double deficient (DKO) mice. Callosal axons defasciculate and stall prior to the midline interaction, or grow astray away from the subventricular zone (SVZ) into ipsilateral cortical plate. Here, I have shown that restoration of either NeuroD2 or NeuroD6 expression by *in utero* electroporation in NeuroD2/6 DKO mice enables callosal fibers to maintain fasciculation across the midline, indicating that these transcription factors regulate long-range axonal projection cell intrinsically. Many potential NeuroD2/6 downstream targets are identified by an expression scanning, including transcription factors, axonal adhesion and guidance molecules. For the promising candidates, I have performed *in vivo* gain-of-function experiments and analyzed downstream signaling pathways.

The genetic deletion of NeuroD2/6 has little effect on determination of callosal projection neuron fate or cortical layer organization. However, NeuroD2/6 modulate callosal axon guidance cues, especially Eph-ephrin signaling. A number of genes involved in Eph-ephrin signaling display altered expression patterns, including Ephrin-A4 ligand (EfnA4). EfnA4, which normally follows high laterally - low medially expression gradient in upper layer neurons, acts downstream of NeuroD2/6 to promote callosal axogenesis. This finding is supported by the observation that EfnA4 electroporation into NeuroD2/6 DKO embryos facilitates the fasciculation of callosal axons and steers outgrown axons towards the midline. Neither secreted EfnA4 (glycosylphosphatidylinositol-attachment signal replaced by flag tag) nor mutated EfnA4 variant (no interaction with EphA receptors) is able to rescue corpus callosum agenesis in DKO embryos. Notably, restoration of ephrin receptors or other ligands fails to rescue the acallosal phenotypes, suggesting that EfnA4 functions in a specific manner.

EfnA4 and Ntrk2 (TrkB) are both expressed in developing neocortex and can be co-immunoprecipitated with each other *in vitro*. Co-electroporation of EfnA4 with kinase-dead Ntrk2, but not kinase-dead Ntrk3, prevents EfnA4 mediated rescue, implicating that Ntrk2 might be a *cis*-interacting co-receptor for EfnA4 reverse signaling. The EfnA4-Ntrk2 interplay modulates intracellular phospho-AKT signaling *in vitro* and *in vivo.* Furthermore, mutation of the Ntrk2's SHC binding site (Y515F), but not the PLCγ1

binding site (Y816F), specifically interferes with EfnA4 promoted callosal axon growth. Considering the expression patterns of EphA receptors and their interaction with EfnA4-Ntrk2 complexes *in trans*, I propose a model that the expression of Eph receptors in the medial neocortex and ventricular zone creates a permissive channel for callosal axons carrying EfnA4-Ntrk2 complexes in the SVZ.

I also find that NeuroD2/6 may intrinsically and extrinsically regulate the differentiation of Tbr2+ and Olig2+ progenitors, respectively.

Zusammenfassung:

Die Entstehung des Corpus Callosum ist in NeuroD2/6 defizienten Mäusen massiv gestört. Die Axone callosaler Neurone defaszikulieren vor Erreichen der Mittellinie. Gezieltes callosales Wachstum findet nicht statt und viele Axone wachsten stattdessen ungezielt in die ipsilaterale Kortikalplatte. Ich zeige hier, dass die experimentelle Wiederherstellung der NeuroD2- oder NeuroD6-Expression durch In-Utero Elektroporation in NeuroD2/6 defizienten Embryonen ausreicht, um das gezielte und faszikulierte Wachstum callosaler Neuronen bis zum erreichen des kontralateralen Kortex sicher zu stellen. NeuroD2/6 regulieren also das callosale Axonwachstum auf zellintrinsische Weise. Weiterhin identifiziere ich mit Hilfe einer Expressionsanalyse eine Reihe potentieller Effektorgene von NeuroD2/6, darunter Transkriptionsfaktoren und axonale Adhäsions- und Lenkungsmoleküle. Die wichtigsten Kandidaten untersuche ich auch funktionell über Gain-of-Function Experimente und die Analyse der nachfolgenden Signalwege.

Im Rahmen des Projekts zeige ich, dass die Deletion von NeuroD2/6 wenig Einfluß auf die Determination von callosalen Projektionsneuronen und die Organisation der Kortikalen Schichtung hat. Trotzdem modulieren die beiden Transkriptionsfaktoten das Wachstum callosaler Axone und insbesondere den Eph-ephrin Signalweg. Eine Reihe von Genen die in Beziehung zu diesem Signalweg stehen zeigen veränderte Expressionsmuster. Ich zeige, dass Ephrin-A4 (EfnA4), dessen Expression in den Neuronen der oberen Schichten des Neokortex normalerweise einem latero-medial orientieren Gradienten folgt, unter der Kontrolle von NeuroD2/6 steht und das callosale Axonwachtum beeinflusst. Die Elektroporation von EfnA4 in den Neocortex von NeuroD2/6 defizienten Embryonen führt ebenfalls zur Wiederherstellung der Faszikulation und des gezielten Wachstums callosaler Axone Richtung Mittellinie. Weder eine sekretiere Form von EfnA4 (der GPI-Anker wurde durch ein Flag Tag ersetzt) noch eine mutierte Variante die nicht mehr in der Lage ist, Eph-Rezeptoren zu binden, führen zu einer vergleichbaren Wiederherstellung der callosalen Axogenese in NeuroD2/6 defizienten Mäusen. Da auch die Elektroporation von Eph-Rezeptoren oder anderen Ephrinen zu keinem vergleichbaren Effekt führt, kann davon ausgegangen werden, dass die Funktion von Efna4 bei der Entstehung des Corpus Callosum spezifisch ist.

Sowohl EfnA4 also auch Ntrk2/3 werden im sich entwickelnden Neokortex exprimiert und können in-vitro miteinander co-immunoprezipitiert werden. Die Co-elektroporation von EfnA4 mit einer dominant negativen (kinase-dead) Variante von Ntrk2 (aber nicht von Ntrk3) in NeuroD2/6 deficienten embryonen verhindert die Wiederherstellung der callosalen Axogenese. Die impliziert, dass Ntrk2 ein cis-interagierender Co-Rezeptor für den reverse EfnA4 Signalweg seien könnte. Das Zusammenspiel von EfnA4 und Ntrk2 moduliert intrazellular den PI3K-Akt Sinalweg *in vitro* und *in vivo*. Weiterhin zeige ich, dass die Mutation der Shc Bindedomäne (aber nicht der PLCγ1 Bindedomände) von Ntrk2 mit der Wiederherstellung des callosalen Axonwachtums in NeuroD2/6 defizienten Embryonen interferiert. Unter Berücksichtigung der Expressionsmuster von Eph-Rezeptoren in der medialen Kortikalplatte und Ventrikularzone und der Interaktion von Eph-Rezeptoren mit EfnA4-Ntrk2 Komplexen *in trans*, schlage ich als Modell vor, dass die trans-Interaktion von Eph-Rezeptoren mit EfnA4-Ntrk2 Komplexen zur Axonalen Repulsion führt und dass die Abwesenheit von Eph-Rezeptoren in der Intermediärzone des medialen Kortex einen permissiven Kanal für die Entstehung des Corpus Callosum bildet.

In weiteren Experimenten konnte ich zeigen, dass NeuroD2/6 auf zell-intrinsische und zell-extrinsische Weise die Differenzierung von Tbr2-positiven und Olig2-positiven Vorläuferzellen beeinflussen können. Die zugrundelegenden Mechanismen müssen allerdings noch identifiziert werden.

1. Introduction

1.1 Cerebral cortex development

Mammalian cerebral cortex is a highly organized structure, which consists of a wide variety of cell types, including different subclasses of progenitors, neurons and glia cells. Neurons are the main functional cell populations and can be categorized into two major groups: ~20% are GABAergic inhibitory interneurons and ~80% are glutamatergic excitatory pyramidal neurons. While interneurons establish local circuits with adjacent cells, cortical pyramidal neurons tend to form long-range projections. Glutamatergic projections contact and signal the contralatetal hemisphere, the thalamus and the spinal cord. Pyramidal projection neurons in neocortical plate segragate into six layers, which are dorso-ventrally termed as layer I to layer VI in order. Traditionally, layer V-VI are regarded as deeper layers (DL) and layer II-IV are regarded as upper layers (UL). Layer I is devoid of pyramidal neurons and is also called marginal zone (MZ). The cells in each layer exhibit distinct morphology, electrophysiological status, gene expression patterns and transcription factor (TF) codes[1]. Therefore, functions and axonal connectivity of neocortical pyramidal neurons are very diverse.

1.1.1 Layering and wiring of the neocortex

During embryonic development, the neocortex is generated from a thin primordial neuroepithelium, a proliferative progenitor pool located in ventricular zone (VZ) and subventricular zone (SVZ)[2]. It is situated ventrally in the developing cortex. One population of primary progenitors resides at the apical surface of the VZ. These cells are called apical progenitors (APs) or radial glia (RG) cells as they exhibit a unique morphology with a radial extension towards the outer surface of cortex. These progenitors undergo either symmetrical divisions (division plane perpendicular to the apical surface of VZ) to proliferate, or asymmetrical divisions to create different daughter cells. One of the daughter cells is an AP to maintain the pool, and the other is a differentiating cell that will give rise to a neuron, astrocyte, oligodentrocyte, or secondary progenitor[3,4]. Secondary progenitors mainly exist in the SVZ or the basal aspect of the VZ (hence also called basal progenitors (BPs) or intermediate progenitors). These cells, unlike RG cells, only transiently renew themselves in a limited

cycles and then mainly give rise to UL neurons[5]. Recent reports have suggested that BPs possess the potentials to produce all layers of projection neurons[6].
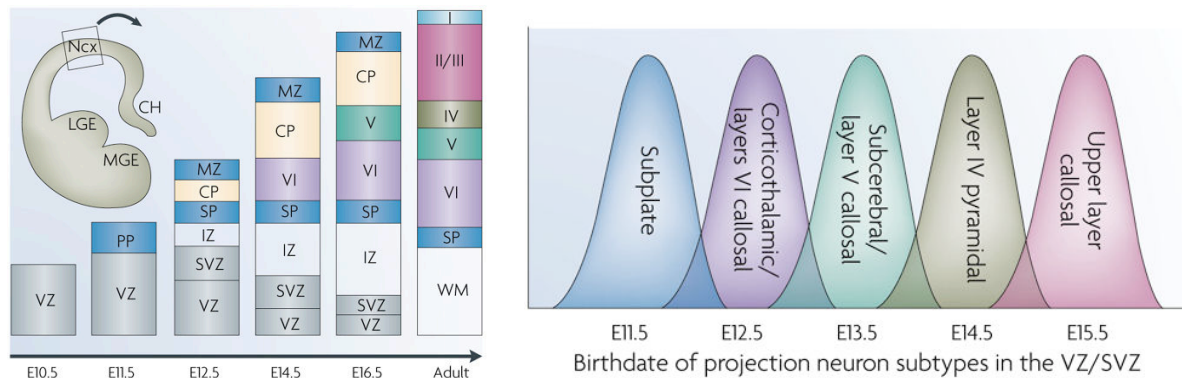
Figure 1.1: Neocortex development and sequential layer formation

Adapted from Molyneaux et al., 2007. The left shows the sequential formation of neocortical layers at each stage. Ncx: neocortex; LGE: lateral ganglionic eminence; MGE: medial ganglionic eminence; VZ: ventricular zone; PP: preplate; SVZ: sub ventricular zone; IZ: intermediate zone; SP: subplate; CP: cortical plate; MZ: marginal zone; WM: white matter; I – VI: layer I – VI. The right shows the birthdate paradigm of distinct projection neuron subpopulations.

The production of neocortical pyramidal neurons is a very precisely regulated campaign regarding to positioning, timing and identity. It is initiated around the embryonic day 11.5 (E11.5) in mice. The earliest born projection neurons (layer VI neurons) invade a population of existing pioneer neurons (preplate, PP), which are subsequently separated into two parts: the dorsal MZ (layer I) and ventral subplate (SP), a process termed as PP splitting. While layer VI neurons are invading the cortical plate (CP), a new wave of neurons from VZ migrate along the processes of RG cells and pass by the layer VI cells. The second wave of neurons settle eventually between layer VI and MZ, thereby forming layer V. Following the same logic, later born neurons always pass earlier born neurons and sequentially form layer IV, III and II in an inside-first outside-last fashion[7,8] (left, Figure1.1). The progressive birthdates of pyramidal neurons in layer VI to II follows a tight timing in mice: the peak of layer VI neurogenesis occurs around E12.5; layer V neurons are largely born around E13.5; layer IV and layer II/III neurons are mainly produced around E14.5 and E15.5, respectively[7] (right, Figure1.1). The lamination- and timing-dependent cell fate specification also restricts their patterns of axonal projection: layer VI cells generally send their axons subcortically to the thalamus in a well-defined topographic map; subcerebral projection axons from layer V neurons connect to the hindbrain,

midbrain and spinal cord via internal capsule; connections bridging two hemispheres originate largely from layer II-III neurons and constitute the two of cerebral commissural tracts - corpus callosum (CC) and anterior commissure (AC). Excitatory projection neurons can be categorized into two subclasses: those projecting their axons away from cortex are called corticofugal neurons and those projecting to ipsi- or contra-lateral hemispheres are called intracortical projection neurons, respectively[8].

The precision of this developmental program is determined by synchronized efforts of various intrinsic and extrinsic factors. Intrinsically, lineage commitment of progenitors and cell fate specification of postmitotic neurons are coded by a series of TFs, as in turn serve as signatures for the corresponding cell types, and by their genetic interactions. Pax6, a VZ marker, was reported to promote neurogenic capacity of multipotent RG cells[9,10]. Tbr2, which is expressed in BPs, is sufficient to convert an AP into a BP[11]. Tbr1 is essential for layer VI cortico-thalamic projection neurons to achieve their identities by inhibiting the layer V cell fate regulator Fezf2[12,13]. Fezf2 and Ctip2 act in the same genetic axis to regulate layer V development and the formation of subcerebral axon projections[14]. UL neurons can be labeled by a few TFs, such as Brn1/2, Cux1/2 and SatB2[8,15–18]. Others and our lab have shown that Satb2, an AT-rich DNA binding protein, is a determinant gene for the callosal projection neuron (CPN) fate as well as an inhibitor for Ctip2. This finding is strongly substantiated by the observation that SatB2 null UL neurons display ectopic Ctip2 up-regulation and mis-project subcerebrally rather than callosally[17,18].

To build such an elegant cerebral cortical architecture also relies on environmental cytokines and growth factors. For instance, Reelin released from Cajal–Retzius cells in MZ plays critical roles for appropriate positioning and migration of projection neurons. In Reelin deficient mice (Reeler mutants), neocortical lamination is organized in an aberrantly inverted outside-first inside-last pattern[19,20]. Additionally, others and my colleagues have unraveled that secreted neurotrophins from newly born neurons in the CP can diffuse to progenitors and alter their subsequent cell fate choices by feedback signaling[21]. Another well-known example for feedback signaling is fibroblast growth factors (Fgf) mediated pathways. Several Fgf ligands have been demonstrated to suppress neurogenic divisions of the progenitor cells and lengthen cell cycles by modulating cell cycle regulators[21–23]. As a result, timing-dependent acquisition of cell

identities is disrupted, and precocious later-produced cell types expand markedly at expenses of earlier-produced cell types (UL neurons instead of DL neurons; glia cells instead of UL neurons).

1.1.2 Formation of the corpus callosum

The two hemispheres of a human brain are interconnected by three commissural axonal tracts: the AC (mainly made by piriform cortical neurons), the hippocampal commissure (HC, made by hippocampal pyramidal neurons) and the CC. The CC is the most prominent commissure in the brain, and it comprises more than 200 million axons in human beings. The CC is important for the lateralization of brain functions and associated with cognitive and behavioral abilities. However, it is a relatively fragile structure indicated by a high incidence of CC agenesis (1:4000 human individuals) and more than 50 associated neurodevelopmental disorders[24]. My PhD project mainly focuses on the regulation and functions of genes that are involved in CC formation during mouse corticogenesis.
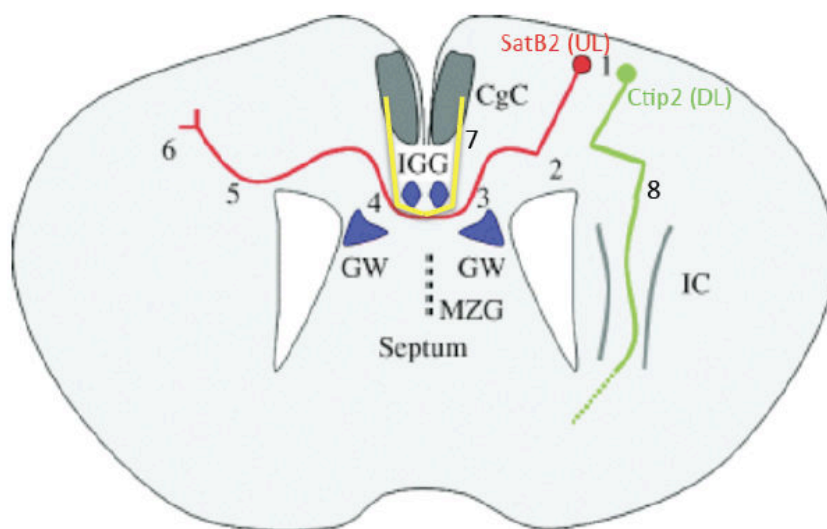
Figure 1.2: Sequential events of callosal axon tract formation
Modified from Richards et al., 2004. 1: Callosal projection neuron fate determination by SatB2; 2: Axon callosal projection decision; 2 – 3: Callosal fibers fasciculate and are guided by guidepost cells; 3 – 4: Midline interaction and crossing; 5 – 6: Innervation into contralateral targets; 7: Pioneering axons from cingulate cortical neurons; 8: Subcerebral projections regulated by Ctip2. CgC: cingulate cortex; IGG: indusium griseum glia; GW: glial wedge; MZG: midline zipper glia; IC: internal capsule; UL: upper layers; DL: deeper layer.

The formation of CC is a multi-stage process including cell fate determination, axon outgrowth, fasciculation, pathfinding, midline interaction and contralateral innervation [24,25] (Figure1.2). After establishing the CPN identity controlled by SatB2 during radial migration, these neurons grow axons that fasciculate into bundles in the SVZ or intermediate zone (IZ) and make a decision to navigate medially towards the later CC. In parallel with CPN development and axon outgrowth, a glial complex of mirrored symmetry forms at the cortical midline, including indusium griseum glia, glial wedge and midline zipper glia. These gila cells can serve as a structurally supportive substrate. Additionally, these cells can either provide membrane located clues (for regional instruction, like Eph-ephrin[26–28]) or secret diffusible signals (for remote projection, like Robo-slit[29–31], wnt5a-Ryk[32], and netrins-DCC/Unc5c[33]) to shape a permissive corridor for callosal fibers carrying cognate responsive molecules around the midline. Growing fibers sense environmental repelling or attracting information by their growth cones to approach and cross the midline. Later, these axons invade homotopic areas of contralateral cortex and establish synaptic transmissions with local neurons[25].

A number of hypothesized or experimentally verified mechanistic models have been posed to explain how callosal axons are able to traverse such a complicated path to find their designated correspondents. Many scientists argue that a group of cingulate cortical neurons project their pioneering axons across the midline earlier, which facilitate later coming axons to follow the correct path more easily (Figure1.2). Another model proposes that CPN growth cones can interact with some neurons resident in the IZ (so called postguide cells) in order to sustain a stereotyped trajectory in this cell sparse region. Intriguingly, both models may require signaling mediated by Semaphorin family members[34–36]. As callosal axogenesis is a bilateral process, direct interactions of opposing axons have been assumed (handshake theory): afferent and efferent callosal axons would communicate and grow along each other so as to eventually target their homotopic destination. More experimental evidence is still needed for these models.

1.2 Basic helix-loop-helix transcription factors

Helix-loop-helix (HLH) proteins are generally deemed as transcriptional activators involved in the regulation of cell survival, differentiation, migration and fate specification. They can be categorized into two subclasses: I and II, of which the former are also termed as E-box proteins, and the latter are basic helix-loop-helix (bHLH) TFs. E-box

proteins and bHLH TFs form inter-subclass heterodimers when binding to DNA and recognize an E-box motif with the elementary sequence of 'CANNTG'[37]. However, the DNA-binding specificity of these TFs still remains inconclusive as canonical and non-canonical E-box motifs widely spread in regulatory regions of numberless genes. Many bHLH TFs distribute and function in distinctive cell types. For instance, TFs belonging to neurogenin (Ngn) family are well-known proneural genes expressed in neocortical progenitors to promote neuronal fate specification and radial migration of pyramidal neurons[38,39]. Olig family genes, for another example, are master regulators determining the switch from neural progenitors to glia progenitors as well as the subsequent glial differentiation, migration and the myelination timing of oligodendrocytes[40,41]. Besides, in genetically modified mice lacking Math1, specific proprioceptive sensory lineages, like cerebellar granule cells, inner ear hair cells and spinal D1 interneurons, are absent[42–44].

1.2.1 NeuroD family transcription factors
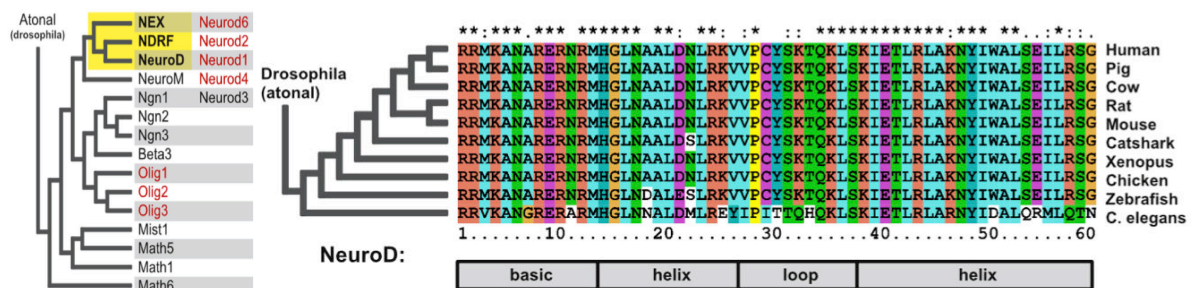
Figure 1.3: Phylogenic tree of bHLH TFs and evolutionary conservation of NeuroD1
Summarized from Ledent et al., 2001 and 2002. The left is the phylogenic analysis of main family members of neural bHLH TFs in flies. The right shows the high conservation of amino acid sequences in NeuroD1's bHLH domains across different species.

NeuroD1, NeuroD2 and NeuroD6, three phylogenetically closely related bHLH TFs (left, Figure 1.3), are jointly termed NeuroD family TFs in my thesis. NeuroD family TFs are highly evolutionarily conserved molecules[45]. Taking NeuroD1 for example, the protein composition in its DNA-binding domain is rather similar ranging from worms to human beings, implicating its functional significance[37,45] (right, Figure 1.3). Indeed, NeuroD1 was first found to promote neuronal differentiation, strongly supported by the observation that ectopic expression of NeuroD1 in frog epidermal cells could convert these cells into neurons[46]. In mouse brains, the deletion of NeuroD1 results in complete loss of the hippocampal dentate gyrus as a consequence of neuronal apoptosis[47,48].

NeuroD2 plays positive roles in neuron survival in cerebellum, and it is essential for the integration of thalamo-cortical connection into neocortex as well as the formation of somatosensory whisker barrel cortex[49]. My colleagues and I have recently reported that, in NeuroD2/6 double deficient (DKO) mice, callosal axon projections are defective[50]. Cepco and her colleagues also claimed that all three NeuroD family TFs coordinate to regulate retinal neuronal fate and neurite lamination[51]. Collectively, NeuroD family TFs essentially control neuronal survival, differentiation, maturation and neurite patterning in nervous system. NeuroD1 and NeuroD2 have previously been reported to interact with E-box proteins such as Tcf3, Tcf4 and Tcf12[37,52].

1.2.2 NeuroD2/6 double deficient mice as a model for axogenesis study
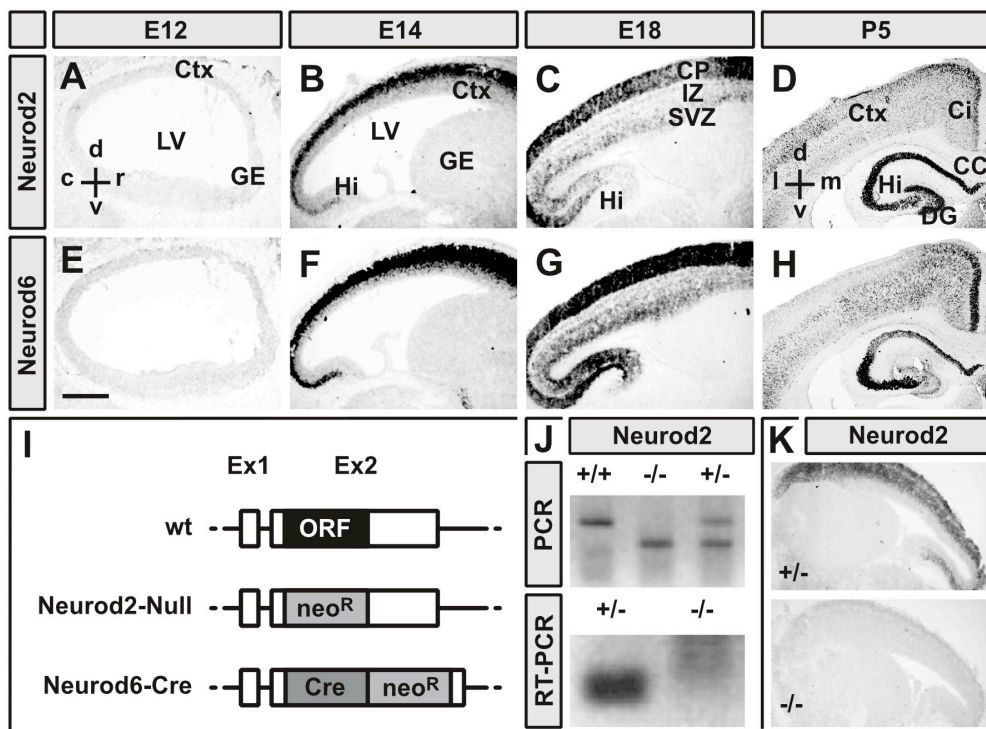
Figure 1.4: Developmental expression patterns of NeuroD2/6 during neocortical development and generation of NeuroD2/6 double deficient (DKO) mice

Cited from Bormuth and Yan et al., 2013. **(A – H)** Expression patterns of NeuroD2 (A – D) and NeuroD6 (E – H) detected by *in situ* hybridization (ISH) in cerebral cortex at E12, E14, E18 and P5. Ctx: cerebral cortex. LV: lateral ventricle; GE: ganglionic eminences; Hi: hippocampus; IZ: intermediate zone; Ci: cingulate cortex; CC: corpus callosum; DG: dentate gyrus. **(I)** The strategy for generating NeuroD2/6 DKO mice. Ex1 and Ex2: exon 1 and 2 for NeuroD2/6 transcripts. Neo[R]: neomycin resistant cassette. Genetic deletion of NeuroD2 can be verified by genomic PCR and reverse transcriptional PCR (RT-PCR) **(J)** or mRNA detection by ISH **(K)**.

NeuroD6 expression starts during early neocortical neurogenesis (E12) in a subset of SVZ progenitors[50,53]. Throughout cortical development, NeuroD6 is expressed in SVZ, albeit weakly, and maintains their strong expression in postmitotic pyramidal neurons in CP (E – G, Figure 1.4). At early postnatal stage (P5), it can be detected in projection neurons in both CP and hippocampus (H, Figure 1.4). Strikingly, NeuroD2 shares overlapping spatio-temporal expression patterns with NeuroD6 during embryonic neurogenesis (A – C, Figure 1.4), implying that they might function redundantly in the same process. As the loss of NeuroD6 was found dispensable for neocortical development, my colleagues generated NeuroD2/6 DKO mice by replacing the NeuroD2 coding exon with a neomycin resistant cassette and the NeuroD6 coding region with Cre recombinase (NeuroD6-Cre line). The genetic deletion of NeuroD2 can be verified by reverse transcriptional PCR and mRNA detection[50] (J and K, Figure 1.4).
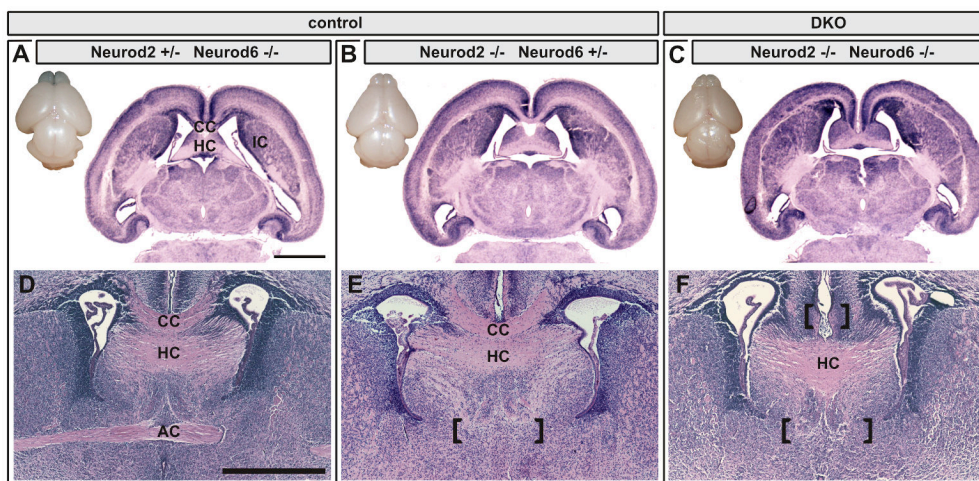
Figure 1.5: Histological staining for NeuroD2 or NeuroD6 single deficient and NeuroD2/6 DKO brains

Cited from Bormuth and Yan et al., 2013. Histological staining for transversal brain sections **(A – C)** from P1 control (single deficient) and NeuroD2/6 DKO mice and the enlarged views of commissures **(D – F)**. HC: hippocampal commissure; AC: anterior commissure.

The formation of both CC and AC is severely damaged in NeuroD2/6 DKO brains, while the HC is still present (C and F, Figure 1.5). Of note, CC is basically intact in either NeuroD2 or NeuroD6 single deficient mice, but absent in NeuroD2/6 DKO mice, consistent with the hypothesis that NeuroD2/6 share functional redundancy. Given this point, single mutant littermates (mostly $Neuro6^{Cre/Cre}; Neuro2^{+/-}$) of the DKO mice are generally used as controls in my study. In sharp contrast with controls, callosally

projecting axons in DKO brains labelled by membrane-localized green fluorescent proteins (GFP) stall axonal growth before turning ventrally along the cingulate cortex and therefore fail to reach the midline. Rather than being tightly bundled in the SVZ/IZ as controls (B, Figure 1.6), NeuroD2/6 null callosal fibers defasciculate and grow astray back to the ipsilateral CP (C, Figure 1.6). Immunostaining for glial fibrillary acidic protein (GFAP), an intermediate filament protein used as glia cell marker, shows that midline glial structures are grossly normal[50] (A, Figure 1.6).
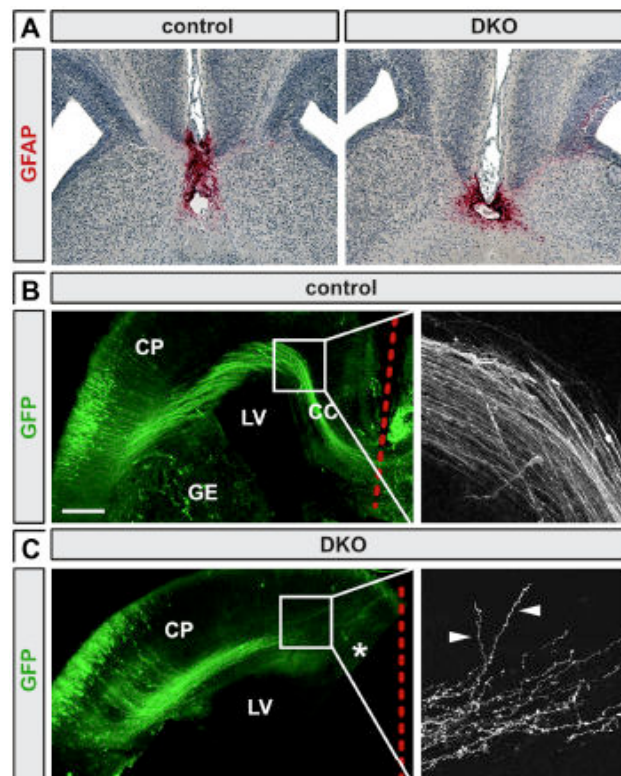
Figure 1.6: Callosal agenesis in the NeuroD2/6 DKO brain

Cited from Bormuth and Yan et al., 2013. **(A)** Immunostaining for glial fibrillary acidic protein on P1 control and NeuroD2/6 DKO brain sections. **(B – C)** Immunofluorescent (IF) staining for GFP on the vibratome sections of P1 control (**B**) and NeuroD2/6 DKO (**C**) brains with E15 GFP eletroporation.

1.3 Ephrin-Eph signaling

Ephrin-Eph signaling has been extensively investigated during the last decades. Unlike most of the other ligand-receptor pairs, 'Ephrin ligands' and 'Eph receptors' are both cell surface bound proteins and transduce bidirectional signals between neighboring cells. Ephrins can not merely activate Eph mediated responses (forward signaling) but can also act as receptors that trigger effects in the host cells in response to Eph binding (reverse signaling)[54]. Forward and reverse signaling can happen synchronously. Both,

Ephrins and Ephs, are classified into A and B subclasses. Mice harbor five EphrinAs (EfnA1 – EfnA5), three EphrinBs (EfnB1 – EfnB3), nine EphAs (EphA1 – EphA8 and EphA10) and five EphBs (EphB1 – EphB4 and EphB6). Binding and signaling occur preferentially between Ephrins and Ephs of the same subclass, but functional inter-subclass interactions do exist[55]. EphA4 can be activated by both EphrinAs and EphrinBs. EfnA5 can bind to and stimulate EphB2, but not any other EphB, to control neurite retraction[56,57]. More research is still needed to shed light on the functional specificity of Ephrin-Eph signaling in the developing central nervous system (CNS).
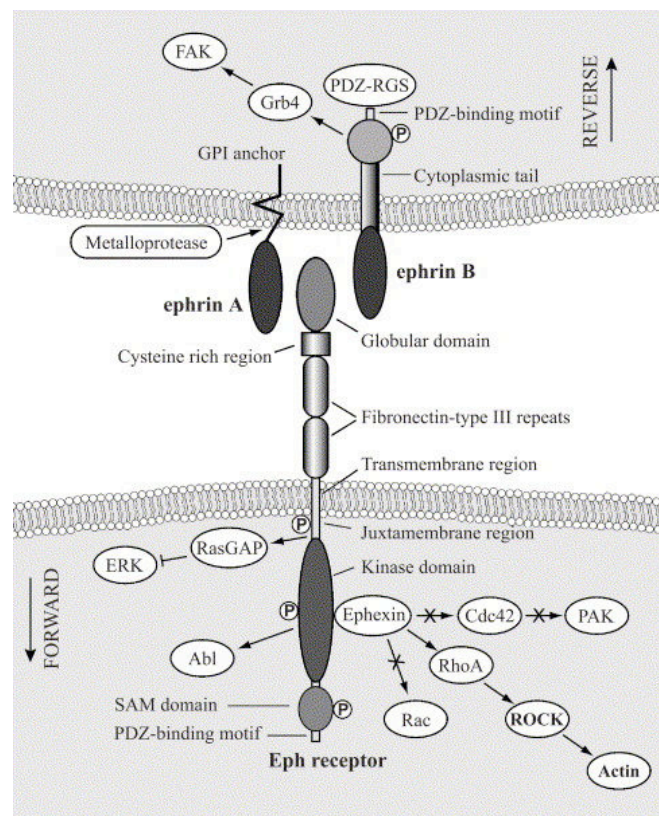
Figure 1.7: The bidirectional Eph-ephrin signaling and structures of the Eph receptors and ephrin ligands

Adapted from Hout, 2004. Eph receptor, denoting a common structural illustration for A and B subclasses, mediates forward signalling. EphrinAs (GPI-anchored) and EphrinBs mediate reverse signaling. The domain organization is marked for all Ephrin-Eph molecules. Major downstream responses regulated in forward signaling, such as ERK and Ephexin pathways, a reverse signaling mediated by ephrinB-Grb4-FAK pathway and the cleavage of ligands by metalloprotease are also representatively depicted.

Structurally, the extracellular domains of Eph receptors consist of two fibronectin type III repeats, a cysteine-rich region and an immunoglobulin (Ig) domain. The Ig domain is mainly responsible for the recognition and binding to ephrin ligands. The intracellular

moieties of the receptors commonly consist of a juxtamembrane region (containing two conserved tyrosines), a tyrosine-rich kinase domain, a sterile α motif (SAM, essential for oligomerization) and a PSD95 disc large zonula occludens-1 (PDZ)-binding motif. The activation of Eph forward signaling is a multi-step process. Autophosphorylation first happens to the tyrosines of juxtamembrane domains upon ligand binding, which in turn has the other tyrosines in kinase and SAM domains phosphorylated. A number of intracellular phospho-tyrosines create docking stations to activate multiple downstream interactive signaling molecules. One well-studied example is Src homology domain-2 (SH2)-containing adaptor complex, which can mediate intracellular biochemical cascades (e.g. ERK1/2 pathway) to influence a wide range of cell activities, such as axon repulsion/attraction, synaptic plasticity, cell migration, border segregation and so on[54,55]. However, some molecules can be constantly bound to Eph receptors irrespectively of ligand binding. One of the known, for instance, is Ephexin, which regulates cytoskeleton remodelling via balancing the activities of RhoA, Cdc42 and Rac1[58] (Figure 1.7).

Each of ephrinB ligands possesses a short intracellular tail consisting of a PDZ binding motif and several tyrosine residues. The phosphorylation of these tyrosines in reverse signaling enables the recruitment and activation of downstream responsive molecules. One well-elucidated example is Grb4, an SH2-containing adaptor, can modulate axon pruning, spinogenesis and synapse formation in hippocampal pyramidal neurons[59]. Unlike ephrinBs, none of the ephrinAs has the cytoplasmic protein domain. Instead, the C-terminal hydrophobic peptide tail is replaced by a glycosylphosphatidylinositol (GPI) anchor during protein maturation, rendering the ephrinA molecules impossible to directly interact with other intracellular proteins[60]. It has been recently found, however, that ephrinAs can mediate reverse signaling by interacting with other transmembrane co-receptors, such as neurotrophin receptors[54]. Additionally, a group of metalloproteases belonging to ADAM superfamily, can associate with Eph receptors *in cis* to cleave the *trans* ligands during ligand-receptor pairing, and vice versa[61] (Figure 1.7).

1.3.1 Eph-Ephrin signaling in axon guidance

Eph-ephrin signaling is involved in a huge spectrum of functions in different developmental processes. In my dissertation, I will mainly focus on their roles in axon guidance in the nervous system. EfnB1 deficient callosal axons fail to cross the cortical

midline and are misrouted to septum because they lose the interaction with EphB receptors expressed by the midline glia cells[62]. Forward signaling via EphB receptors is also important for the formation of CC and AC, supported by the finding that genetic deletion of EphB1/2 coding sequences for their intracellular (but not extracellular) domains in mice causes partial CC and AC agenesis[26]. Virtually, the repelling EphB receptors can create a permissive corridor for ligand-expressing AC fibers to establish inter-hemispheric connectivity, suggested by the fact that posterior AC axons in EphB2 deficient mice grow astray into diencephalic tissues[26,63,64].
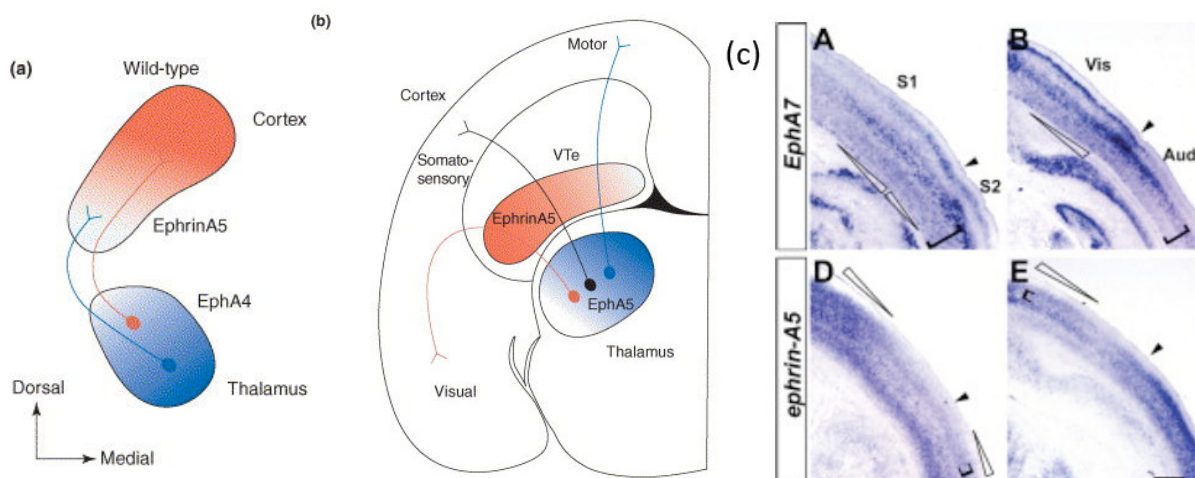
Figure 1.8: Organisation of cortico-thalamic and thalamo-cortical topography

Modified from review, Klein, 2004 and Masaaki, et al., 2005. **(a)** The axons originating from ventral thalamic nuclei with high EphA4 expression project to the cortical area with low ephrinA5 expression (blue axon), and vice versa (red axon). **(b)** The axons originating from the thalamic nuclei with low lateral to high medial EphA5 graded expression are guided along opposing ephrinA5 gradient to the layer IV neurons of different cortical areas (anterio-posteriorly: motor, somatosensory and visual cortex). **(c)** EphA7 and ephrinA5 display mutually complementary expression in the neocortex.

EphA-ephrinA signaling is also critical for brain wiring. Interference with endogenous EphA5 by a truncated variant can prevent callosal axons to approach the midline[27]. Interestingly, EphA4 has been suggested by Prof. Klein's group to act either as kinase-active receptor for instructing axonal cortico-spinal projection or as ligand for promoting AC formation[65]. The establishment of axonal topography also relies on EphA-ephrinA signaling. A good example is cortico-thalamic inter-projections (a and b, Figure 1.8). During thalamo-cortical mapping, EfnA5 functions as the repelling instructor for EphA4/5 positive axons according to the principles that axons with high expression of EphAs are guided to target territories with low expression of EfnA5, and vice versa[66]. On the other

hand, EphA7 displays complementary expression with EfnA5 in the neocortex (c, Figure 1.8) and directs the efferent axons from cortical Layer VI to the thalamus based on a similar mechanism. Artificial alteration of EphA7 expression in the cortex leads to shifted inter-areal projection patterns[67]. Likewise, retinotectal and vomeronasal axonal topography is also shaped by EphA-ephrinA signaling[66,68]. Consequently, the differentially expressed ligands and receptors function in orchestration to pattern the axonal connectivity.

Eph-ephrin signaling regulates axonal guidance through several mechanisms. Cellularly, the axons carrying receptors or ligands react in a repelled/attracted way along the graded expression of the counterparts, such as the above-described formation of axonal topography. Subcellularly, the Eph forward signaling tends to induce growth cone collapse and repulsion, while the ephrin reverse signaling more often leads to growth cone survival and attraction. The dynamic guidance of growth cones, which frequently express both receptors and ligands, depends on the relative balance of signal inputs and the subcellular distribution of Eph/ephrin molecules[69,70]. It was suggested that the compartmentalization of EphrinAs on cell surface might be regulated by Src family kinase Fyn and integrins[71]. Besides, *cis* interaction of ligands and receptors has been experimentally verified and hypothesized to desensitize forward signaling activities[72,73]. In any case, the regulation of Eph-ephrin signaling is achieved through remodelling the cytoskeleton organization of growth cones. It is also known that a single mutation in EfnA5 can abolish its capacity of interaction with EphA3 receptor *in trans*[72]. This finding suggests a useful tool for Eph-ephrin functional research.

1.3.2 Diversified functions of ephrinAs mediated reverse signaling

Despite being far less studied than Eph forward and ephrinB reverse signaling, the ephrinAs mediated reverse signaling has been reported to play active roles in different biological contexts. For instance, EfnA5 reverse signaling can promote adhesive abilities of the fibroblasts *in vitro* by regulating Fyn[71]. Moreover, EfnA5 is able to substantially elevate the insulin yield by up-regulating Rac1 activities in primary pancreatic β cells when these cells are treated with a soluble chimeric protein consisting of the extracellular moiety of EphA5 and the Fc fragment of human IgG1 (EphA5-Fc)[74]. In the cultured T cell line Jurkat TAg, EfnA4 dependent signaling can induce the phosphorylation of Fyn and AKT to prevent cell apoptosis[75].

EphrinA reverse signaling does also play important roles in the nervous system. The EfnA2 reverse signaling, when activated by interaction with EphA7, is required for neural progenitors to maintain normal cell proliferation in adult mouse brains. This finding is supported by the observation that these progenitors exhibit shorter cell cycle length and thus enhanced neurogenesis in EfnA2 knockout mice[76]. Another example is that protein complexes of ephrinAs and the proto-oncogene Ret (Ret) on motor axons can be synergistically stimulated by EphAs and GDNF (a diffusible Ret ligand) and guide the host axons attractively along the EphA expression gradient to innervate limb musculature[77]. Additionally, Prof. Drescher's lab have also argued that, during topographic migration of vomeronasal axons, EfnA5 directs the fibers to the EphA6-expressing olfactory bulb in a high-concentration dependent manner and has a positive role in focal adhesion, although the downstream mechanisms remain still elusive[78]. EphrinAs are also able to regulate axon guidance and branching via interaction with neurotrophin receptors, which will be described in the following sections. However, the functions of ephrinAs concerning CC formation have been barely dissected.

1.4 Neurotrophin signaling

There are four neurotrophins in rodents: nerve growth factor (NGF), brain derived neurotrophic factor (BDNF), neurotrophin-3 (NT-3) and neurotrophin-4 (NT-4). All of them are secreted and soluble cytokines. The neurotropin receptors also consist of four members: three Tropomyocin related kinases (TrkA, TrkB and TrkC, the current nomenclature: Ntrk1, Ntrk2 and Ntrk3, respectively) and the farther related p75NTR belonging to the tumor necrosis factor receptor superfamily. Each of the neurotrophins can bind to a specific receptor with highest affinity, but can also trans-activate other receptors at lower levels. The pairing of ligand-receptor with maximal preference: NGF binds to Ntrk1; BDNF and NT-4 bind to Ntrk2; NT-3 binds to Ntrk3[79–81] (Figure 1.9).

The three Ntrk receptors constitute a subfamily of receptor tyrosine kinases (RTK) and share very similar protein secondary structures. Extracellularly, a number of leusine-rich repeats flanked by two cysteine-rich domains are situated in the N-terminal region of the Ntrk molecules. These N-terminal domains are required for ligand binding. Two Ig domains follow, which are used for inhibiting homo-dimerization when inactivated. Intracellularly, each of the receptors contains a tyrosine kinase domain (Figure 1.9). A common functional paradigm of the RTK also applies to Ntrks. Ligand binding induces

homo-dimerization and autophosphorylation of the cognate receptors, which in turn create phospho-tyrosine docking sites and phosphorylate downstream interacting partners[82,83] (Figure 1.9).
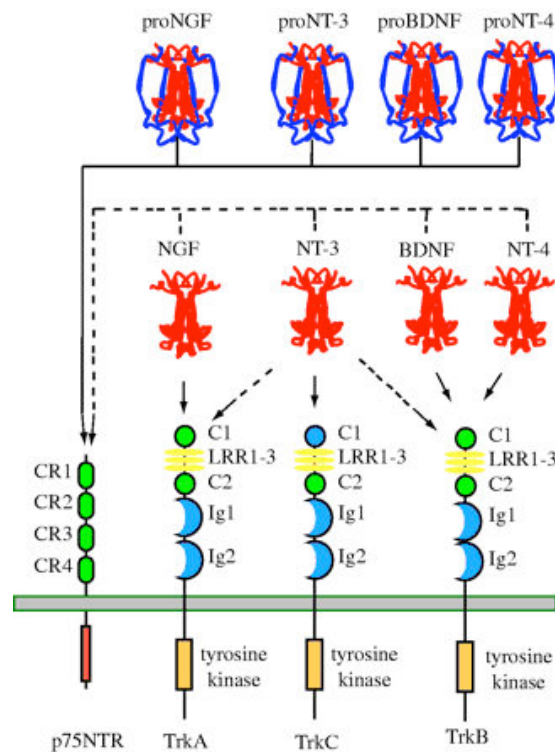
Figure 1.9: Ligand-receptor pairing patterns and protein structures of neurotrophin receptors
Adapted from review, Reichardt, 2006. LRR: leusine-rich repeats; C1 and C2: cysteine-rich domains; Ig1 and Ig2: immunoglobulin domains; CR1 – CR4: cysteine-rich regions in p75NTR. Arrows in real line stand for high affinity binding and arrows in dotted line stand for low affinity binding.

1.4.1 Ntrk2 downstream signaling

Upon binding to BDNF or NT-4, the full-length Ntrk2 (TrkB) can activate three main intracellular cascades via phospholipase C gamma1 (PLCγ1), Ras-mitogen activated protein kinases (MAPK or ERK) or phosphatidylinositol 3 kinase (PI3K)-AKT[81]. These downstream events are mediated by the phosphorylation of two different tyrosines: Y816 and Y515. The abolishment of either tyrosine does not impede the cascade mediated by the other one. Phosphorylation of Y816 results in direct interaction of Ntrk2 with PLCγ1 as well as PLCγ1 phosphorylation, which in turn activates the selective cleavage of its downstream substrates. Ras-ERK and PI3K-AKT cascades both derive their activities originally from the phosphorylated Y515. An adaptor complex, including SH2 domain containing protein 1 (SHC), fibroblast growth factor receptor substrate 2,

growth factor receptor-bound protein 2 (Grb2), son of sevenless (SOS) and Grb2 associated binding proteins, can bind to phosphorylated Y515 directly via SHC (Figure 1.10). The interaction of Ntrk2 and the adaptor complex may activate Ras-ERK and PI3K-AKT cascades. Ras-ERK signaling is involved in a broad range of biological processes, such as cell survival, differentiation and proliferation[84,85]. The activation of AKT cascade is critical for the survival of various cell types, and more importantly to my interest, is of vital significance for axon growth, guidance and the resistance to growth cone collapse in cultured neurons[86–90]. An alternative downstream pathway mediated by FRS2-SHP2 may play a role in maintaining high phosphorylation levels of ERK[83].

1.4.2 The functions of neurotrophin signaling in nervous system

While Ntrk1 is mainly expressed in the peripheral nervous system and promotes the survival of dorsal root and sympathetic ganglia[91,92], Ntrk2 and Ntrk3 are more widely expressed in the nervous system, including CNS[79,93]. Phosphorylation of Ntrk2 at Y816 can modulate synaptic plasticity through protein kinase C and long-term potentiation through Ca^{2+}/calmodulin (Ca^{2+}/CaM)-dependent protein kinases in hippocampal neurons [81,83,94] (Figure 1.10). Phosphorylation of Ntrk2 at Y515 promotes the survival and axon growth of sympathetic neurons[88]. Suppression of both Ntrk2 and Ntrk3 using dominant negative variants leads to reduced proliferation of neural progenitors in cerebral VZ, and hence impaired neuron production[95]. Ntrk1 and Ntrk3, nut not Ntrk2, can induce programmed cell death *in vitro* and *in vivo*, whereas the presence of the compatible ligands prevents the pro-apoptotic effects. This finding has revealed a novel mechanism to control brain size[96]. Several independent groups have showed that BDNF and NT-4 positively regulate dendritic growth and arborization of cortical pyramidal neurons[97–100].

Additionally, it has been reported that Ntrk2 facilitates axon branching via interaction with EfnA5 or EfnA6 in cultured chicken neurons. But this effect can be blocked by application of EphA7-Fc. The p75NTR receptor can also interact with ephrinAs to regulate the axon migration of retinal ganglion cells to the targeted termination zones.

Since receptor homo-dimerization is strictly required for Ntrks activation, the dominant negative approach provides a valuable strategy for loss-of-function studies[88,95,101]. Indeed, the truncated variants of Ntrk2 and Ntrk3 that lack cytoplasmic kinase domains

exist in nature and can suppress the activities of the full-length receptors[102–104]. The Prof. Miller's lab in Canada have reported a kinase-dead version of Ntrk2 with a single mutation on its ATP binding site, which entirely attenuates the kinase activity with minimal change on the protein structure[88]. Since then the kinase-dead Ntrk2 has been frequently used as a dominant negative variant to interfere with the full-length Ntrk2 in quite a few lines of *in vitro* and *in vivo* experiments[95,105–108].
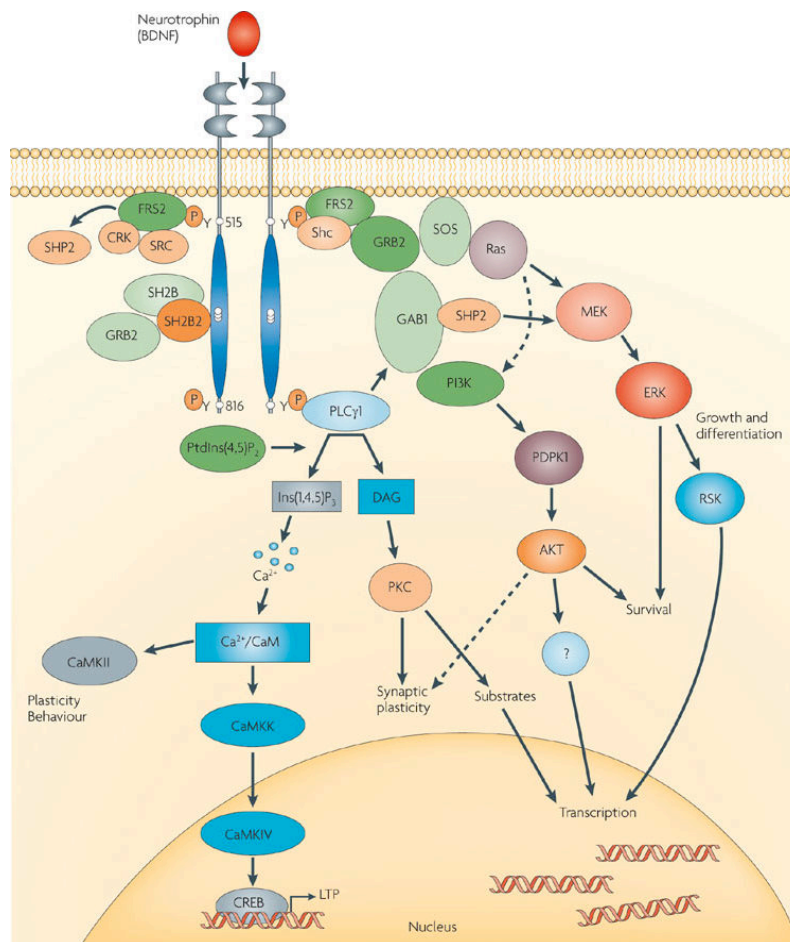
Figure 1.10: Dissection of Ntrk2 downstream signaling

Adapted from review, Minichiello, 2009. Ntrk2 receptor mediates intracellular signaling mainly via three pathways. The phosphorylation of Y816 results in activation of PLCγ1 cascade, which regulates the long-term potentiation (LTP) and memory formation via Ca^{2+}/calmodulin (Ca^{2+}/CaM)-dependent protein kinases and its substrate cAMP response element-binding protein (CREB), and also regulates synaptic plasticity via protein kinase C (PKC). The adaptor complex (including SH2 domain containing protein 1 (SHC), fibroblast growth factor receptor substrate 2 (FRS2), growth factor receptor-bound protein 2 (Grb2), son of sevenless (SOS) and Grb2 associated binding proteins 1 (GAB1)) associated with phosphorylated Y515 can activate Ras-ERK or PI3K-AKT cascades (depending on the cellular contexts), which regulate a wide range of biological activities, such as cell survival, growth, differentiation and axon guidance.

2. Aims:

The transcription factors belonging to basic helix-loop-helix superfamily are well-known gene regulators that control various cell behaviors in nerve systems. Thanks to my colleagues and other researchers, the genetically modified mouse line carrying homozygous deficient NeuroD6 and heterozygous deficient NeuroD2 alleles (NRX line: Neuro6$^{Cre/Cre}$; Neuro2$^{+/-}$) was produced a few years ago. Our collaborators (Prof. K.A. Nave's lab) in Max Plank Institute for Experimental Medicine, Göttingen, Germany, had been studying this transgenic mouse line for years and found that these mice were viable, and that their cerebral neocortical development was grossly normal. NeuroD2/6 DKO embryos could be easily accessible by breeding NRX mouse line and had been briefly characterized by my colleague, Ingo Bormuth, when my PhD project was started. He managed to show that NeuroD2 and NeruoD6 were both strongly expressed in postmitotic neurons of cerebral cortex and followed similar spatio-temporal expression patterns during corticogenesis. It had also been found that NeuroD2/6 DKO mice displayed early postnatal death (around P1) as a result of failure to milk intake and severely disrupted brain commissural structures (details are described in introduction part of the thesis). These data reveal that NeuroD2/6 play critical roles in brain development and wiring with functional redundancy. With such unpublished information in 2011, I commenced this PhD project aiming to address the questions below:

(**I**) How do NeuroD2 and NeuroD6 control axonal wiring in the brains? Cell intrinsically or extrinsically?

(**II**) Which steps of commissural formation are regulated by NeuroD2/6?

(**III**) What are the downstream molecular mechanisms underlying the NeuroD2/6 regulated commissural formation?

(**IV**) Do NeuroD2/6 regulate other developmental processes in the brain?

3. Methods and Materials:

3.1 Mouse mutants:

All mouse experiments were carried out according to German law and approved by the Bezirksregierung Braunschweig and Landesamt für Gesundheit und Soziales Berlin. Generation of NeuroD2/6 DKO embryos: a male and a female in NRX line (NeuroD6$^{Cre/Cre}$/NeuroD2$^{+/-}$) were bred for producing embryos of mixed genotypes (25% incidence of NeuroD2/6 double mutants: NeuroD6$^{Cre/Cre}$/NeuroD2$^{-/-}$). The embryos of other genotypes (NeuroD6$^{Cre/Cre}$/NeuroD2$^{+/+}$ or NeuroD6$^{Cre/Cre}$/NeuroD2$^{+/-}$) were used and termed as controls in the project. The mice of all different genotypes were originally C57BL/6 genetic background. The day of plug discovery was considered as embryonic day 0.5 (E0.5). Male and female embryos were not discriminated in this study. I have participated in the course of "Introductory course in laboratory animals: Handling, Techniques and Theory" from 21st – 24th, Sept, 2010, and have been permitted to do animal experiments on 24th, Sept, 2010.

3.2 Genotyping and polymerase chain reaction:

The double mutant genotype was determined by polymerase chain reaction (PCR). The following primers were used:

NDRFFw: 5′-TTC TCG CTC AAG CAG GAC-3′,

NeoRFw: 5′-AGT GAC AAC GTC GAG CAC AG-3′,

NDRFRev: 5′-CCC ACA GCT AAG AGA GCA CG-3′.

A 20μl PCR reaction was performed as below:

5x buffer (Promega):   4 μl

10mM dNTPs (Invitrogen):   0.4 μl

10nmol/ml each of the primers: 0.5 μl

Go-taq polymerase (Promega): 0.1 μl

Isolated tail DNA: 2 μl

Distilled deionized H$_2$O (ddH$_2$O):   13 µl

Amplification program:

94°C – 15 sec

60°C – 18 sec

72°C – 1 min

Amplification was set for 35 cycles. The final elongation last 5 min at 72°C and samples were cool down to room temperature (RT) for DNA gel electrophoresis.

3.3 *In utero* electroporation:

Mostly, the pregnant mice carrying E12.5 or E13.5 embryos were operated in this study. Plasmids (1 µg/µl) were mixed with fast green dye (1:20, 000). During the entire process, the pregnant mice on surgery were kept laid down on a heating pad and anesthetized by constant inhalation of isoflurane mixed with oxygen. The abdominal region was cleaned by 70% ethanol and Iodine followed by subcutaneous administration of temgesic before operation started. An incision of ~15mm was made on the fur and skin along the abdomen midline. The embryos wrapped in the uterine wall were pulled out with ring-headed forceps gently enough without damaging the blood vessels and visceral organs. DNA loaded in a fine glass capillary (pulled by HEKA-PIP6 capillary puller) was enforced by a vacuum pico-pump (WPI) into either of the cerebral lateral ventricles (fast green dye spreading over the injected hemisphere). Electrodes were placed on both sides of a head with the positive on the electroporated side. Electroporation was achieved by an electroporator (CUY21, Sonidel) with setup: 6 times pulses, 35 V voltage, 50 ms pulse duration and 1 sec interval time. Consistent application of 1x PBS containing antibiotics (1000 units/ml Penicillin-Streptomycin, Gibco) to each operated embryo was carried out during and after electroporation. After all embryos were electroporated, they were returned carefully into the abdominal cavity filled with more 1x PBS containing antibiotics. The skin was sewed up with sterilized sutures. The fur was closed with surgical staples. After surgery, the mice were put back to an individual cage marked with genes and dates of the electroporation. The operated mice were monitored every day for their health and sacrificed when embryos reached E18.5.

3.4 Molecular cloning, constructs and mutagenesis:

For TA cloning: full transcript sequences of targeted genes were downloaded from UCSC genome browser, based on which primer sequences were procured using online Primer3 software. The parameters for primer designing were set: the melting temperature was ~60°C, oligo length was ~25 bases and GC proportion ranged from 30% ~ 70%. The targeted sequences ranging from 500 to 800 base pairs (bp) were amplified by PCR (similarly as described in part 3.2, the annealing temperature was usually 57°C) and immediately isolated by gel extraction with ready-to-use kits (QIAGEN, solutions and procedures according to manufacturer's instructions). Ligation was set up as below and last over night (O/N) at 4°C.

2x Ligation Buffer (Promega):   5 µl

10x T4 Ligase (Promega):   1 µl

50ng/µl pGMT vector (Promega): 1 µl

Isolated inserts: 3 µl

On the next day, 2.5 µl ligation products were transformed into competent cells by heat shock (15 min on ice -> 45 sec at 42°C -> 5 min on ice) followed by 1 hour agitating incubation in LB media at 37°C). The transformed bacteria were then spread evenly on the LB plates containing selective antibiotics (mostly 100 µg/ml ampicillin) and kept at 37°C O/N. Positive clones were screened out by colony PCR (2 µl bacterial cultures as templates for PCR). The plasmids were amplified by continuous agitating incubation of the positive bacterial clones at 37°C in LB media (with antibiotics) O/N and then isolated by ready-to-use miniprep kits (QIAGEN, solutions and procedures according to manufacturer's instructions). Subsequently, ~10 µg plasmids were incubated at 37°C O/N with properly chosen restriction enzymes. The linearized plasmids were purified by gel extraction kits and served as templates for *in vitro* transcription. The concentrations of plasmids and templates were determined by Nanodrop machine (Eppendorf).

Constructs: Cre-activatable plasmid (pCAG-FPF-GFP) was generated and verified by Dr. S. Parthasarathy in our lab. Briefly, it was modified from pCAGIG (Addgene) that contained pCAG promoter, multiple cloning sites (MCS), internal ribosome entry site (IRES) and the coding sequence for GFP. For generating pCAG-FPF-GFP, a stop

cassette (flox-mCherry-flox) was inserted between pCAG and MCS of the pCAGIG vector. The open reading frame (ORF) of NeuroD2 or Neurod6 with the original Kozak sequence was cloned in pCAG-FPF-GFP for IUE and pCAGIG for *in vitro* experiments. The ORFs of EfnA1, EfnA3, EfnA4, EfnB1, Cntn2, Ntrk2 and Ntrk3 were cloned into pCAGIG for IUE. The C-terminal myc-tagged Ntrk2 and Ntrk3 were also cloned into pCAGIG for *in vitro* assays. The ORF of EfnA4 was also cloned in pCRC-dsRed vector, which had been reported to express membrane located dsRed[109], for co-IUE with different variants of Ntrk2/3.

Mutagenesis: the full-length ORFs of targeted genes were first cloned into pGMT vectors by TA cloning for subsequent mutagenesis. The different variants of EfnA4 or Ntrk2/3 were created with Q5 Site-Directed Mutagenesis kit (New England Biolabs, NEB) as below via tag- or point mutation-containing primers.

Step I: Q5 site-directed mutagenic PCR amplification

98°C	15 sec
60 - 72°C (annealing temperature determined by NEB website)	20 sec
72°C (30 sec for 1 kb)	2-4 min

Amplification was set for 25 cycles and achieved by Q5 high fidelity polymerase (NEB).

Step II: Self-ligation of the amplified plasmids by KLD enzyme mix (NEB)

PCR product:	1 µl
2x KLD reaction buffer:	5 µl
10x KLD enzyme mix:	1 µl
ddH$_2$O:	3 µl

The reaction mix was incubated at RT for 15 min and then 5 µl ligation products were transformed into competent cells. The transformation, positive clone screening and plasmids isolation were the same as described above. The wanted inserts were eventually transferred from pGMT into pCAG expression vectors by restriction enzyme release and re-ligation. All cloned full-length ORFs and fragments of targeted transcripts were verified by sequencing. The plasmid containing EphA2 transcript fragment was a

kind gifts provided by Dr. S. Parthasarathy in our lab. All used primers are listed below:

Table 3.1 Primers for TA cloning:

Oligo Name	Sequence
EfnA1-Fw	TACATCTCCAAACCTATCTACCATC
EfnA1-Rv	CGTCTTTACCAAGTTCAGTGTCC
EfnA2-Fw	TACATCCTGTACATGGTGAATGGT
EfnA2-Rv	CAGCACCATGAAAGAGAAGCAG
EfnA3-Fw	GGCCAAGAATACTACTACATCTCCA
EfnA3-Rv	GGGCAAAGAGGGAGGGCACCAAGG
EfnA4-Fw	ATAGCTGCTTTGATGGTCTTGTCT
EfnA4-Rv	GTAGCATGTTCGAAGGACAACTTT
EfnA5-Fw	GATGTTGCACGTGGAGATGTTGACG
EfnA5-Rv	GGGAGGAGACTGTGCTATAATGTCA
EphA4-Fw	GTCAACGAGACATCGGTGAACT
EphA4-Rv	CTTCTTGTTTCGCTTTGCTGTAC
EphA5-Fw	GCTGGATATGAAGAGAAAAATGGTA
EphA5-Rv	CTTTAAGAGTTTTGATAGCCACAGG
EfnB1-Fw	GCGCTAGGGGATCCTGAAGTGCATT
EfnB1-Rv	CAGTAGTTGTTCTCTGTAGTCCGTA
EfnB2-Fw	GCAGAACTGGGAGCGGCTTGGGCAT
EfnB2-Rv	GCACGATGTACACCGGGTGCCCATA
EfnB3-Fw	CTAACCAGAGGCATGAAGGTG
EfnB3-Rv	ATAGTCACCGCTCACCTTCTC
EphA2-Fw	GTCATGTGGGAAGTGATGACTTATG
EphA2-Rv	GTACTGTTGCATCTTGATGCTCTC
EphA3-Fw	GTCCAAATGCCTTAAAATGGAATTG
EphA3-Rv	CAATAGCATTTGGCACTTGGCTGT
EphA4-Fw	GTCAACGAGACATCGGTGAACT
EphA4-Rv	CTTCTTGTTTCGCTTTGCTGTA
EphA5-Fw	GCTGGATATGAAGAGAAAAATGGTA
EphA5-Rv	CTTTAAGAGTTTTGATAGCCACAGG
Ret-Fw	ATGAGACTACTGGCCTTCTCTACCT
Ret-Rv	CTCCTGTTGAGAATCAGCTTGTAAT
p75NTR-Fw	AGCATATAGACTCCTTTACCCACGA
p75NTR-Rv	CAGACCCCTAGATCTGACACAGTTA
Ntrk1-Fw-1st	CTAGGCAGTCTGATGACTTCGTT
Ntrk1-Rv-1st	AGAGTCATGAAGCGTCTGTGTATG
Ntrk1-Fw-2nd	CAGTGATCTCAACAAGAAGAATGTG
Ntrk1-Rv-2nd	GGTATCACTGAAGTACTGTGGGTTC
Ntrk1-Fw-3rd	GTATATCTAGCCAGCCTGCACTTT
Ntrk1-Rv-3rd	GTGAGAGACTTGAATGTGGTAGCTC

Ntrk2-Fw	AAACCAGAAAAGGCTAGAAATCATC
Ntrk2-Rv	CGTTATTCATATGAGTGGGGTTATC
Ntrk3-Fw	ATTACGGACATCTCAAGGAATATCA
Ntrk3-Rv	TAGTAGACAGTGAGAGCAACACTGG
Cntn2-Fw	GGATATGAGATTCGCTACTGGAAAG
Cntn2-Rv	GACCAATGTCTTCAGGTACTGGTAT
Robo1-Fw	AACATGAGTGCTGTTGTGATCC
Robo1-Rv	CCTCTTGATGACATAGAGCTGG
NfiA-Fw	ACTGAAGAAGTCTGAGAAGTCTGGTT
NfiA-Rv	TGAGAAATTACGACAGTCCCTAAAGTA
NfiB-Fw	TCAATGTATCAGAGCTTGTGAGAGTAT
NfiB-Rv	TTAAGGGAATTAGTGACTGTAAGTGCT
Cux1-Fw	CGATCCAGCCTAGAAGTAGAGTTGGC
Cux1-Rv	AAGATATGGAGTTTGTGCTGTAAGGA
Cux2-Fw	GATGGAGACAGCCAGCCCCAGGAT
Cux2-Rv	TTCAGAATTCCCACTCCAGGACCTC
Ptn-Fw	GCCTACCCGTCCAAATATCCCGCCA
Ptn-Rv	TGCCAGTTCTGGTCTTCAAGGCGG
Limch1-Fw	AGCCAGACACGAAAGGAATGCAG
Limch1-Rv	GCAAACACCTCCGAGAGAAGCCG

Table 3.2 Primers for full-length ORF cloning:

Oligo Name	Usage	Sequence
NeuroD2-Fw	NeuroD2 full length cloning	TTTTGAATTCCACCATGCTGACCCGCCTGTTCAGC
NeuroD2-Rv		TTTTGCGGCCGCTTATCAGTTATGGAAAAATGCGTTG
NeuroD6-Fw	NeuroD6 full length cloning	TTTTGAATTCAACCATGTTAACACTACCGTTTGAC
NeuroD6-Rv		TTTTGCGGCCGCTCATTAATTATGAAAAACTGCATTT
EfnA4-Fw-EcoRI	EfnA4 full length cloning	TTTTGAATTCGGGCGATGCGGCTGCTGCCCCTGC
EfnA4-Rv-NotI		TTTTGCGGCCGCTTATCACAGAACTCTCAGGAGACGGAG
EfnA4-Rv-EcoRI	Reverse primer for cloning EfnA4 into pCRC vector	TTTTGAATTCTCACAGAACTCTCAGGAGACGGAG
sEfnA4-Rv-NotI	Reverse primer for generation of secreted EfnA4	TTTTGCGGCCGCTTATCACCCAACAGGATGAGCTGACTCATGT
EfnA1-Fw-XhoI	EfnA1 full length cloning	TTTTCTCGAGCGCTATGGAGTTCCTTTGGGCCCCT
EfnA1-Rv-NotI		TTTTGCGGCCGCTCACTGAGATTGCAGCAGCAGCAGT
EfnA3-Fw-xhoI	EfnA3 full length cloning	TTTTCTCGAGGGGATGGCGGCGGCTCCGCTGCTG

EfnA3-Rv-NotI		TTTTGCGGCCGCCTAGGAGGCCAAGAGCGTCATGAGG
EfnB1-Fw-xhoI	EfnB1 full length cloning	TTTTCTCGAGGAAAATGGCCCGGCCTGGGCAGCG
EfnB1-Rv-NotI		TTTTGCGGCCGCTCAAACCTTGTAGTAGATGTTCGCC
Cntn2-Fw-xhoI	Cntn2 full length cloning	TTTTCTCGAGCACCATGGGAGCACCGGCCAGGAAAAG
Cntn2-Rv-NotI		TTTTGCGGCCGCTCAGAGCCTCTGGCATCCGGCGAG
Ntrk2-Fw-EcoRI	Ntrk2 full length cloning	TTTTGAATTCGGGATGTCGCCCTGGCTGAAGTG
Ntrk2-Rv-NotI		TTTTGCGGCCGCTAGCCTAGGATATCCAGGTAGACG
Ntrk3-Fw-XhoI	Ntrk3 full length cloning	TTTTCTCGAGGAGATGGATGTCTCTCTTTGCCCA
Ntrk3-Rv-NotI		TTTTGCGGCCGCACTAGCCAAGAATGTCCAGGTAGATC
EfnA4-Cflag-Fw	Insert flag tag in C-terminal of cloned EfnA4	GACGACGATAAGGGGAGTCCTGGAGAAAGC
EfnA4-Cflag-Rv		ATCCTTGTAATCAACAGGATGAGCTGACTC
EfnA4-Mut-Fw	Generation of EfnA4^{E126K} on cloned EfnA4	CCCGCTGGGCTTTAAGTTCTTGCCT
EfnA4-Mut-Rv		AAGGGTGTGTAGCGCTGAATCT
Ntrk2-DK-Fw	Generation of kinase dead Ntrk2^{K571N}	GGTGGCTGTGAACACGCTGAACGACGCCAGCGACAA
Ntrk2-DK-Rv		AGGATCTTATCCTGCTCTGGGCA
Ntrk3-DK-Fw	Generation of kinase dead Ntrk3^{K572N}	GTGGCAGTGAACGCCCTGAACGATCCCACCTTGGCT
Ntrk3-DK-Rv		TAGCATCTTGTCTTTGGTGGGGCTT
Ntrk2-Myc-Fw	Insert myc tag in C-terminal of cloned Ntrk2	GATCAGTTTCTGTTCGCCTAGGATATCCGGTAGACG
Ntrk2-Myc-Rv		TCTGAAGAAGACCTGTAGAATCCCGCGGCCAGG
Ntrk3-Myc-Fw	Insert myc tag in C-terminal of cloned Ntrk3	TCTGAAGAAGACCTGTAGTGCGGCCGCAAAAAT
Ntrk3-Myc-Rv		GATCAGTTTCTGTTCGCCAAGAATGTCCAGGTAG
Ntrk2-Y515F-Fw	Generation of mutation TrkB^{Y515F}	GATGCCAAAGAACTGGGGGTT
Ntrk2-Y515F-Rv		ACCAACAGTCAGCTCAAG
Ntrk2-Y816F-Fw	Generation of mutation Ntrk2^{Y816F}	GATATCCAGGAAGACGGGAGATG
Ntrk2-Y816F-Rv		CTAGGCGAACAGAAACTG

3.5 Bromodeoxyuridine pulse chase:

300 μl BrdU solution (10 mg/ml BrdU dissolved in 1xPBS) was injected intraperitoneally into mouse abdominal cavity with sterile needles. Then the time points and embryonic stages (E14.5 – E17.5) of the injections were carefully labelled on the cage. The injection time points at different stages were tightly controlled (± 0.5 hour).

3.6 In situ hybridization:

In vitro transcription for synthesis of *in situ* hybridization (ISH) probes: the reaction mixture below was incubated for 3 hours at 37°C.

Linearized plasmids as template:	2 µg
10x transcription buffer (Roche):	2 µl
Digoxigenin-labeled RNA mix (Roche):	2 µl
RNAse inhibitor (NEB):	1 µl
T7 or Sp6 RNA polymerase (Roche):	2 µl
DEPC-treated H_2O:	up to 20 µl

The synthesized anti-sense RNA probes were mixed with 3 µl lithium chloride (4 M) and incubated at -20°C O/N. The probe precipitation was achieved by centrifugation (13.2 krpm at 4°C for 20 min). The RNA pellets were washed twice by centrifugation as before in 150 µl 70% Ethanol and then resuspended with 33 µl DEPC-treated H_2O. 3 µl of each probe was subject to fast DNA gel electrophoresis to monitor the RNA quality, and the remaining was mixed with 170 µl hybridization buffer (HB, 50% deionized formamide (AppliChem), 5x SSC, 1% blocking reagent (Roche), 5 mM EDTA, 0.1% Tween20 (SIGMA), 0.1% CHAPS (SIGMA), 0.1 mg/ml Heparin (SIGMA), 100 µg/ml yeast RNA (Invitrogen)). The probes were kept at -20°C.

ISH: on the 1st day, tissue sections were dried in vacuum for 30 min, and fixed in 4% paraformaldehyde (PFA) dissolved in DEPC-treated 1x PBS (DPBS) for 15 min followed by twice quick washes in DPBS (5 min each, the same below), and then were incubated in pK solution (20 mM Tris pH7.5, 1 mM EDTA pH8.0, 20 µg/ml proteinase K) for 2.5 min. Subsequently, sections were washed in 0.2% glycine (AppliChem) in DPBS, quickly washed twice in DPBS, and post-fixed in 4% PFA containing 0.2% glutaraldehyde (SIGMA) in DPBS for 15 min, quickly washed twice in DPBS, pre-hybridized in HB at 65°C for 2 hours, and eventually hybridized with the denatured probes (10 µl probe in 160 µl HB, heated at 90°C for 5 min, kept on ice) at 68°C O/N.

On the 2nd day, the sections were washed once in 2x SSC pH4.5, incubated in RNase solution (0.5 M NaCl, 10 mM Tris pH8.0, 20 µg/ml RNase (SIGMA)) for 30 min at 37°C, washed once in 2x SSC pH4.5, and then washed stringently 3 times in 50% formamide/ 2x SSC pH4.5 (30 min each) at 63°C, and eventually washed 3 times in KTBT buffer (50 mM Tris pH7.5, 150 mM NaCl, 10 mM KCl, 1% Triton X-100) for 10 min each. Subsequently, the sections were incubated in blocking solution (BS, KTBT containing 20% sheep serum (SIGMA)) for 2 hours, and were incubated with anti-digoxigenin antibody (alkaline phosphatase (AP)-conjugated, Roche, 1:1500) in BS at 4°C O/N.

On the 3rd day, the sections were washed 4 times in KTBT for 30 min each, washed twice in NTMT buffer (100 mM Tris pH9.5, 100 mM NaCl, 50 mM MgCl$_2$, 0.1% Tween20) for 15 min each, and were eventually incubated in NTMT containing NBT/BCIP (AP substrates, Roche). The staining was monitored hourly until the signals showed up. The stained sections were subject to an ascending alcohol series (50% - 100%), incubated in clearing solution (benzyl alcohol:benzyl benzoate = 1:2) for 5 min, and finally mounted using Eukitt (O. Kindler). All solutions used before hybridization were prepared using DEPC-treated H$_2$O. If not noted otherwise, all incubations in the section of 'Methods and Materials' were at RT.

3.7 Immunohistochemistry and immunocytochemistry:

Immunohistochemistry (IHC): on the 1st day, the cryo-sections (16 µm in thickness) were dried in vacuum for 30 min, and fixed in 4% PFA (dissolved in 1x PBS) for 15 min followed by twice quick washes in 1x PBS. Subsequently, the sections were incubated in blocking solution (1x PBS containing 0.5% Triton X-100, 2% BSA and 10% horse serum (SIGMA)), and then incubated with primary antibodies in blocking solution at 4°C O/N. On the next day, the sections were quickly washed 3 times in 1x PBS, incubated with secondary antibodies in blocking solution for 1.5 hours and then were washed 3 times in 1x PBS for 10 min each. The slides were then mounted with DAKO anti-artifact medium (DAKO).

Immunocytochemistry (ICC): on the 1st day, HEK293 cells adhering to 0.1 mg/ml poly-

lysine coated cover slips were co-transfected with 50 ng EfnA4 variant-expressing plasmids and 450 ng empty vector (no insert or GFP expression). On the 2nd day, the cells were fixed in 4% PFA (dissolved in 1x PBS) for 20 min, and then were quickly washed twice in 1x PBS. Procedures for blocking and antibody incubation were the same as IHC. After staining, the cover slips were mounted reversely on a slide with the cells in between using DAKO medium. In the case of mutated EfnA4, 3 μg/ml EphA4-Fc-6xHis (mouse, R&D) was applied into the media 1 hour before fixation.

Primary antibodies used in IHC and ICC: anti-SatB2 (rabbit, homemade, 1:800), anti-Ctip2 (rat, Abcam, 1:500), anti-Brn2 (goat, Santa Cruz, 1:200), anti-Tbr1 (rabbit, Abcam, 1:200), anti-Tbr2 (rabbit, Abcam, 1:200), anti-nestin (mouse, Millipore, 1:300), anti-Sox5 (goat, Santa Cruz, 1:200), anti-Cux1 (rabbit, Santa Cruz, 1:200), anti-phospho-p44/42 MAPK (ERK1/2) Thr202/204 (rabbit, Cell signaling, 1:300), anti-Pax6 (rabbit, Abcam, 1:400), anti-Foxp2 (rabbit, Abcam, 1:200), anti-NeuroD1 (goat, Santa Cruz Biotechnology, 1:100), anti-Cre (mouse, SIGMA, 1:200), anti-Tuj1 (mouse, Covance, 1:1000), anti-Olig2 (rabbit, a kind gift from Prof. Charles Stiles, Harvard Medical School, 1:200), anti-GFP (goat, Rockland, 1:500; chicken, Abcam, 1:1000), anti-dsRed (rabbit, Clontech, 1:600), anti-L1 (rat, Millipore, 1.500), anti-BrdU (rat, Abcam, 1:300), anti-6xHis (rabbit, Abcam, 1:1000), anti-flag (mouse, SIGMA, 1:1000). Secondary antibodies: all fluorochromes (Fluor 488, Cy3 and 647) conjugated secondary antibodies (raised in donkey) were from Jackson Immunoresearch and used at 1:500.

3.8 Microscopy and image acquisition:

Bright field images (for ISH results) were acquired with microscope Olympus BX60 and software AxioVision 4.8 (Zeiss). Fluorescent images (for IHC and ICC results) were acquired with confocal microscope Leica TCS SL and configured software (Leica). The same manipulations (such as background subtraction, contrast adjustment and photo-merge) were carried out on the paired images of the control and DKO brain sections by Adobe photoshop CS3 or ImageJ.

3.9 Tissue processing:

For tail DNA purification: the tails with identity labels were incubated in lysis solution (100 mM Tris-HCl pH8.0, 5 mM EDTA, 150 mM NaCl, 0.2% SDS, 100 mg/ml proteinase K (Merck)) in an agitating incubator at 55°C O/N. The tubes containing the lysates were centrifuged at 13.2 krpm for 15 min and then the supernatants were transferred into new tubes. Subsequently, the supernatants were mixed with equal volume of isopropanol thoroughly till the flocculent DNA appeared. The mixtures were centrifuged again as before to remove supernatants. The DNA pellets were washed with 70% Ethanol twice by centrifugation as before and eventually resuspended with 150 μl ddH$_2$O.

For ISH: the pregnant mice were sacrificed by injection of Avertin followed by cervical dislocation when they had lost consciousness. The brains (E15.5 onwards) or whole heads (till E14.5) of littermate control and DKO embryos were immediately isolated and fixed for 6 hours in 4% PFA in DPBS and then quickly washed twice with DPBS. The fixed tissues were incubated in DPBS containing 25% sucrose at 4°C O/N and embedded in Tissue-Tek O.C.T. ^{TM} Compound (Sakura) on the next morning. Tissue sections (16 μm) were processed by cryo-microtome, collected on adhesive glass slides and kept in -80°C freezer. For IHC: the similar procedures were applied as described in ISH except for that the PFA fixation last O/N instead of 6 hours.

For cortical protein extraction: all E18.5 littermate embryos were transferred in pre-chilled 1x PBS (on ice) as soon as they were taken out from the sacrificed mouse. Cerebral cortices were immediately and carefully separated from the diencephalic tissues following delicate manipulation to remove the hippocampi and basal ganglia with micro-forceps. The remaining cortical tissues were lysed in Flag buffer (50 mM Tris pH7.5, 100 mM NaCl, 1 mM EDTA, 1% Triton X-100) containing inhibitors (1x Protease inhibitor cocktail (SIGMA), 1x PhosStop (Roche), 10 mg/mL leupeptin, 5 mg/mL pepstatin) by pipetting up and down. The lysates were centrifuged at 13.2 krpm at 4°C for 20 min, and then the supernatants were transferred into new tubes and maintained at -80°C. The embryos and tissues were always kept on ice during all the processes.

3.10 Cell culture, transfection and neurotrophin stimulation:

Cell culture: HEK293 cells were cultured in standard media composed of basal Dulbecco's modified Eagle's medium (DMEM, Gibco), 10% fetal calf serum (FCS, Biochrom) and 1% penicillin/streptomycin (Gibco) in a 37 °C and 5% CO_2 incubator. All the manipulations (passages, transfection and neurotrophin stimulation) were carried out under a well-ventilated hood.

Transfection: the plasmids (2 μg for a well of 6-well plate and 600 ng for a well of 24-well plate) and lipofectamine 2000 (Invitrogen, 5 μl for a well of 6-well plate and 1.5 μl for a well of 24-well plate) were incubated with equal volume of Opti-Mum (Invitrogen, 200 μl for a well of 6-well plate and 50 μl for a well of 24-well plate) in separate tubes for 5 min. Then the solutions of plasmids and lipofectamine were mixed well and incubated for 30 min. In the meanwhile, the standard media were exchanged into antibiotic free media. The reaction mix was applied to the cells after 30min-incubation, and the plates were gently rotated and returned to the incubator. The transfection was generally performed on 70-80% confluent cells. Fluorescence was monitored 24 hours after transfections.

Neurotrophin stimulation: the transfected HEK293 cells were stimulated with 25 ng/ml human BDNF (Invitrogen) for verification of kinase-dead Ntrk2 and quantification of the phosphorylation levels of Ntrk2 downstream effector proteins. The transfected cells were stimulated with 50 ng/ml human NT-3 (Peprotech) for verification of d kinase-dead Ntrk3.

3.11 Luciferase Assay:

5 kbp genomic sequence upstream of EfnA4 transcription initiation site was obtained from UCSC genome browser. Among this genomic region, six selected DNA fragments (EC1 – EC6) containing 2 - 5 potential E-box motifs were subcloned into pMCS-GL vector (Thermo Scientific) expressing secreted luciferase. The primers of PCR amplification for EC1 – EC6 subcloning are below:

EC1Fw: 5′-CCA CAA TGG TCA CCC AGC ACG ATG C-3′,

EC1Rv: 5′-TAT GTT TAG ATC TTG TCC TTT GTG T-3′.

EC2Fw: 5′-CAA GAA TGT GTC ACT TAG GAT GCC T-3′,

EC2Rv: 5′-GAC ACA GCC TGC CCC TTA TCC GCA C-3′;

EC3Fw: 5′-GGG CTG GGC CTT GCC CTG GCT CAG G-3′,

EC3Rv: 5′-ACA CTA CCC AGG GGT CGA CAT GCA A-3′;

EC4Fw: 5′-CAA GGA CTC AGG ACC AGT AAG TAG C-3′,

EC4Rv: 5′-AGA TTT ACC TGG AGT TTC TTG GGC A-3′;

EC5Fw: 5′-GGC CTG CTC CTC AGC CTC CTG TTG T-3′,

EC5Rv: 5′-TCT GAG TCT TGA ACC CTT AGT GCT A-3′;

EC6Fw: 5′-CCC GTC TTT GCC ACT TCC CAG GAT A-3′,

EC6Rv: 5′-GGA CCA CTT CCC TGT GTA TGG CTT T-3′;

250 ng pMCS-GL carrying DNA fragments of interest (pMCS-EC1 - pMCS-EC6) were co-transfected with 250 ng pCAG-GFP or pCAG-NeuroD6 in HEK293 cells in a well of a 24-well plate by lipofectamine 2000. 100 ng of an AP expressing plasmid was also co-transfected in each sample for normalization. After 48-hour incubation, the supernatants to be used for the assays were collected and centrifuged at 13.2 krpm at 4°C for 15 min. The cleared supernatants were transferred into new tubes. Triplicate sampling was applied to each transfection condition. The luciferase assays were performed with the Secrete-Pair Dual Luminescence kit (Genecopoeia) as below:

Step I for AP activity measurement: 50 µl aliquote from each sample was heated at 65°C for 15 min and then kept on ice. In the meanwhile, 1x AP substrate (100x provided) was prepared in pre-thawed 1x buffer (10x provided) and incubated for 10 min. 10 µl aliquote of each heated sample was pipetted into a well of 96-well microplate followed by mixed with 100 µl substrate per well. The reaction mixtures were incubated for 8 min and sent for measurement.

Step II for luciferase activity measurement: 1x luciferase substrate (100x provided) was dissolved in pre-thawed 1x buffer (10x provided) and incubated for 25 min. 10 µl aliquote of each sample (on ice) was pipetted into a microplate well followed by mixed

with 100 µl luciferase substrate per well. The reaction mixtures covered with aluminium foil were incubated for 1 min and sent for measurement.

The signal intensity resulted from the AP and luciferase reactions was measured in duplicate by Glomax reader (Promega). The mean value of luciferase reactions (averaged by the triplicate sampling and duplicate measurement of each sample) was normalized to the mean value of AP reactions to achieve the data that denoted luciferase activities for each transfection condition. The up- or down-regulation was indicated by normalizing the luciferase activity of NeuroD6 transfection to that of corresponding GFP transfection.

3.12 Bicinchoninic acid assay and western blot:

Bicinchoninic acid (BCA) assay: the assays were carried out using Pierce BCA Protein Assay kit (life technologies) to determine protein concentrations. 10 µl aliquote of a protein sample was diluted with 50 µl ddH$_2$O, and 25 µl of the dilution was pipetted into a well of transparent microplate. Then 200 µl working reagent (reagent A (transparent): reagent B (blue) = 1:50) was immediately mixed with the sample dilution. The complete reaction was achieved by 30 min incubation (light proof) at 37°C. In parallel, protein standards with concentration gradient (minimally 0.05 mg/ml to maximally 2 mg/ml, provided in the kit) were prepared in the same way. All protein samples and standards were prepared and measured in duplicate by Varioscan Flash (Thermo Scientific, version 2.4.3) and configured software SkanIt^{TM}. The mean values were obtained by Excel software and considered to be the protein concentrations of the samples.

Western Blot (WB): the protein samples in Flag buffer or Ripa buffer (50 mM Tris pH8.0, 150 mM NaCl, 1% NP-40, 0.1% SDS, 0.5% sodium deoxycholate) from *in vitro* and *in vivo* samples were separated by SDS-polyacrylamide gel electrophoresis (PAGE) with standard Bio-Rad WB devices. The protein samples (equal amounts if the subsequent quantification was required) were heated at 95°C for 5 min in 1x Laemmli buffer (5x stock: 12.5 ml Tris pH6.8, 3.86 g DTT, 5.0 g SDS, 250 mg Bromophenol blue, 17.5 ml glycerol dissolved in 50 ml ddH$_2$O) and then subject to PAGE with the protein ladders (protein plus, Thermo Scientific). Polyacrylamide gel recipes are as below:

Running gel (20ml, 10%):

40% Acrylamide/Bisacrylamide (29:1):	5 ml
1.5 M Tris-HCl pH8.8:	5 ml
10% SDS:	0.2 ml
ddH$_2$O:	9.9 ml
10% Ammonium persulfate (APS):	0.1 ml
TEMED:	20 µl

Stacking gel (10ml, 4%):

40% Acrylamide/Bisacrylamide (29:1):	1 ml
1 M Tris-HCl pH6.8:	1.25 ml
10% SDS:	0.1 ml
ddH$_2$O:	7.65 ml
10% APS:	0.1 ml
TEMED:	20 µl

As for the samples from *in vitro* assays, 40 µg of each sample was applied; as for the samples from cortices, 50 µg of each sample was applied. The proteins on the gel were transferred onto a PVDF membrane (pre-activated by 100% Methanol, Immobilon-P, Millipore) after PAGE. The membrane was then blocked in TBST (TBS (50 mM Tris pH7.5, 150 mM NaCl) + 0.5% Tween20 + 3% BSA) for 1 hour and then incubated in TBST containing primary antibodies at 4°C O/N on a horizontally agitating incubator. On the next day, the membrane was washed 3 times in TBS (10 min each), incubated with secondary antibodies in TBST for 2 hours and then washed 3 times in TBS. The membrane was treated with horseradish peroxidase (HRP) substrates (Perkin Elmer) and immediately detected using Bio-Rad ChemiDoc XRS+ machine and software 'Image lab'. The WB band intensities were quantified by software 'Image lab' as well. Antibody stripping was performed if necessary: the membrane was washed twice with 1x PBS (5 min each), twice with Glycine solution (0.15 M glycine pH2.5, 0.4% SDS) (15 min each) and twice with 1x PBS. The stripped membrane would be blocked again in TBST and then used for the detection of a new epitope.

Primary antibodies used for WB: anti-total Akt (rabbit, Cell signaling, 1:3000), anti-phospho-Akt Ser473 (rabbit, Cell signaling, 1:3000), anti-phospho-Akt Thr308 (rabbit, Cell signaling, 1:2000), anti-phospho-p44/42 MAPK (ERK1/2) Thr202/204 (rabbit, Cell signaling, 1:3500), anti-p44/42 MAPK (ERK1/2) (rabbit, Cell signaling, 1:3000), anti-phospho-PLCγ1 Tyr783 (rabbit, Cell signaling, 1:2500), anti-total PLCγ1 (mouse, BD Transduction Laboratories™, 1:2000), anti-α tubulin (mouse, SIGMA, 1:40000), anti-flag (mouse, SIGMA, 1:3000), anti-myc (mouse, Cell signaling, 1:3000). Secondary antibodies: anti-mouse and anti-rabbit HRP conjugated secondary antibodies (Abcam) were used at dilution 1:5000.

3.13 Co-immunoprecipitation and pull-down assay:

The transfected HEK293 cells were lysed with either Flag buffer or Ripa buffer containing a variety of inhibitors (1x Protease inhibitor cocktail (SIGMA), 1x PhosStop (Roche), 1 mM Na_3VO_4, 10 mM NaF, 10 mg/mL leupeptin, 5 mg/mL pepstatin) and the protein supernatants were transferred into new tubes after centrifugation (13.2 krpm at 4°C for 20 min). Before any co-immunoprecipitation (co-IP) and pull-down assay, 10 µl aliquote of each sample was isolated for input. For co-IP, each protein sample (500 µl) from fully confluent cells in a well of 6-well plate was divided evenly into two tubes (250 µl each) for separate trials.

During co-IP, 0.5 µl of a specific primary antibody was added into the 250 µl protein sample, and subsequently the mixture was incubated on a rotator at 4°C for 2 hours. Then the mixture was incubated with protein G sepharose beads (pre-washed with TBS, GE Healthcare) at 4°C for 1.5 hours, followed by 3 times washes with Flag buffer (or Ripa buffer), 3 times washes with TBS and eventually were heated at 95°C for 5 min in 2x Laemmli buffer. All heated samples were examined by WB. For pull-down assays, each protein sample was incubated with 3 µg/ml EphA4-Fc-6xHis instead of the primary antibodies. Antibodies used for co-IP: anti-flag (mouse, SIGMA, F1804), anti-myc (mouse, cell signaling, 2276S).

3.14 Quantification for axonal fasciculation:

Callosal axonal fasciculation was analyzed by densitometry of GFP (for the GFP electroporated control and DKO brains, and EfnA4 electroporated DKO brains) or of dsRed (for the EfnA4/Ntrk2^{WT}, EfnA4/Ntrk2^{K571N}, EfnA4/Ntrk2^{Y515F} and EfnA4/Ntrk2^{Y816F} co-electroporated DKO brains) in the electroporated ipsilateral hemispheres. The fluorophores could label the electroporated cell bodies and the outgrown axons. Three regions of interest were selected for quantification: callosal tract (CT) in the SVZ/IZ (1' – 4', CC, Figure 4.15, 3200 µm latero-medially x 300 µm dorso-ventrally), CP (1 – 4, Ctx, Figure 4.15, 3200 µm x 600 µm) and the electroporated cell bodies (IUE, Figure 4.15). In each region, the GFP or dsRed positive areas on confocal photomicrographs were analyzed with ImageJ software: the 'Threshold' program was used to define fluorescence positive areas, the 'Analyze particles' program was used to define the minimal size for evaluation, and the 'Measure' program was used to summate areal values. The areal values of all fluorescence positive particles in CT or CP were then normalized to the areal values of electroporated cell bodies. The resultant data represent fasciculated (in CT) and defasciculated (in CP) callosal axons, respectively. For each embryo, three sections at similar coronal planes were quantified and the averaged value denoted axonal (de)fasciculation. In each IUE situation, three embryos were selected for quantification (except for EfnA4 and EfnA4/Ntrk2^{Y816F} IUE: only 2 embryos were quantified by the moment of dissertation completion) to achieve statistical data (n=3).

3.15 Statistics:

The relative quantitative data of WB and the ratios (indexes) of axonal (de)fasciculation were analyzed statistically with paired two-tailed Student's t-test for their significance using Excel. The relative quantitative data of luciferase assays were analyzed with paired one-tailed t-test. The charts were made with GraphPad Prism software and presented as mean ± standard error. Probability assignment: $p > 0.05$ (not significant, ns), $0.01 < p < 0.05$ (*), $0.001 < p < 0.01$ (**) and $p < 0.001$ (***).

4. Results:

Part I: NeuroD2/6 regulate corpus callosum formation via EfnA4

4.1 Restoration of NeuroD2 or NeuroD6 in DKO embryos rescues callosal agenesis

We have previously shown that callosal axogenesis depends on NeuroD2/6 expression in mice[50]. With the aim to understand the regulation of callosal axon guidance in the ipsilateral neocortex, my first question is whether NeuroD2/6 serve primarily cell intrinsic functions in callosally projecting neurons (CPNs). I used *in utero* electroporation (IUE) to restore NeuroD2 or NeuroD6 expression only in a small subset of postmitotic neurons in the developing cerebral cortex of NeuroD2/6 double deficient (DKO) embryos. To avoid possible artifacts caused by over-expression of NeuroD2/6 in apical progenitors (APs), a Cre-activatable expression plasmid was generated by inserting a loxP site-flanked 'stop' cassette between pCAG promoter and the coding sequences of NeuroD2/6 (A, Figure 4.1). The 'stop' cassette consists of the mCherry (red) open reading frame (ORF) and a transcriptional stop signal. NeuroD2/6 are bicistronically co-expressed with GFP using an internal ribosomal entry site. IUE of such constructs into the cerebral cortex of NeuroD6-Cre carrying embryos restricted mCherry expression to progenitors while NeuroD2/6 and GFP were exclusively expressed in postmitotic neurons (B and C, Figure 4.1).

In order to analyze NeuroD2/6 functions in long-range axonal navigation *in vivo*, E13.5 embryos were electroporated with plasmids expressing GFP alone or NeuroD2/GFP. NeuroD6/GFP was also electroporated at E12.5. Brains were fixed at E18.5 and axons of electroporated neurons were visualized using immunofluorescent (IF) staining for GFP. IF staining for the cell adhesion molecule L1 was used to visualize the most remaining non-electroporated axons. In control brains, GFP positive axons formed a fasciculate callosal axon bundle just below the large number of L1-positive ipsilaterally projecting fibers. This callosal tract (CT) turned ventrally around the cingulate cortex across the midline to reach the contralateral hemisphere (A, Figure 4.1). In DKO brains, GFP labelled axons defasciculated, grew astray into the ipsilaterally projecting regions and got lost prior to midline interaction (B, Figure 4.1). L1 staining also showed that DKO mice possessed far less callosally projecting axons in the SVZ/IZ and separated midline (E and D, Figure 4.1). These data were in line with our previous finding that CC development was severely impeded in DKO mice. Interestingly, *in vivo* gain-of-function

of either NeuroD2 at E13.5 or NeuroD6 at E12.5 in DKO embryos was sufficient to establish fasciculate callosal axon growth towards the midline (F and G, Figure 4.1). Many axons followed the stereotypical trajectory and migrated into the contralateral hemisphere. This is in agreement with our assumption that NeuroD2 and NeuroD6 share redundant cell intrinsic functionality in CC formation.
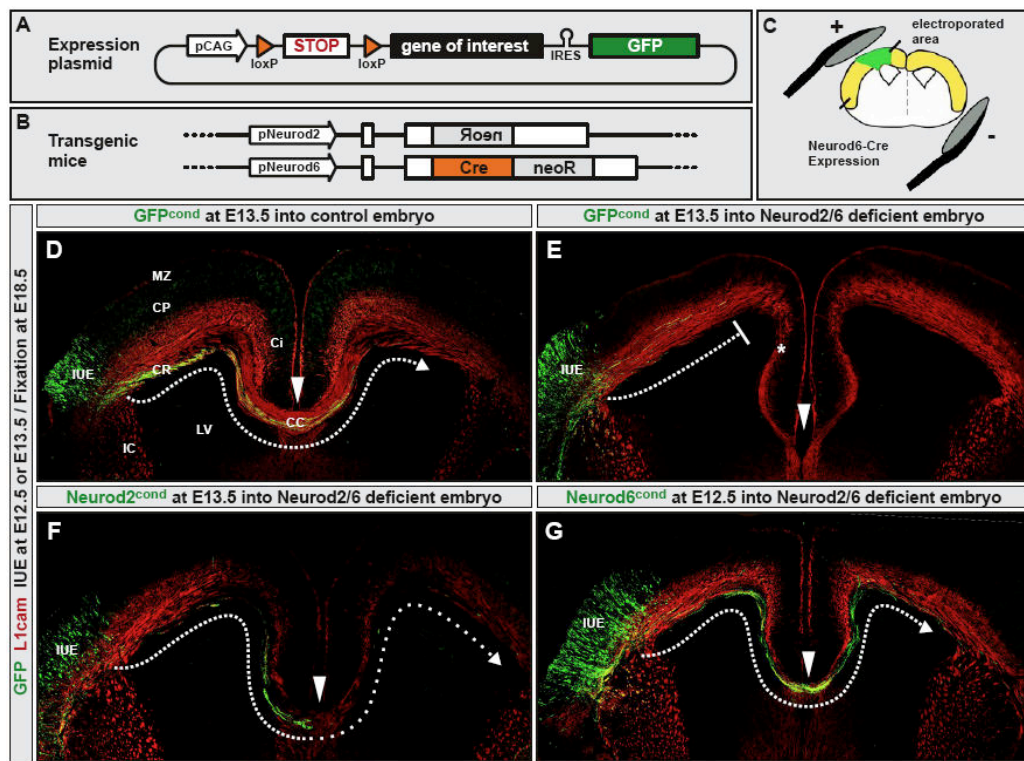
Figure 4.1: Restoration of NeuroD2/6 expression in the DKO brains by IUE

(A) Vector map for Cre activatable electroporated expression constructs. pCAG: strong synthetic promoter consisting of cytomegalovirus early enhancer element, chicken beta-actin promoter (including the first exon and intron) and rabbit beta-globulin splice acceptor. STOP: mCherry coding sequence including stop codon and SV40 late poly-A signal. IRES: encephalomyocarditis virus internal ribosome entry site. GFP: green fluorescent protein. **(B)** Strategy for generating NeuroD2/6 double deficient (DKO) mice: the coding sequence of NeuroD2 was replaced with a reversely oriented neomycin resistance expression cassette (Neurod2-Null). The coding sequence of NeuroD6 was replaced with Cre recombinase (NeuroD6-Cre). **(C)** *In utero* electroporation of the Cre-activatable expression vector into neocortex of NeuroD6-Cre mice restricted gene expression to postmitotic pyramidal neurons. **(D–E)** Immunofluorescent (IF) staining for GFP (green) and L1 (red) on coronal sections of E18.5 control (D) and NeuroD2/6 DKO (E) brains electroporated with Cre-activatable GFP expression plasmids. **(F–G)** IF staining for GFP and L1 on coronal sections of E18.5 NeuroD2/6 DKO brains electroporated with Cre-activatable NeuroD2 (at E13.5, F) or NeuroD6 (at E12.5, G). IUE: electroporated area. MZ: marginal zone; CP: cortical plate; CR: coronal radiation; IC: internal capsule; LV: lateral ventricle; Ci: cingulate cortex; CC: corpus callosum.

4.2 Neuron identities and lamination are grossly normal in NeuroD2/6 DKO cortex
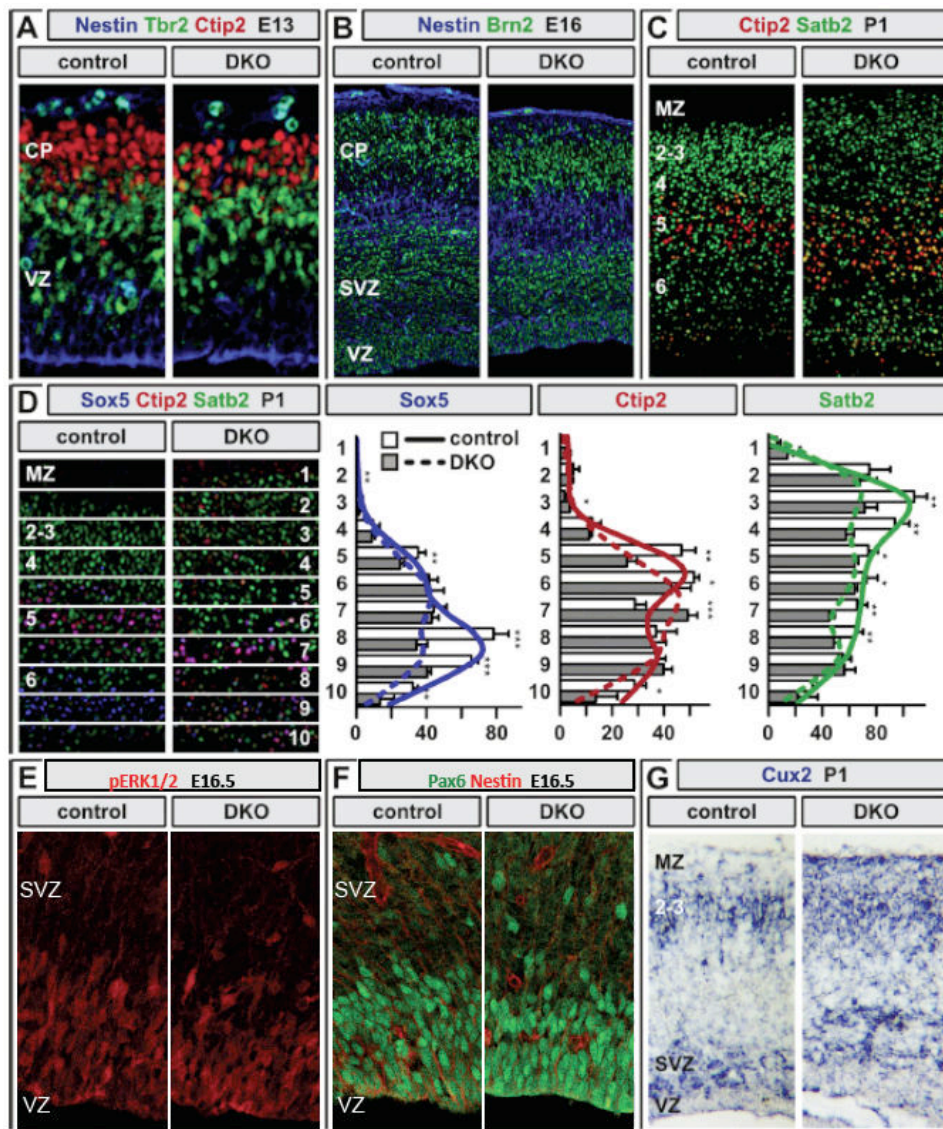
Figure 4.2: Neocortical cell production and lamination were only mildly disturbed in DKO brains
(A) IF staining for Nestin (blue), Tbr2 (green) and Ctip2 (red) on E13 brain sections. **(B)** IF staining for Nestin (blue) and Brn2 (green) on E16 brain sections. **(C)** IF staining for Ctip2 (red) and SatB2 (green) on P1 brain sections. **(D)** IF staining for Sox5 (blue), Ctip2 (red) and SatB2 (green) on P1 brain sections. The neocortex was divided into 10 equally sized horizontal bins, in which the numbers of immuno-positive cells were blindly quantified for each bin (collaborated with my colleague) and presented by bar and flow charts. **(E and F)** IF staining for phosphorylated ERK1/2 (E), Pax6 (green) and Nestin (red) (F) on E16.5 brain sections. **(G)** *In situ* hybridization (ISH) for Cux2 on P1 brain sections. All IF staining and ISH were performed on littermate control and DKO brains. VZ: ventricular zone; SVZ: subventricular zone.

As development of the neocortical architecture could directly influence cortical wiring patterns, we asked if CC agenesis in DKO brains might simply be due to abnormalities

in the differentiation and migration of distinct pyramidal neuron subpopulations. I performed IF staining for various cell subtype markers at different stages of cortex development in order to estimate to what extend the cortical architecture was abnormal in DKO mice. Pax6 and phosphorylated ERK1/2 (pERK1/2) are normally expressed in VZ during corticogenesis and play important roles in regulating neurogenic activity of apical precursors[110–113]. At E16.5, I could not identify significant alterations of Pax6 or pERK1/2 signals in DKO brains (E and F, Figure 4.2). I concluded that the inactivation of NeuroD2/6 did not severely affected apical precursor cells. Co-staining for Nestin, Tbr2 and Ctip2 at E13 confirmed that RG cells, BP and DL neurons were produced and positioned properly during early cortical neurogenesis (A, Figure 4.2). Brn2 is an essential regulator for development of neocortical UL neurons[15]. Immuno-staining for Brn2 on E16 and E18.5 brain sections indicated basically normal production of UL neurons in DKO neocortex (B, Figure 4.2 and E – E', Figure 4.3). SatB2, a marker for CPN mainly situated in UL, was also positively stained in P1 DKO neocortex (C, Figure 4.2). Furthermore, normal expression for Cux2 was detectable by ISH in P1 DKO brains, which also added to the conclusion that the majority of UL neurons differentiated and migrated properly in the absence of NeuroD2/6 (E and G, Figure 4.2).

IF staining for SatB2, Ctip2 and Sox5 at P1 demonstrated that the lamination of UL and DL neurons was grossly normal. Nevertheless, the less compacted distribution of SatB2-positive (SatB2+) neurons implied subtle defects in UL neuron development in DKO (D, Figure 4.2). The quantification of SatB2+, Ctip2+ and Sox5+ neurons at P1 stage revealed a moderate reduction of Satb2+ cells [control: 673 ± 60; DKO: 520 ± 40 cells per radial unit; p = 0.074, ns] and of Sox5+ DL cells [control: 318 ± 30; DKO: 216 ± 18; p = 0.026, *], while the number of Ctip2+ cells [control: 258 ± 21; DKO: 237 ± 16; p = 0.57, ns] was hardly altered (D, Figure 4.2).

4.3 NeuroD2/6 regulate gene expression in upper layer neurons

As the expression patterns of Brn2 and SatB2 (two genes essentially required for UL neuron development) were not severely disturbed, I wondered if NeuroD2/6 were genuinely modulating gene expression in UL neurons. I performed ISH for two CPN specific genes, pleiotrophin (Ptn) and LIM-And-Calponin-Homology-Domains 1 (Limch1)[114]. Both were notably down-regulated in E18.5 DKO cortex (A – A' and B – B',

Figure 4.3). Expression for Cux1, a widely employed UL neuron marker, was also reduced in DKO as shown by ISH (C – C', Figure 4.3) and IF staining (D – D', Figure 4.3). Most Brn2+ UL neurons did co-express Cux1 in controls, however, Brn2+ cells in DKO brains rarely showed Cux1 staining (D – D' to F – F', Figure 4.3). Furthermore, Cux1 expression could be specifically restored in cortical neurons by electroporation of NeuroD2 (G – G', Figure 4.3). All these results suggested that NeuroD2/6 be critical regulators for patterning gene expression in UL neurons.
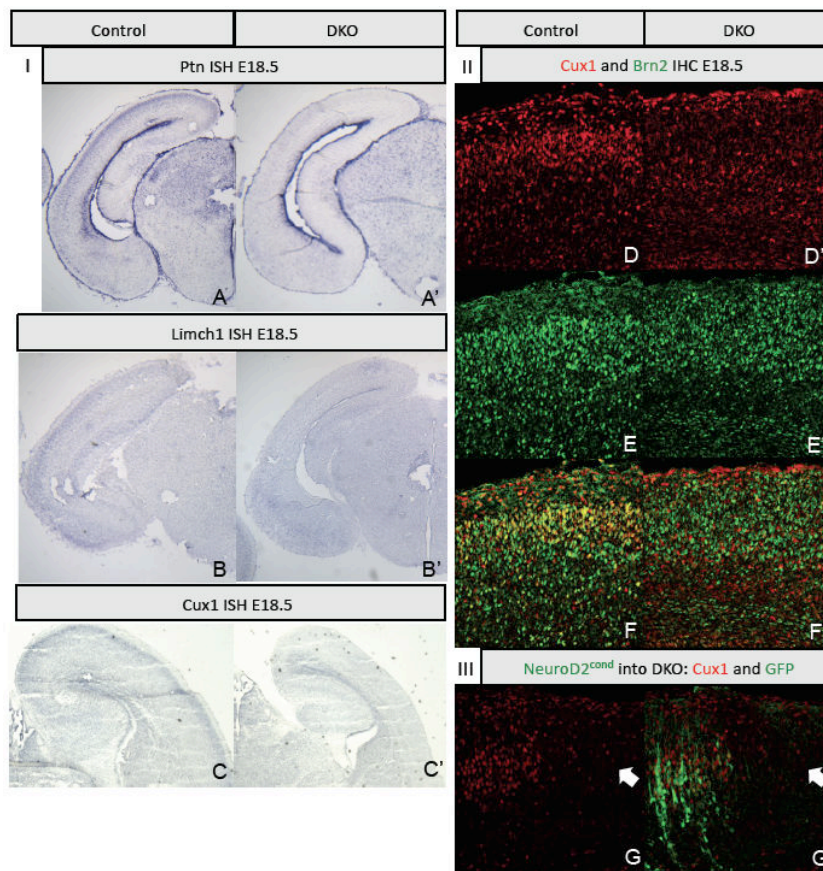
Figure 4.3: Gene expression patterns in UL neurons were disrupted in NeuroD2/6 DKO cortex
(I) ISH for Limch1 **(A – A')**, Ptn **(B – B')** and Cux1 **(C – C')**. **(II)** IF staining for Cux1 (red, **D – D'**), Brn2 (green, **E – E'**) and the overlay **(F – F')**. All ISH and IF staining in (I) and (II) were performed on E18.5 littermate control and DKO brains. **(III)** Cux1 expression was restored in NeuroD2 electroporated cells in DKO brains. IF staining for GFP (NeuroD2, green) and Cux1 (red) **(G – G')**. Arrowheads indicate the Cux1 negative area in DKO. IUE was performed at E13.5 and the brain was fixed at E18.5.

4.4 Ephrin ligands are down-regulated in NeuroD2/6 DKO cortical plate

As UL neuron production and lamination in the DKO neocortex were relatively normal, I

hypothesized that CC agenesis was a consequence of failed axon guidance and not due to modified neuronal identities. Based on the data obtained in ISH-based screening project (details described in section 4.28), I focused primarily on axonal guidance cues, such as the Eph-ephrin superfamily of membrane associated signaling molecules. I first analyzed expression patterns by ISH for A and B subclass ephrin ligands at E16.5, the stage when callosal axons normally approach the cortical midline. EfnA1 and EfnA3 presented marginally decreased expression in DKO compared with the littermate control (A – A' to C – C', Figure 4.4). EfnB1 was also gently down-regulated in cortical postmitotic compartment (F – F', Figure 4.4). Most strikingly, EfnA4 displayed substantial down-regulation in migrating UL neurons at E16.5 (D – D', Figure 4.4) but unaltered expression pattern in the VZ. Additional evidence was attained by ISH at E18.5 that EfnA4 expression, as normally follows a high lateral to low medial gradient in UL neurons, was completely absent in the lateral cortex of DKO mice (B – B', Figure 4.13). Other ephrins did not show obviously changed expression levels (Figure 4.4).

To investigate whether EfnA4 was directly regulated by NeuroD2/6, I combined *in silico* analysis of the EfnA4 promoter region and an *in vitro* luciferase assay. There were 21 potential E-box motifs (CANNTG) clustered in six genomic fragments within 5 kbp upstream of the EfnA4 transcription initiation site: EC1 (4 motifs in 400 bp), EC2 (3 motifs in 400 bp), EC3 (3 motifs in 324 bp), EC4 (5 motifs in 542 bp), EC5 (2 motifs in 635 bp) and EC6 (4 motifs in 625 bp). To test each element, the chosen fragments were cloned in front of a luciferase expression cassette. These constructs were subsequently co-transfected with either a NeuroD6 expressing plasmid or an empty backbone plasmid (pCAG-GFP) into HEK293 cells. An alkaline phosphatase (AP) expressing plasmid was also co-transfected in every sample for normalization. Triplicate sampling and duplicate measurements were applied to each experimental line. Relative luciferase values were calculated by comparison of data in NeuroD6 experimental lines to empty vector lines. NeuroD6 expression promoted luciferase expression up to 4.52 folds (p=0.00613, **) in statistically consistent fashion via EC1, which is closest to EfnA4 transcription initiation site. NeuroD6 binding to EC2, EC4 and EC6 facilitated mild luciferase up-regulation as well [EC2: 1.53 folds, p = 0.151, ns; EC4: 1.34 folds, p = 0.00781, **; EC6: 1.81 folds, p = 0.083, ns] (I, Figure 4.4). Summarized from ISH and luciferase assay, EfnA4 can be regarded as a direct downstream target of NeuroD2/6.
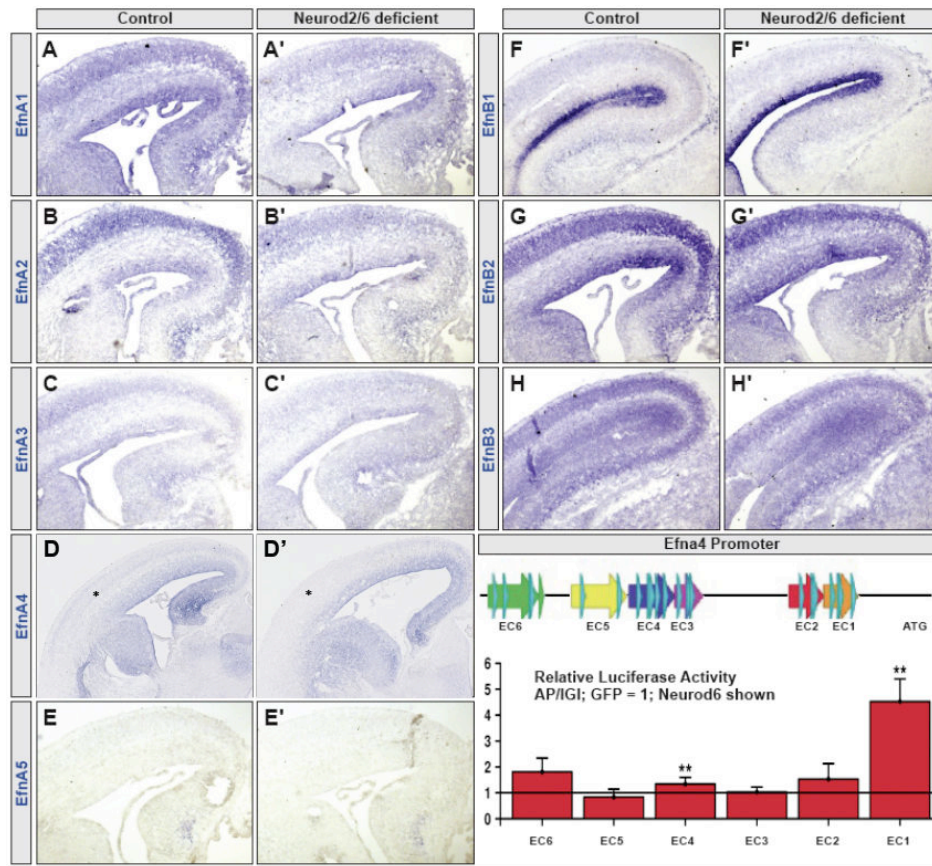
Figure 4.4: EfnA4 is directly regulated by NeuroD2/6

(A – A' to E – E') ISH for EfnA1 – EfnA5. **(F – F' to H – H')** ISH for EfnB1 – EfnB3. All ISH were performed on E16.5 littermate control and DKO brain sections. **(I)** Design and results of luciferase assay for EfnA4's promoter region. EC1 – EC6 denote six E-box motif clusters in the 5 kbp genomic sequence upstream of the transcription initiation site. Cloned DNA fragments for E-box clusters vary in length from 324 to 635 bp. A blue arrow denotes a potential E-box motif. EC1 is closest to EfnA4 transcriptional start. The relative quantification was achieved by normalizing the values of NeuroD6 experimental line to those of empty vector line (baseline set to 1).

4.5 Restoration of EfnA4, but not of the other ephrins, rescues callosal agenesis

As some ephrins had been reported necessary for axon guidance in callosal and other projection tracts[54,62,70], I wondered if the down-regulation of ephrin ligands in the DKO neocortex might be a cause of CC agenesis. Gain-of-function experiments were performed to address this issue. The ORF of EfnA4 was subcloned into a bicistronic GFP expression construct under control of the pCAG-promoter and was subsequently electroporated into the lateral ventricle of E13.5 DKO embryos. IF staining for GFP on

E18.5 tissue showed that the restoration of EfnA4 expression was sufficient to bundle most callosal fibers in a single fascicle in the IZ and to guide their growth ventrally in the cingulate cortex towards the cortical midline (A, Figure 4.5). The capacity of EfnA4 to rescue axon growth in the ipsilateral cortex of DKO embryos suggests strongly that EfnA4 be critical for callosal axonal fasciculation and guidance. The expression levels of EfnA1, EfnA3 and EfnB1 were also reduced in DKO as well, but electroporation of any of them could not significantly improve the callosal defects in DKO embryos (B – D, Figure 4.5). Growth of the CT did always stall in the ipsilateral cingulate cortex. Interestingly, over-expression of EfnA1 and EfnB1 induced radial columnar aggregation of neocortical pyramidal neurons, an effect that was barely seen when EfnA3 or EfnA4 was over-expressed.
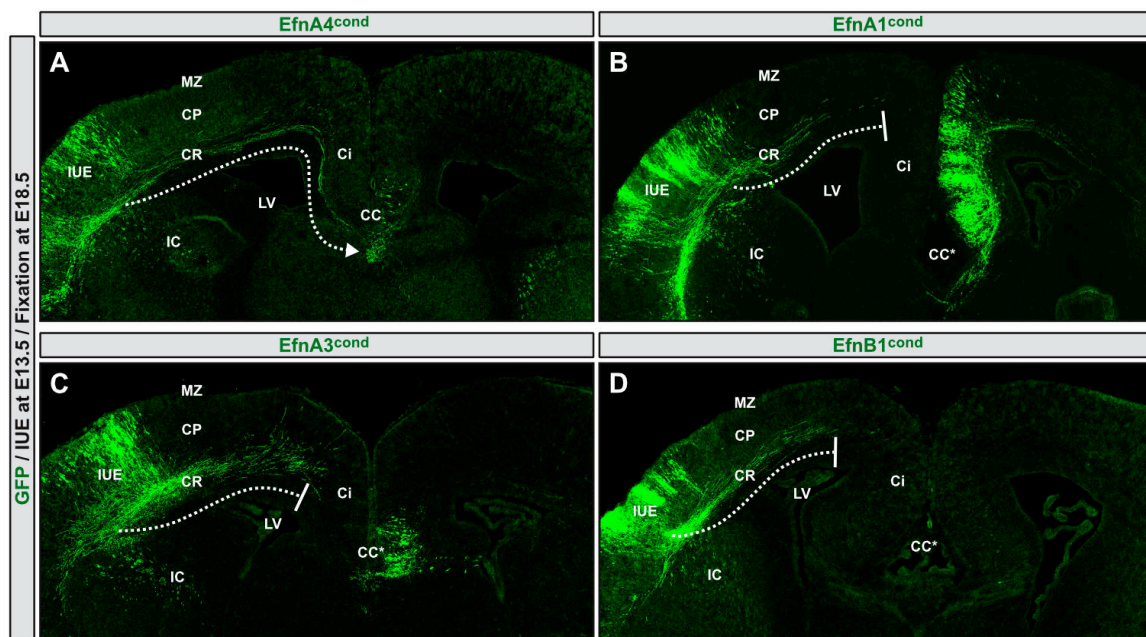
Figure 4.5: Callosal axon growth can be rescued by EfnA4 expression, but not any other ephrins
(A) Electroporated EfnA4 at E13.5 resulted in fasciculate callosal axonal growth and guidance towards the cortical midline (n=3). **(B - D)** Over-expression of EfnA1 (B, n=2), EfnA3 (C, n=3) or EfnB1 (D, n=2) at E13.5 failed to rescue CC agenesis in DKO embryonic brains.

4.6 Over-expression of EphA receptors does not rescue callosal agenesis in DKO

Based on the EfnA4 mediated rescue and the necessity of ligand-receptor interplay in Eph-ephrin signaling, I turned to investigate the receptor axis as a matter of course.

Since A subclass ligands generally interact with A subclass receptors, I did ISH for the members of EphA family that had previously been shown to be involved in CC formation. EphA3, which was shown weakly but specifically expressed in layer II CPNs[114], was not detectable in DKO neocortex (B – B', Figure 4.6). EphA4 was also slightly down-regulated (C – C', Figure 4.6), while EphA5 maintained similar expression level in the neocortex of DKO with control mice (D – D', Figure 4.6). Unexpectedly, EphA2 was significantly up-regulated in the progenitor zone and CP of DKO brains, but not in the IZ (A – A', Figure 4.6), where callosally projecting axons normally grow. EphA3 or EphA4 expressing constructs were co-electroporated with pCAG-GFP plasmids at E13.5 and the brains were analyzed at E18.5. IF staining for GFP showed that neither of them was able to rescue CC agenesis. The majority of GFP labeled fibers did not follow the typical callosal trajectory and axonal growth was still stuck before midline interaction (E and F, Figure 4.6).
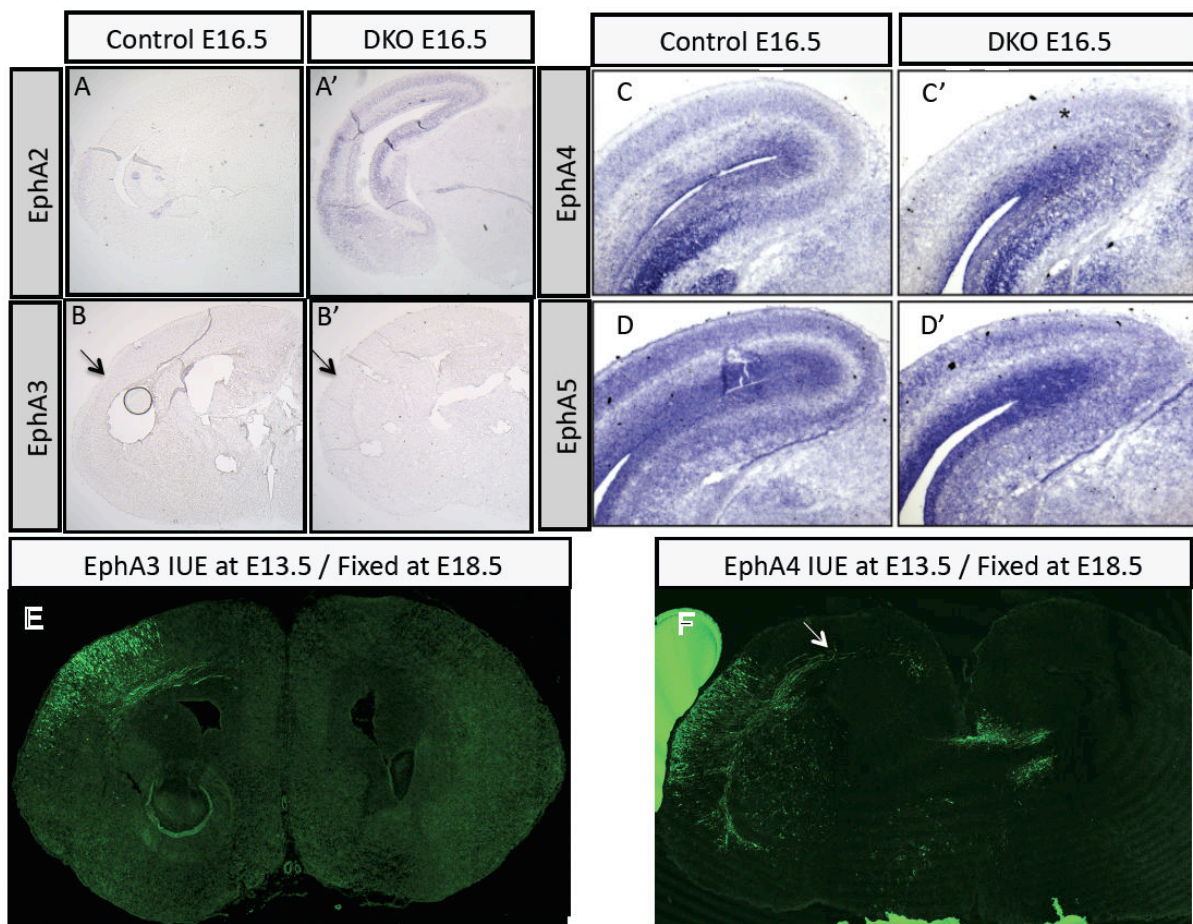
Figure 4.6: Expression and gain-of-function analysis for EphA receptors
(A – A' to D – D') ISH for EphA2, EphA3, EphA4 and EphA5, respectively, on E16.5 littermate control

and DKO brains. **(E and F)** Electroporation of either EphA3 (E, n=2) or EphA4 (F, n=3) at E13.5 could not rescue axonal fasciculation and growth.

4.7 A secreted variant of EfnA4 does not rescue callosal agenesis in DKO mice
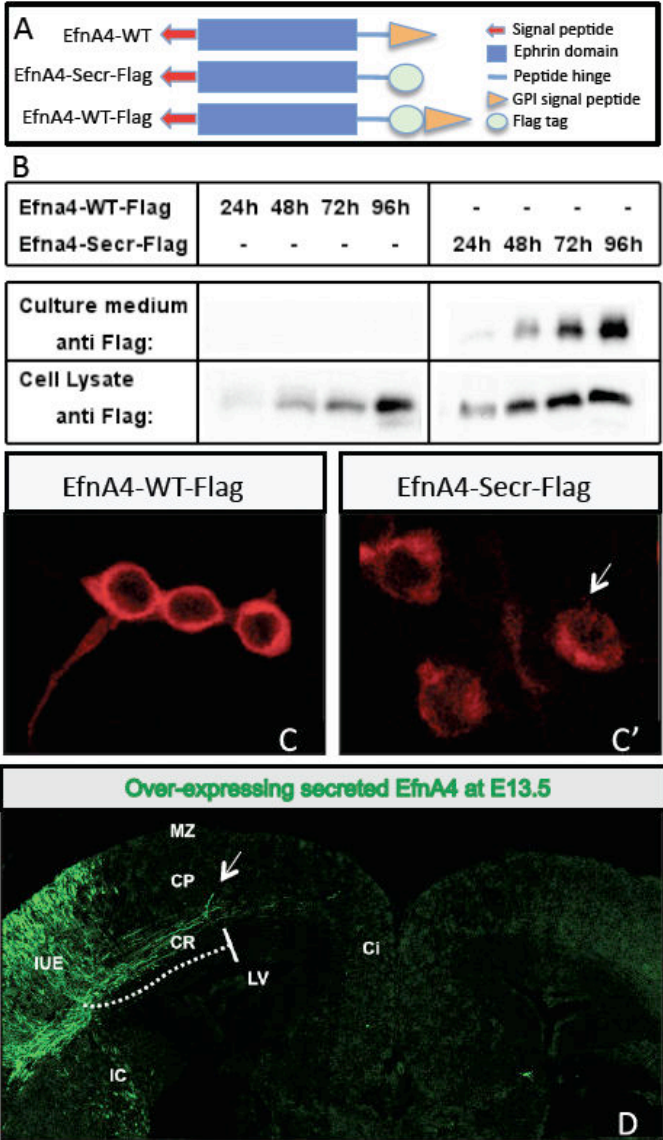
Figure 4.7: Over-expression of secreted EfnA4 variant can not rescue CC agenesis in DKO embryos

(A) Schematic illustration of EfnA4, flag-tagged wild type (WT) EfnA4 (EfnA4-WT-Flag) and secreted EfnA4 variant (EfnA4-Secr-Flag). **(B)** Verification of EfnA4-WT-Flag and EfnA4-Secr-Flag by WB. **(C – C')** Verification of EfnA4-WT-Flag and EfnA4-Secr-Flag by immunocytochemistry (ICC). **(D)** Electroporation of EfnA4-Secr-Flag at E13.5 failed to rescue CC agenesis in DKO embryos (n=3).

Based on the finding that EfnA4 had a selective function in callosal axogenesis, I asked whether the involved mechanism was majorly cell autonomous to CPNs, or alternatively relied on exogenous signals. Class A ephrins are GPI-anchored proteins, whose premature peptide chains possess GPI signal peptides containing the ω residues, the GPI-anchor transamidation sites. In human, the ω residue of EfnA4 (S^{170}) has been previously predicted[60]. The amino acid (AA) sequences in the C terminal regions of the human and mouse EfnA4 proteins are evolutionarily conserved, and the ω residue in mouse EfnA4 could thus be speculated as its S^{175}. For more convenient *in vitro* and *in vivo* studies, flag tag (DYKDDDDK) was artificially conjugated with different versions of EfnA4, which allowed direct detection of these proteins in the absence of a specific EfnA4 antibody. The tagged secreted variant of EfnA4 (EfnA4-Secr-Flag) was generated by replacing the GPI signal peptide with flag tag, and the tagged WT EfnA4 (EfnA4-WT-Flag) was generated by inserting flag tag between the ephrin domain and the GPI signal peptide (between V^{169} and G^{170}) to avoid the cleavage of the tag during protein maturation (A, Figure 4.7). The C-terminal AA sequences of the indicated EfnA4 versions are below:

Human WT EfnA4: SAHPVGSPGE ***S***^{170}GTSGWRGGDTPSPLCLLLLLLLLILRLLRIL

Mouse WT EfnA4: SAHPVGSPGE ***S***^{175}GTSGWRGGHAPSPLCLLLLLLLPILRLLRVL

Mouse EfnA4-Secr-Flag: SAHPVGSPGE ***DYKDDDDK***

Mouse EfnA4-WT-Flag: SAHPV ***DYKDDDDK*** GSPGE***S***^{170}GTSGWRGGHAPSPLCLL…

To test if the different variants of EfnA4 functioned as expected, EfnA4-WT-Flag and EfnA4-Secr-Flag constructs (driven by pCAG promoter) were transfected in HEK293 cells in separate wells and cultured for 24, 48, 72 and 96 hours. At each time point, culture media and cell lysates were collected for WB analysis using flag primary antibody. There was visible accumulation of flag-tagged proteins in the media as well as cell lysates with increasing culture duration when EfnA4-Secr-Flag constructs were transfected. In contrast, flag-tagged proteins were never detectable in the media where EfnA4-WT-Flag construct transfected cells were cultured, even though those cells were also producing increasing amounts of flag-tagged WT EfnA4 (B, Figure 4.7). On the other hand, I also performed immunocytochemistry (ICC) experiments to examine

subcellular localization of EfnA4-WT-Flag and EfnA4-Secr-Flag. IF staining for flag tag clearly depicted that WT EfnA4, albeit tagged, was enriched at the cell surfaces (C, Figure 4.7), however, EfnA4-Secr-Flag proteins were dispersedly distributed in the cytoplasm and could be found in the vesicles to be released (C', Figure 4.7). Taken WB and ICC data together, EfnA4-Secr-Flag was clearly not membrane associated, but instead secreted. I cloned the EfnA4-Secr-Flag into a pCAG-promoter expression vector (with bicistronic GFP) and over-expressed the construct in E13.5 DKO embryos. I found that the secreted EfnA4 variant was not able to properly guide callosal axons (D, Figure 4.7), suggesting that EfnA4 functioned cell autonomously to callosal fibers *in vivo*.

4.8 Expression patterns of potential EfnA4 co-receptors
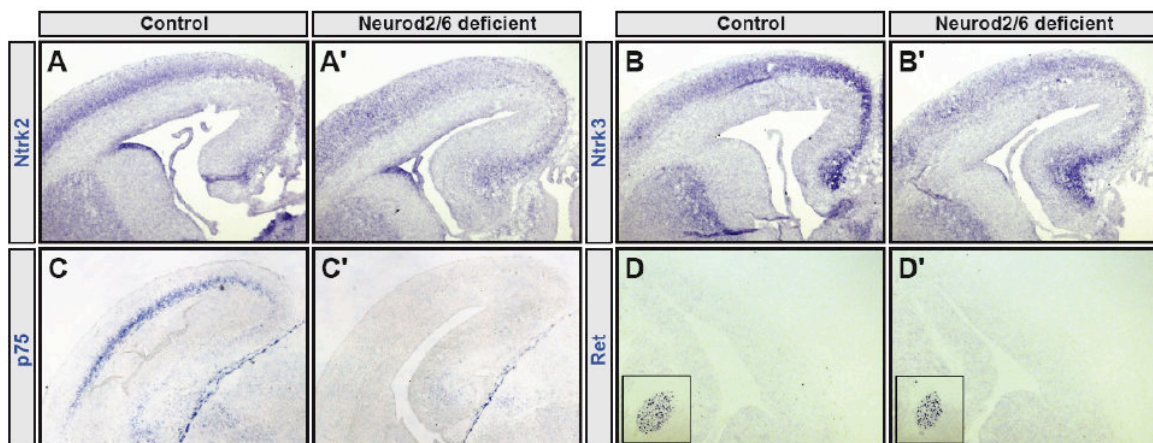
Figure 4.8: Expression patterns for potential EfnA4 co-receptors in the cerebral cortex
(A – A' to C – C') ISH for Ntrk2 (A – A'), Ntrk3 (B – B') and p75NTR (C – C') on E16.5 littermate control and DKO brain sections. **(D – D')** ISH for Ret on E14.5 littermate control and DKO brain sections.

Class A ephrins usually mediate reverse signaling with the help of other membrane bound co-receptors. Three groups of co-receptors have been reported in different tissues so far: p75NTR, Ret and Ntrks[54]. Expression of the potential co-receptors in both control and DKO neocortex is a prerequisite for EfnA4 mediated axon guidance. To find out which molecule might be EfnA4's co-receptor in CC formation, I performed ISH experiments for p75NTR, Ret, Ntrk2 and Ntrk3 on the cryo-sections of littermate control and DKO brains. It was found that Ret expression was barely detectable by ISH in

developing neocortex of E14.5 control and DKO embryos (D – D', Figure 4.8). The expression of p75NTR in control DL neurons was entirely missing in the E16.5 DKO brains (C – C', Figure 4.8). Ret and p75NTR could thereby not be EfnA4's co-receptor in the scenario of callosal axon growth and were excluded from further analysis.

Ntrk2 and Ntrk3 were both strongly expressed in cortical pyramidal neurons at comparable expression levels in control and DKO brains (A – A' and B – B', Figure 4.8). I was also trying my best to clone Ntrk1 by reverse transcriptional PCR with three pairs of primers targeting different regions of Ntrk1 transcript from a pool of E16.5 cerebral complementary DNA, from which hundreds of fragments were once subcloned. None of these trials succeeded (data not shown). I thus supposed that Ntrk1 is rarely expressed in the E16.5 neocortex, consistent with the previous report that Ntrk1 was mainly expressed in peripheral nerve system[91]. According to the expression patterns, Ntrk2 and Ntrk3 might be potential co-receptors to mediate EfnA4 reverse signaling in callosal projection axons.

4.9 Generation and verification of dominant negative Ntrk2 and Ntrk3

For following functional investigation of Ntrks, I generated pCAG expression constructs for full-length Ntrk2 and Ntrk3 (Ntrk2^{WT} and Ntrk3^{WT}) and their dominant negative variants (kinase-dead) carrying a mutation to abolish the kinase activity. In case of Ntrk2, the lysine at position 571 (K571) was mutated into an asparagine[88] (Ntrk2^{K571N}, according to the latest genome browser). In case of Ntrk3, the homologous lysine (K572) was also mutated into an asparagine (Ntrk3^{K572N}). To verify the invalidation of kinase activity, either Ntrk2/3^{WT} or their corresponding kinase-dead variants were transfected to independent wells of HEK293 cells, which were then incubated for 24 hours in serum free media. Subsequently, protein samples were collected immediately after 5 min stimulation with or without appropriate neurotrophins (final concentration: 25 ng/ml BDNF in case of Ntrk2 and 50 ng/ml NT-3 in case of Ntrk3). Cell lysates from GFP transfected cells were also collected as references. Equal amount of isolated proteins from each sample (40 μg) were subject to WB detection using the primary antibody of pERK1/2, the shared downstream responsive effectors of Ntrk2 and Ntrk3.

The transfection of Ntrk2^{WT} led to strongly up-regulated phosphorylation of ERK1/2 (lane 3 and 4, A, Figure 4.9) when BDNF was applied. However, pERK1/2 activity in case of Ntrk2^{K571N} transfection (lane 5 and 6, A, Figure 4.9) was comparable to that of GFP-alone transfection (lane 1 and 2, A, Figure 4.9), regardless of BDNF application. Similarly, Ntrk3^{K572N} failed to augment the phosphorylation of ERK1/2 in contrast to Ntrk3^{WT}, regardless of NT-3 application (B, Figure 4.9). I thus concluded that the targeted mutations had successfully destroyed kinase activities of Ntrk2 and Ntrk3. Besides, I realized that pERK1/2 activities were also increased in the cases of Ntrk2/3^{WT} transfection without neurotrophin treatment, suggesting that full-length Ntrk2/3^{WT} could be moderately activated in basal DMEM media.
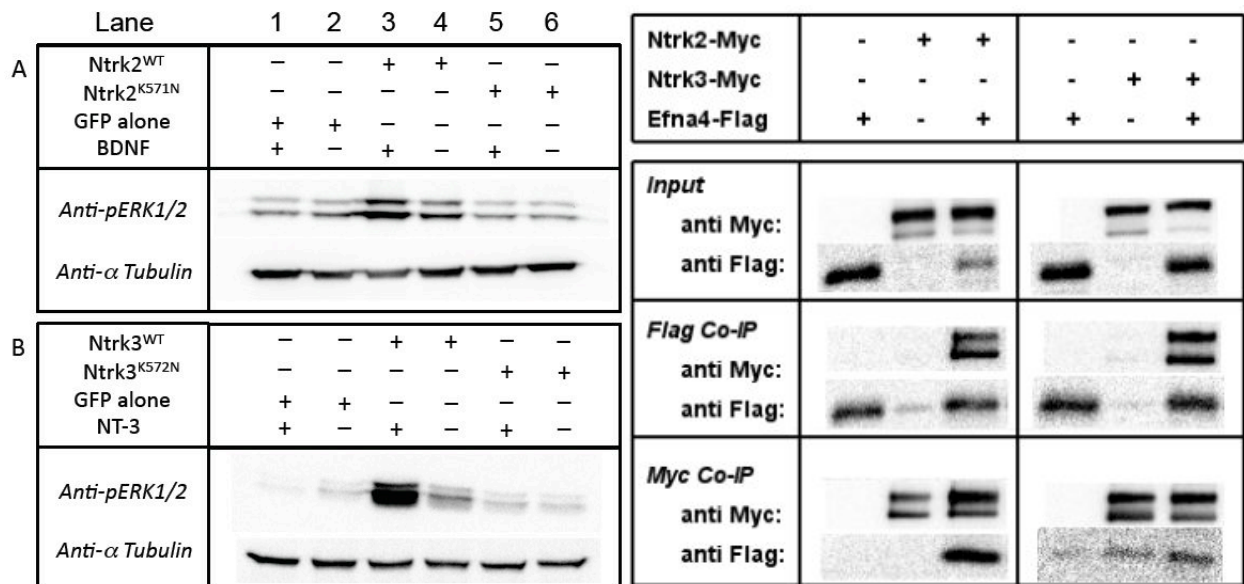
Figure 4.9 (left): Verification of dominant negative Ntrk2 and Ntrk3

(A – B) Ntrk2 ^{WT} and Ntrk3^{WT} were capable of phosphorylating ERK1/2, but Ntrk2^{K571N} (A) and Ntrk3^{K572N} (B) had lost their kinase activity. Equal quantity of proteins were loaded in each lane of WB, as was indicated by α tubulin detection.

Figure 4.10 (right): EfnA4 can be co-immunoprecipitated with Ntrk2 and Ntrk3 *in vitro*.

Immunoprecipitation using primary antibody against flag tag could precipitate myc-tagged Ntrks in the HEK293 cells co-transfected with EfnA4-WT-Flag and myc-tagged Ntrk2 ^{WT} or Ntrk3^{WT}, and verse versa.

4.10 EfnA4 interacts with Ntrk receptors *in vitro*

Chicken EfnA5 and EfnA6 can interact with all three Ntrks in cultured retinal cells[115,116],

but if mouse EfnA4 interacts with Ntrks still remains uncertain. To testify the interplay, I co-transfected EfnA4-WT-Flag with either C-terminal myc-tagged Ntrk2^{WT} or Ntrk3^{WT} in HEK293 cells and maintained the culture for 24 hours in standard DMEM media. The collected protein samples in Flag buffer were divided evenly into two parts: one part was used to co-IP myc epitope with flag primary antibody, and the other part was used to co-IP flag epitope with myc primary antibody. In both cases, EfnA4-WT-Flag and myc-tagged Ntrk2/3^{WT} could co-IP each other (A, Figure 4.10), meaning that EfnA4 could interact with both of Ntrk2^{WT} and Ntrk3^{WT} *in vitro*. The same experiments were replicated in Ripa buffer, a more stringent buffer, and showed the same results (data not shown).

4.11 Function of EfnA4 in callosal axogenesis depends on Ntrk2, but not Ntrk3
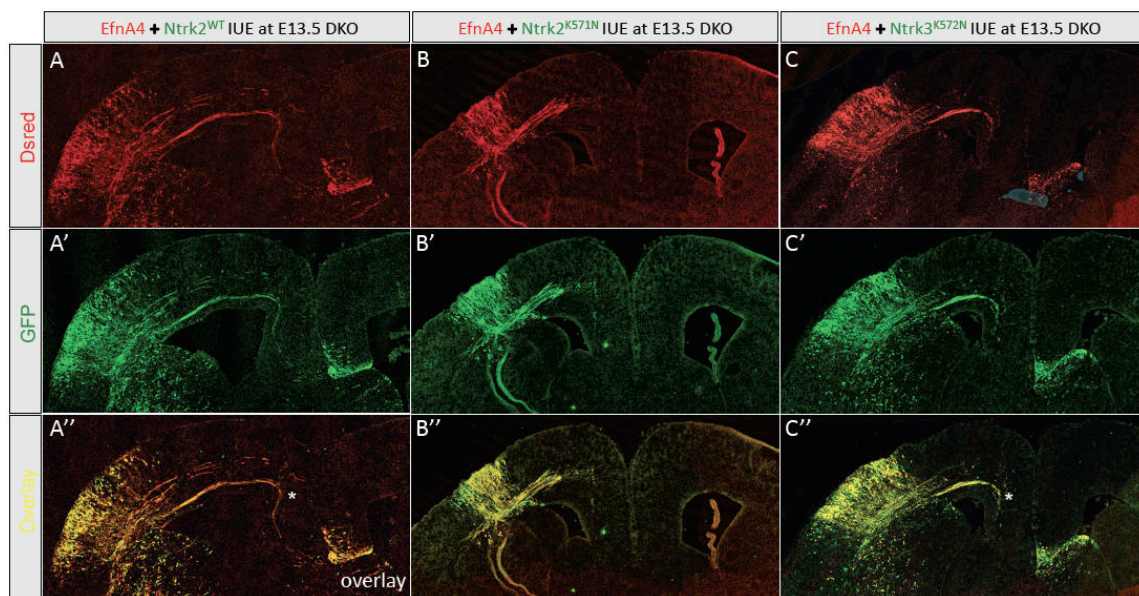
Figure 4.11: The EfnA4 mediated rescue is specifically disrupted by co-IUE with Ntrk2^{K571N}

IF staining for dsRed **(A – C)** and GFP **(A' – C')** on the sections of E18.5 DKO brains co-electroporated with EfnA4/Ntrk2^{WT} (A – A'', n=5), EfnA4/Ntrk2^{K571N} (B – B'', n=6) and EfnA4/Ntrk3^{K572N} (C – C'', n=3). DsRed: EfnA4 (A – C); GFP: Ntrk2^{WT} (A'), Ntrk2^{K571N} (B') and Ntrk3^{K572N} (C'), and the overlays **(A'' – C'')**.

To deepen our understanding of EfnA4/Ntrk interactions in the scenario of CC formation, I implemented a functional assay to examine Ntrks mediated effects *in vivo*. EfnA4 ORF was cloned in a vector (pCRC) under control of pCAG promoter and bicistronically expressing dsRed, which had been utilized in cortical electroporation

previously[109]. Ntrk2/3^{WT} and the dominant negative variants (Ntrk2^{K571N} and Ntrk3^{K572N}) were cloned in above-mentioned pCAG-GFP vector so that neurons and axons carrying electroporated EfnA4 or Ntrk2/3 variants could be labelled by distinguishable colours. I co-electroporated EfnA4 together with either Ntrk2^{WT} or Ntrk2^{K571N} at concentration ratio: 1:1 (1 µg/µl each) in E13.5 DKO embryos. IF staining for dsRed and GFP at E18.5 showed that most EfnA4/Ntrk2^{WT} double positive callosal axons in the DKO bundled compactly and travelled towards the midline (A – A'', Figure 4.11, n=5), mimicking the EfnA4 mediated rescue. However, co-electroporation of EfnA4/Ntrk2^{K571N} acutely and reproducibly interfered with EfnA4 promoted fasciculation (B – B'', Figure 4.11, n=6). Intriguingly, restored EfnA4 was still capable of re-fasciculating callosal axons when co-expressed with Ntrk3^{K572N} (C – C'', Figure 4.11, n=3), which in turn highlighted the functional relevance and specificity of Ntrk2 *in vivo*. Loss-of-function experiments for Ntrks suggested that Ntrk2 was the most plausible co-receptor for EfnA4 in the context of CC formation.

4.12 EfnA4/Ntrk2 interplay modulates Ntrk2 downstream signaling *in vitro*

To investigate the biological relevance of EfnA4/Ntrk2 interaction, I analyzed the activities of known Ntrk2 downstream effector proteins - (p)AKT, (p)PLCγ1 and (p)ERK1/2 - *in vitro*[81,83]. The Ntrk2 expression construct was co-transfected with either EfnA4 expression plasmids (pCAG promoter, without tags) or with equal amounts of the empty vector backbone into HEK293 cells following 24-hour incubation in serum free DMEM media. Protein samples were collected in Ripa buffer on the next day. A separate experimental line with the same conditions was also performed in parallel, but 5 min BDNF stimulation (25 ng/ml) for both EfnA4- and backbone-transfected cells was carried out before protein isolation. Equal amount of the proteins from each sample (40 µg) were subject to WB (A, Figure 4.12). After visualization, the WB band intensities, which reflected protein levels of targeted molecules (the phosphorylated and according total homogeneous proteins were discriminated by specific antibodies), were measured and relatively quantified using 'Image Lab' software (control lanes were set as 100%). Protein levels for α tubulin were also determined in the same way to denote total quantities of loaded proteins. The values of phosphorylated effector proteins were then normalized to those of α tubulin or total proteins (taking AKT for example, the ratio of

pAKT/α tubulin or pAKT/total AKT) under the same conditions to denote the phosphorylation level of the targeted effectors. The relative quantification was achieved by comparison of the phosphorylation level of a targeted effector in EfnA4/Ntrk2 co-transfected cells to that of Ntrk2-alone transfected cells. Three independent groups of trials were performed to acquire statistical data.

Even without BDNF stimuli, the co-transfection of Ntrk2 with EfnA4 robustly augmented phosphorylation of AKT at T308 (pAKT T308) when compared to the case of Ntrk2-alone transfection. Relative pAKT T308 protein levels were increased by 103% (p=0.00245, **) or 119% (p=0.00777, **) when normalized to α tubulin or total AKT, respectively. This effect was similar in case of BDNF stimulation, where relative pAKT T308 protein levels were increased by 85.83% (p=0.00065, ***) or 103% (p=0.000654, ***) when normalized to α tubulin or total AKT, respectively (B, Figure 4.12). AKT phosphorylation at S473 (pAKT S473) was also increased by the co-transfection of EfnA4/Ntrk2 in comparison to the transfection of Ntrk2 alone, albeit to a lesser extent than pAKT T308. Without BDNF stimulation, relative pAKT S473 protein levels were increased by 45.61% (p=0.000986, ***) or 56.49% (p=0.00936, **) when normalized to α tubulin or total AKT, respectively. With BDNF stimulation, relative pAKT S473 protein levels were increased by 36.95% (p=0.00893, **) and 49.78% (p=0.0104, *) when normalized to α tubulin or total AKT, respectively (C, Figure 4.12).

In contrast, the phosphorylation of PLCγ1 at Y783 (pPLCγ1 Y783) was remarkably reduced by the co-transfection of EfnA4/Ntrk2 when compared to the case of Ntrk2-alone transfection. Without BDNF stimulation, relative pPLCγ1 Y783 protein levels were reduced by 60.56% (p=0.00864, **) or 63.93% (p=0.00237, **) when normalized to α tubulin or total PLCγ1, respectively. With BDNF stimulation, relative pPLCγ1 Y783 protein levels were reduced by 68.42% (p=0.00133, **) or 77.04% (p=0.00852, **) when normalized to α tubulin or total PLCγ1, respectively (D, Figure 4.12).

The phosphorylation of ERK1 and ERK2 at T202/Y204 (pERK1 and pERK2) was moderately (and statistically less consistently) reduced by the co-transfection of

EfnA4/Ntrk2 in comparison to the transfection of Ntrk2 alone. Without BDNF stimulation, pERK1 protein levels were reduced by 28.33% (p=0.0279, *) or 38.39% (p=0.000195, ***) when normalized to α tubulin or total ERK1, respectively; and pERK2 protein levels were reduced by 27.03% (p=0.0234, *) or 41.15% (p=0.00325, **) when normalized to α tubulin or total ERK2, respectively. This mild effect was lost after BDNF stimulation: the relative pERK1 protein levels were 106.80% (p=0.44, ns) or 89.95% (p=0.17, ns) when normalized to α tubulin or total ERK1, respectively; and the relative pERK2 protein levels were 108.77% (p=0.33, ns) or 78.91% (p=0.27, ns) when normalized to α tubulin or total ERK2, respectively (E and F, Figure 4.12).
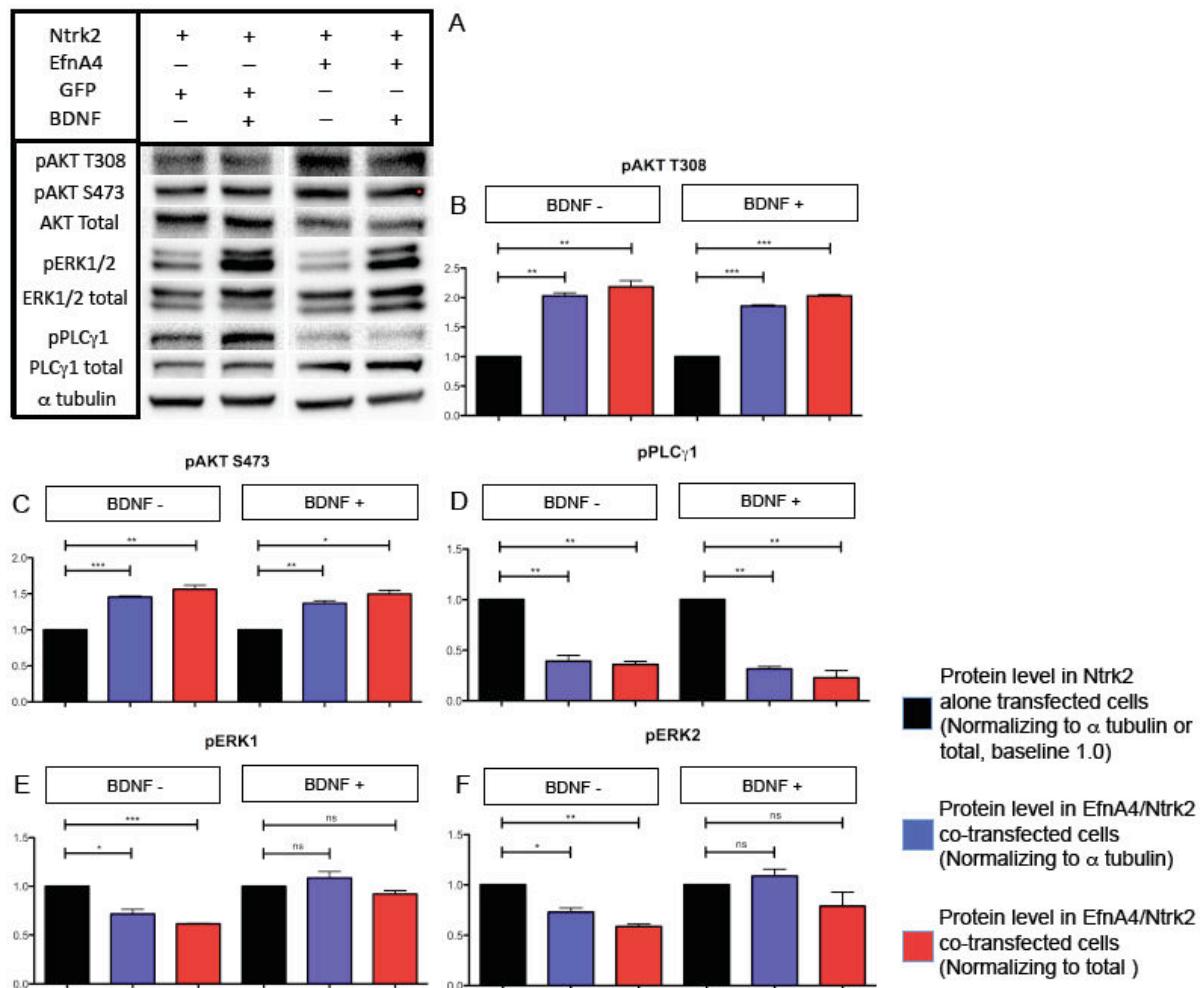
Figure 4.12: EfnA4/Ntrk2 mediated signaling increases AKT phosphorylation *in vitro*
(A) WB detection for AKT phosphorylation at threonine 308 (pAKT T308) and at serine 473 (pAKT S473), for total AKT, for ERK1/2 phosphorylation at threonine 202/ tyrosine 204 (pERK1/2), for total ERK1/2, for PLCγ1 phosphorylation at tyrosine 783 (pPLCγ1 Y783), for total PLCγ1 and for α tubulin in HEK293 cells transfected with EfnA4/Ntrk2 or Ntrk2-alone (in the cases of BDNF application or not). **(B – F)** Relative

quantification (based on three independent experimental groups) for pAKT T308 (B), pAKT S473 (C), pPLCγ1 Y783 (D), pERK1 (E) and pERK2 (F). For each effector protein, the phosphorylation level was determined by normalizing the phosphorylated protein to α tubulin (blue bar) or the total homogeneous proteins (red bar). The quantification was achieved by normalizing the targeted phosphorylated effector in EfnA4/Ntrk2 co-transfected cells to that in Ntrk2-alone transfected cells (black bar, baseline 1.0). The effector phosphorylation was always quantified in two situations: with or without extra BDNF stimulation. Asterisks denote p-values (* <0.05, ** < 0.01, *** < 0.001, ns>0.05) obtained by two-tailed Student's t-test.

4.13 EfnA4/Ntrk2 interplay modulates Ntrk2 downstream signaling *in vivo*

Having shown that EfnA4/Ntrk2 interaction could influence Ntrk2 mediated cascades *in vitro*, I wanted to find out if the loss of EfnA4 in DKO brains resulted in altered phosphorylation levels of AKT, PLCγ1 or ERK1/2 *in vivo*. Equal amount of proteins (50 μg per sample) from cortical lysates of E18.5 embryos were used for WB detection and relative quantification of effector protein phosphorylation (as described in section 4.12). Five pairs, each consisting of one DKO brain and one adjacent littermate control (A, Figure 4.13), were independently processed and the obtained data were used for paired Student's t-statistics. The loss of EfnA4 expression in the lateral cortex of E18.5 DKO embryos was confirmed by ISH (B – B', Figure 4.13).

In coherence with the *in vitro* results, protein levels of phosphorylated AKT (both pAKT T308 and pAKT S473) were significantly reduced in the neocortex of DKO embryos. Relative pAKT T308 protein levels were reduced by 27.5% (p=0.00000037, ***) or 23.33% (p=0.000514, ***) when normalized to α tubulin or total AKT, respectively (C, Figure 4.13). Relative pAKT S473 protein levels were reduced by 21.72% (p=0.00000842, ***) or 17.29% (p=0.000892, ***) when normalized to α tubulin or total AKT, respectively (D, Figure 4.13). EfnA4 expression in the E18.5 neocortex is normally restricted to superficial layers of the CP (B', Figure 4.13). Alteration in Ntrk2 mediated signaling caused by EfnA4 down-regulation was thus only expected in a subset of the lysed cortical cells. The reductions of AKT phosphorylation at both sites by approximately 17-27% in the entire cortex can thus be assumed to reflect much higher changes at the cellular level.

Surprisingly, PLCγ1 phosphorylation was also significantly reduced in DKO brains. Relative pPLCγ1 Y783 protein levels were reduced by 31.07% (p=0.0064, **) or 24.29% (p=0.00157, **) when normalized to α tubulin or total PLCγ1, respectively (E, Figure 4.13). Finally, the phosphorylation of neither ERK1 nor ERK2 was much altered in the DKO brains, in spite of far less statistical consistence. Relative pERK1 protein levels were non-significantly reduced by 7.47% (p=0.44, ns) or 5.57% (p=0.70, ns), and relative pERK2 levels were reduced by 1.82% (p=0.95, ns) or increased by 1.64% (p=0.93, ns) when normalized to α tubulin or total ERK1/2, respectively (F and G, Figure 4.13).
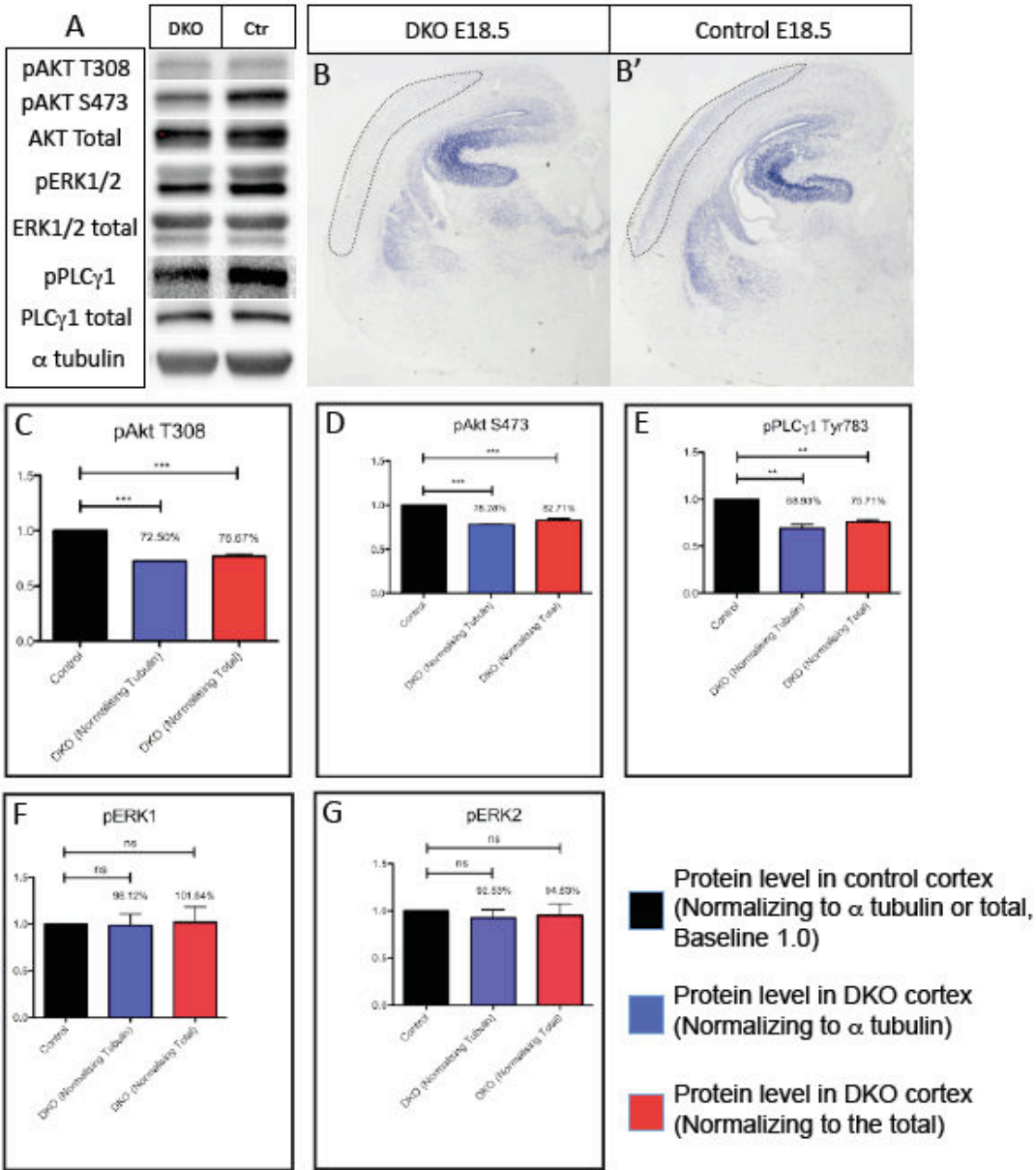
Figure 4.13: The phosphorylation of AKT and PLCγ1 was reduced in Neuro2/6 DKO neocortex

(A) WB detection for pAKT T308, pAKT S473, total AKT, pERK1/2, total ERK1/2, pPLCγ1, total PLCγ1 and α tubulin of cortical lysates from E18.5 control and DKO littermate brains. **(B – B')** ISH for EfnA4 on the sections of E18.5 DKO (B) and control (B') brains. **(C – G)** Relative quantification for pAKT T308 (C), pAKT S473 (D), pPLCγ1 (E), pERK1 (F) and pERK2 (G) in 5 pairs (n=5) of E18.5 control and DKO littermate neocortex. For each effector protein, the phosphorylation level was determined by normalizing the phosphorylated protein to α tubulin (blue bar) or the total homogeneous proteins (red bar). The quantification was achieved by normalizing the targeted phosphorylated effector in DKO neocortex to that in control neocortex (black bar, baseline 1.0). Asterisks denote *p*-values (* <0.05, ** < 0.01, *** < 0.001, ns>0.05) obtained by two-tailed Student's t-test.

4.14 Ntrk2^{Y515F}, but not Ntrk2^{Y816F}, interferes with EfnA4 mediated rescue
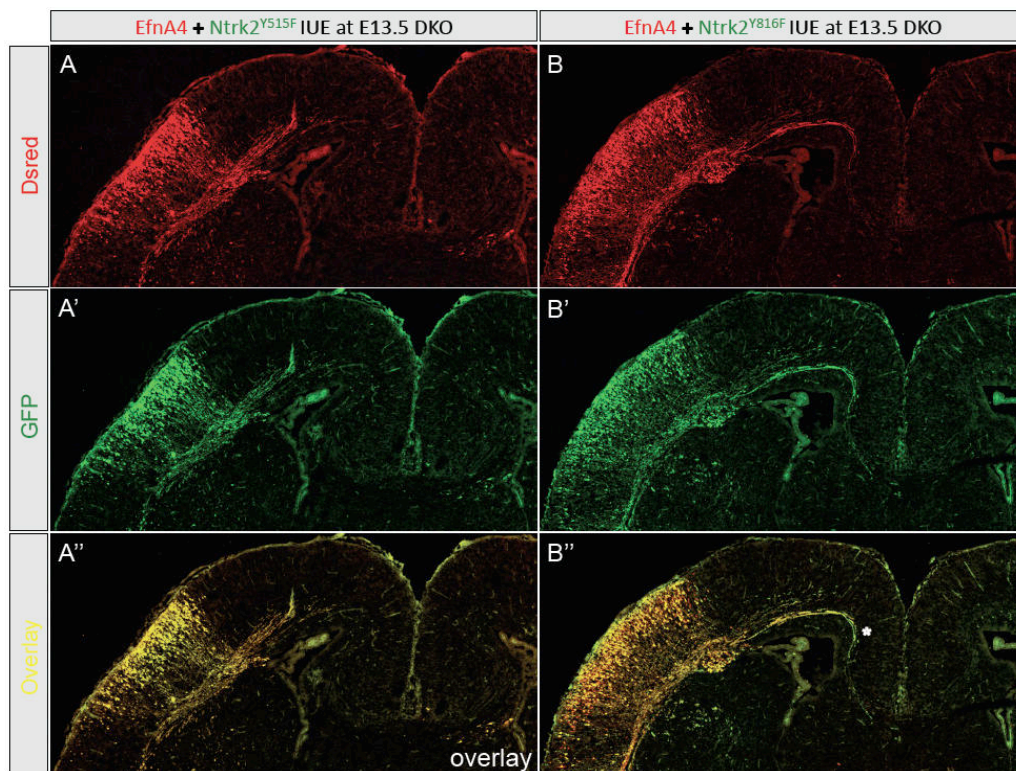
Figure 4.14: EfnA4 promoted axon growth is specifically interfered with Ntrk2^{K515F} (but not Ntrk2^{K816F}) in NeuroD2/6 DKO brains

(A – B to A'' – B'') IF staining for dsRed (A – B) and GFP (A' – B') on the sections of E18.5 DKO brains electroporated with EfnA4/Ntrk2^{K515F} (A – A', n=6) or EfnA4/Ntrk2^{K816F} (B – B', n=4), and the overlays (A'' – B''). The asterisk in (B'') marks the fasciculate callosal tract (CT) towards the midline.

The protein levels of both pAKT and pPLCγ1 were reduced in the NeuroD2/6 DKO neocortex, leaving it equivocal which pathway was primarily necessary for callosal axon growth. It is known that the pAKT and pPLCγ1 cascades are induced by different phospho-tyrosines in Ntrk2 signaling: Y515 and Y816, respectively. I*n vivo* loss-of-function strategy by binding site-specific mutant variants of Ntrk2 could be meaningful to figure out the responsible signaling. To do so, Ntrk2's Y515 or Y816 was independently mutated into a phenylalanine, which is structurally most similar with the tyrosine but not phosphorylatable (Y515F or Y816F). These variants were cloned into pCAG-GFP vector to generate expression constructs (Ntrk2^{Y515F} or Ntrk2^{Y816F}) that were subsequently co-electroporated with EfnA4 (in pCRC vector) at E13.5 (concentration: 1 μg/μl each). IF staining for dsRed and GFP on the sections of E18.5 DKO brains showed that callosal axons projected from EfnA4/Ntrk2^{Y515F} co-electroporated neurons in the DKO defasciculated and were not guided towards the midline (A – A'', Figure 4.14, n=7), while the majority of EfnA4/Ntrk2^{Y816F} double positive axons maintained fasciculate growth towards the midline (B – B'', Figure 4.14, n=4). These data reveal that the Y515 of Ntrk2, a SHC docking site, is necessary for EfnA4/Ntrk2 regulated callosal axon growth. In another word, pAKT signaling is probably the molecular mechanism underlying this biological process.

4.15 Quantification for callosal axon fasciculation

It was noticed that there were still varying subsets of callosal axons of the EfnA4 restored neurons in the DKO brains projecting into the ipsilateral CP. A quantitative method was established to statistically evaluate the (de)fasciculation levels of callosal axons, which allowed more direct and unbiased comparison of the so far described rescue experiments. The method details are described in section 3.14. Briefly, for each brain, three serial brain sections at comparable coronal planes were subject to IF staining for GFP and/or dsRed (DAPI as nuclear counterstaining) to generate high-resolution confocal microscopic images of the entire neocortex. The important anatomical structures (VZ, SVZ, CP and so on) were manually identified and an equally sized grid was positioned medially to the electroporation site to reproducibly define eight rectangular bins that described lateral to medial aspects of the CP and IZ (1-4, Ctx, and 1'-4', CC, respectively, in A, Figure 4.15). The total areal values of fluorescence positive

regions (GFP or dsRed) were determined in each bin, and normalized to the total areal values of the electroporated cell bodies in the lateral CP (IUE in A, Figure 4.15). Averaged values from the three sections denoted axon (de)fasciculation of the specific brain. Seven IUE situations were taken into account: electroporation of control embryos with only GFP (#1, baseline set to 100% or 1.0); electroporation of DKO embryos with only GFP (#2, full callosal defect), electroporation of DKO embryos with only EfnA4 (#3, simple rescue), co-electroporation of DKO embryos with EfnA4/Ntrk2^{WT} (#4), co-electroporation of DKO embryos with EfnA4/Ntrk2^{K571N} (#5, kinase-dead), co-electroporation of DKO embryos with EfnA4/Ntrk2^{Y515F} (#6, interference with SHC binding) and co-electroporation of DKO embryos with EfnA4/Ntrk2^{Y816F} (#7, interference with PLCγ1 binding). Relative quantification was achieved by normalizing the areal values of CP and IZ in (#2) – (#7) to the according values in (#1) (V_{CP} and V_{CC}, in B and C, Figure 4.15). The ratio of labelled axons in the IZ (V_{CC}, normal CC trajectory) versus total labeled axons ($V_{CP} + V_{CC}$) was also calculated to quantify the percentage of callosal axons along the normal callosal path in each situation. In the following section, this ratio is termed as calculated callosal index (ccidx, D, Figure 4.15). Statistical analysis was applied over three independently processed brains in each situation (biological replicas, n=3 (except for (#3) and (#7): n=2)).

The comparison of GFP in (#1, ccidx=1.0, reference) and (#2) confirmed that the ccidx was a good measure for the above-described callosal defect. In contrast, the ccidx in (#2) was only 0.0726 (p=0.00000121, ***), which is a reflection of approximately 96% decrease of labeled axons following the normal CT in the SVZ/IZ (#2, V_{CC}=3.99%, p=0.000241, ***), and 41.18 folds increase of labeled axons following aberrant trajectories into the ipsilateral CP in DKO brains (V_{CP}=42.18, p=0.053, ns). The electroporation of EfnA4 into DKO embryonic brains (#3) was sufficient to restore the ccidx to 0.697 (p=0.12, ns), indicating better fasciculation of labeled axons (V_{CC}=33.30%, p=0.0294, *; V_{CP}=5.29, p=0.094, ns). Co-electroporation of EfnA4/Ntrk2WT into DKO brains (#4) resulted in a ccidx of 0.678 (p=0.00415, **) and more fasciculate axons in SVZ/IZ (V_{CC}=45.79%, p=0.00754, **; V_{CP}=20.28, p=0.0000473, ***). Consolidation of the data in (#3) and (#4) indicated that the activation of Ntrk2 is absolutely necessary for the ability of EfnA4 to rescue callosal axon growth in DKO brains. Co-electroporation of EfnA4 with the kinase-dead variant

Ntrk2^{K571N} into DKO brains (#5) resulted in a ccidx of 0.057 (p=0.000000367, ***) and thus completely abolished the positive effect of EfnA4 (V_{CC}=1.24%, p=0.000188, ***; V_{CP}=25.23, p=0.0335, *).
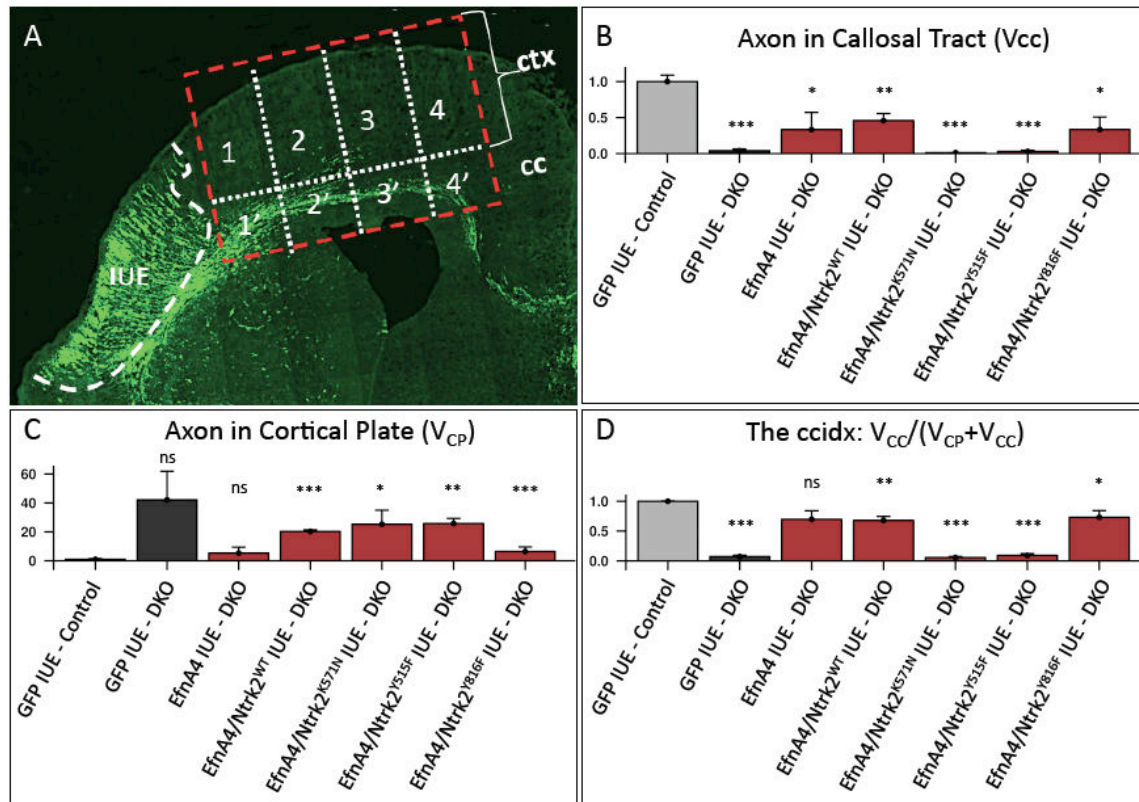
Figure 4.15: Quantification of callosal axon fasciculation by calculated callosal index (ccidx)
(A) Schematic illustration for fasciculation quantification methodology with anatomical annotations. The area marked by IUE and enclosed by white broken line denotes total electroporated area. The axons projected into the area enclosed by red broken line was used for axonal quantification. Ctx: cortical plate area, 1 - 4 mark different subareas latero-medially in Ctx. CC: callosal path area, 1' – 4' mark subareas in CC, opposite to 1 - 4. Ctx and CC are separated by white dotted lines. **(B - C)** The areal values of the fluorescent axon areas in CT (CC, B) and cortical plate (Ctx, C), respectively, for seven situations: GFP electroporated controls, GFP electroporated DKOs, EfnA4 electroporated DKOs, EfnA4/Ntrk2^{WT} co-electroporated DKOs, EfnA4/Ntrk2^{K571N} co-electroporated DKOs, EfnA4/Ntrk2^{Y515F} co-electroporated DKOs and EfnA4/Ntrk2^{Y816F} co-electroporated DKOs. All the axonal areal values have been normalized to the areal values of electroporated cells on the same sections. The mean values of GFP electroporated controls were set as baseline (1.0) to exhibit relative values of the other situations. **(D)** The calculated callosal index (ccidx): ratio of areal values in CT over total labelled axons.

The ccidx also confirmed that EfnA4/Ntrk2 mediated effects on callosal axon growth

were highly specific to Ntrk2 phosphorylation at the SHC, but not the PLCγ1, binding site. Co-electroporation of EfnA4 with the SHC-specific mutant variant Ntrk2^{Y515F} into DKO brains (#6) resulted in hardly any quantifiable increase of the rescue of the callosal defect: the ccidx was 0.0923 (p=0.00000418, ***), the V_{CC}=2.99% (p=0.000213, ***) and V_{CP}=25.77 (p=0.00116, **). Co-electroporation of EfnA4 with the PLCγ1-specific mutant variant Ntrk2^{Y816F} into embryonic DKO brains (#7) resulted in proper rescue of the callosal defect: the ccidx was 0.731 (p=0.0379, *), which reflected an improvement of labelled axons in CT (V_{CC}=33.38%, p=0.0136, *) and less defasciculate axons in the CP (V_{CP}=6.37, p=0.00062, ***) similarly with (#3). Taken together, the restoration of EfnA4 alone or in combination with over-expression of Ntrk2^{WT} or PLCγ1-binding deficient Ntrk2^{Y816F} into the lateral neocortex of NeuroD2/6 DKO embryos results in highly significant rescue of fasciculation in targeted callosal axons. This EfnA4 mediated effect is completely abolished by over-expression of the kinase-dead Ntrk2^{K571N} or SHC-binding deficient Ntrk2^{Y515F}. The signaling via the SHC-binding site of Ntrk2 is thus necessary for EfnA4 promoted fasciculate axon growth in the ipsilateral neocortex.

4.16 Generation and verification of Eph-binding deficient EfnA4 variant

EfnA/co-receptor complexes can regulate either repulsive or attractive migration of axon growth cones when interacting with EphA receptors[77,116,117]. I wanted to know whether the *trans* interaction of EfnA4 with Eph receptors is essential for EfnA4/Ntrk2 regulated callosal axon growth. To study this, I produced and took advantage of the EfnA4 variant, which was EphA receptor binding deficient. It has been shown that the Glu129 (E^{129}) in the G-H loop of EfnA5 is necessary for its interaction with EphA receptors *in trans* (but not *in cis*)[72]. Since the G-H loops of ephrin A class molecules share highly conserved AA sequences, I predicted that the homologous Glu126 (E^{126}) of EfnA4 might also be necessary for EfnA4/EphA interaction. I thus produced the EfnA4^{E126K} variant by mutating E^{126} into a lysine and cloned it into pCAG-GFP expression vector (EfnA4-mut). The flag-tagged EfnA4^{E126K} (EfnA4-mut-flag) was also generated (in the same way as EfnA4-WT-flag) for antibody detection *in vitro* (A, Figure 4.16).

To verify if the targeted mutation indeed abolished EfnA4/EphA interaction, EphA4-Fc-6xHis (a chimeric protein recombined with the EphA4 extracellular moiety, human IgG$_1$-

Fc fragment and 6xHis tag) was utilized to pull down EfnA4-WT-Flag or EfnA4-mut-Flag. I transfected HEK293 cells separately with equal amounts of either of the plasmids. The protein of EfnA4-WT-Flag was obviously detectable in the pull-down assay, however, EfnA4-mut-flag could be hardly precipitated by EphA4-Fc-6xHis (B, Figure 4.16). Additionally, I incubated living EfnA4-WT-Flag or EfnA4-mut-Flag transfected HEK293 cells with 2 μg/ml EphA4-Fc-6xHis for 1 hour and performed ICC experiments for flag and 6xHis tags. Both EfnA4 and EfnA4^{E126K} localized to the cell membranes. Nonetheless, the positive staining for 6xHis (EphA4) at cell surface in the case of EfnA4-WT-Flag transfection was hardly visible on the cells transfected with EfnA4-mut-Flag (C, Figure 4.16). Collected together, I concluded that EfnA4^{E126K} is an EphA4-binding deficient variant of EfnA4.

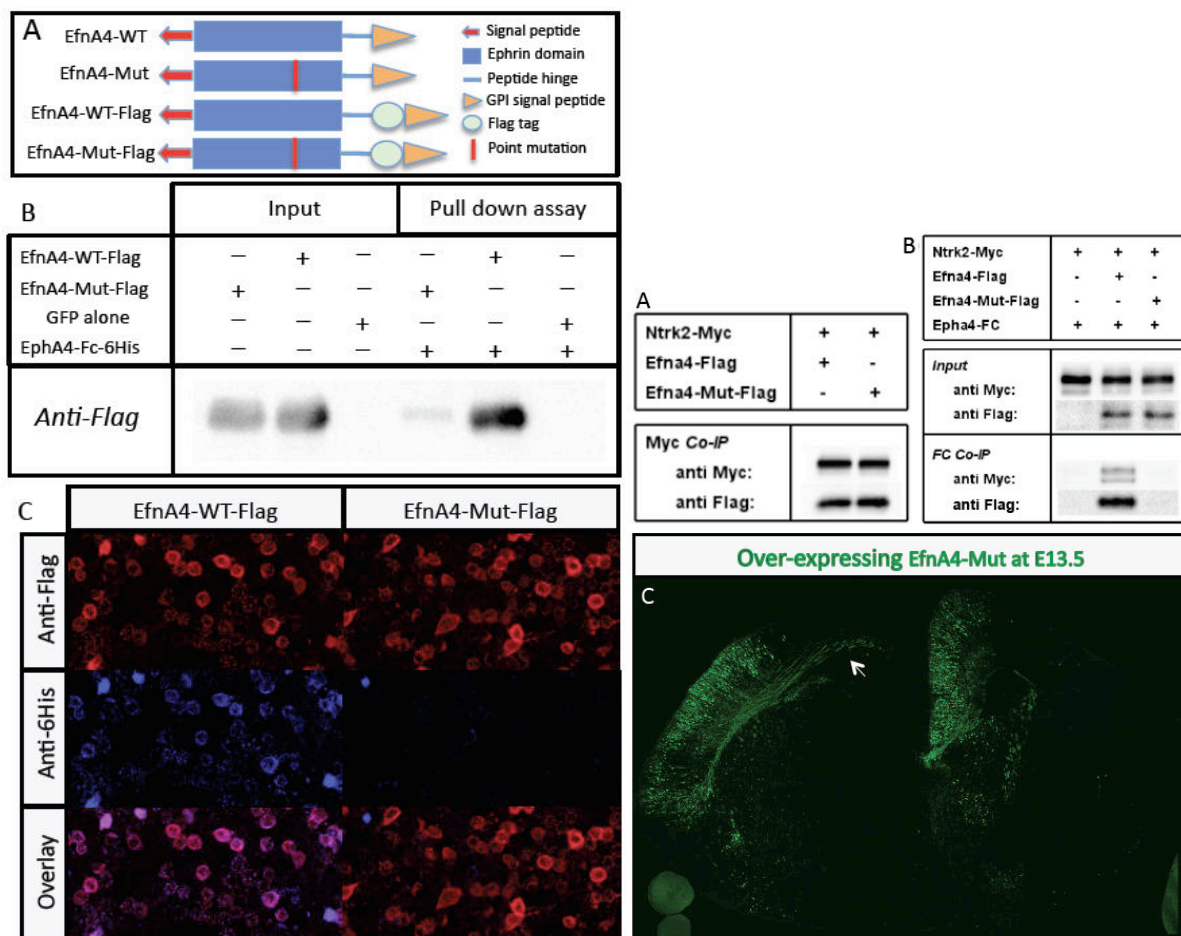## 4.17 EfnA4/Ntrk2 promoted callosal axogenesis depends on interaction with Eph receptors

Figure 4.16 (left): The targeted mutation E126K abolishes EfnA4's *trans* interaction with EphA4
(A) Schematic illustration for generation of mutated EfnA4 variant EfnA4^{E126K} (flag-tagged or not). **(B)** Pull-down assay: EphA4-Fc-6xHis interacted with flag-tagged EfnA4^{WT}, but not with EfnA4^{E126K}. **(C)** ICC staining for HEK293 cells transfected with either flag-tagged EfnA4^{WT} or EfnA4^{E126K}.

Figure 4.17 (right): EfnA4^{E126K} cannot rescue callosal agenesis in the NeuroD2/6 DKO brains
(A) Both flag-tagged EfnA4^{WT} and EfnA4^{E126K} could co-immunoprecipitate myc-tagged Ntrk2. **(B)** Pull-down assay: EphA4-Fc-6xHis could precipitate myc-tagged Ntrk2 through EfnA4, but not via EfnA4^{E126K}.
(C) Over-expression of EfnA4^{E126K} in the E13.5 DKO brains failed to rescue CC agenesis (n=3).

Before functional analysis, I wondered if the mutated variant EfnA4^{E126K} was still able to interact with Ntrk2. The co-IP experiments were performed for protein samples from EfnA4/Ntrk2 or EfnA4^{E126K}/Ntrk2 transfected HEK293 cells. It turned out that the point mutation did not affect EfnA4-Ntrk2 interaction (A, Figure 4.17). I then electroporated EfnA4^{E126K} (without flag tag, in pCAG-GFP vector) into the E13.5 DKO brains. IF staining for GFP on brain sections of E18.5 electroporated DKO embryos showed that NeuroD2/6 null axons carrying over-expressed EfnA4^{E126K} defasciculated in the medial neocortex and failed to approach the midline (n=3, C, Figure 4.17). As EfnA4 could interact with both Ntrk2 and EphA receptors, I wondered whether all these molecules acted in the same complex. Indeed, pull-down assays showed that myc-tagged Ntrk2 could be precipitated by EphA4-Fc-6xHis via EfnA4, but not via EfnA4^{E126K} (B, Figure 4.17). Collectively, the *trans* interaction of EphA receptors with EfnA4/Ntrk2 complex is necessary for the promotion of callosal axon growth via EfnA4 reverse signaling.

4.18 Other potential downstream targets of NeuroD2/6 for axogenesis regulation

In addition to Eph-ephrin family members, I also found more genes that had been previously reported involved in CC formation were dys-regulated in the DKO mice.

Cntn2 (also called Tag-1, a GPI-anchored neural adhesive glycoprotein) was shown to promote neurite outgrowth *in vitro* and *in vivo* via interaction with L1[118]. Cntn2 expression was remarkably reduced in the neocortex (but not changed in the hippocampus) of E18.5 DKO mice (A, Figure 4.18). I cloned the full ORF of Cntn2 into the Cre-activatable expression vector and then restored Cntn2 expression in the E13.5 DKO neocortex by IUE. However, Cntn2 expression alone was not sufficient to rescue

CC agenesis caused by NeuroD2/6 deficiency (E, Figure 4.18).

Robo1 is one of the Roundabout guidance receptors (Robo1/2/3). These receptors and their ligands (Slit1/2/3) comprise another family of well-studied axon guidance cues. Robo/Slit interaction is also important for the midline crossing of callosal axons[29,30]. Robo1 was strongly up-regulated in the CP of DKO mice. At E18.5, the Robo1 ISH signal was very robust and equally strong in the entire DKO CP, while it was normally relatively weak and confined to the DL in the control (B, Figure 4.18). I planned to over-express Robo1 in the neocortex of control mice to see if Robo1 mis-expression could interfere with CC formation, but the coding sequence of Robo1 (~4.8 kb) was too long to be cloned. Currently, the work about Robo1 functional analysis is still in progress.

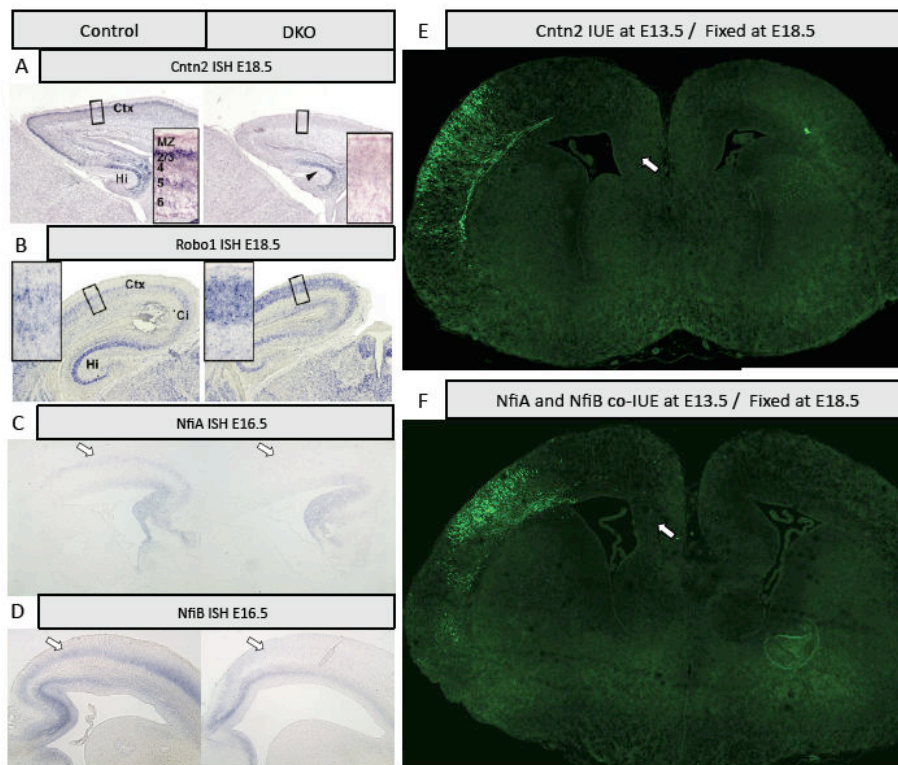**Figure 4.18: Expression patterns and over-expression of additional NeuroD2/6 regulated targets**
(A – D) ISH for Cntn2 (E18.5), Robo1 (E18.5), NfiA (E16.5) and NfiB (E16.5) on the littermate control and DKO brains. **(E)** Restoration of Cntn2 at E13.5 failed to rescue CC agenesis in the DKO (n=3). **(F)** Co-electroporation of NfiA/B mixed constructs at E13.5 could not rescue CC agenesis in the DKO (n=5).

NfiA and NfiB are related transcription factors that control organogenesis in a number of systems, including the brain. Mice that are genetically deficient for NfiA or NfiB have severe defects in CC formation[119,120]. In E16.5 NeuroD2/6 DKO brains, the expression of NfiA and NfiB were reduced in postmitotic DL neurons, but relatively normal in SVZ progenitors (C and D, Figure 4.18). Considering that NfiA and NfiB share similar molecular structures, known functions and expression patterns, I co-electroporated the mixture of NfiA/NfiB expression constructs (concentration ratio 1:1, 1 μg/μl each), which was contributed by the lab of Prof. L. Richards in Australia, into E13.5 DKO brains. However, even the combined restoration of NfiA/NfiB expression failed to rescue CC agenesis in DKO mice (F, Figure 4.18).

Part II: NeuroD2/6 regulate cell differentiation during corticogenesis

4.19 NeuroD1 expression is ectopically up-regulated in postmitotic neurons of NeuroD2/6 DKO neocortex and hippocampus

NeuroD family TFs are known to promote cell survival and differentiation. Clear developmental defects had been expected in the CP when generating the NeuroD2/6 DKO mice, however, their size and lamination of the neocortex were only mildly affected. The question how the majority of cortical neurons survived from the loss of two key regulators remained to be answered. NeuroD1 is normally expressed in the SVZ/IZ, and immediately down-regulated in CP pyramidal neurons (A – C, Figure 4.19). By IF staining, however, I found that NeuroD1 expression was aberrantly maintained in the migrating neurons of NeuroD2/6 DKO CP (A' – C', Figure 4.19). In addition, co-IF staining for NeuroD1 with either Ctip2 or Satb2 at E15.5 showed that the NeuroD1 up-regulation occurred in both Ctip2+ (light blue arrowheads in F' and G', Figure 4.19) and emerging Satb2+ neurons (yellow arrowheads in E' and G', Figure 4.19), which implicated that NeuroD1 was activated in both DL and UL neurons of NeuroD2/6 DKO brains. The earliest ectopic expression of NeuroD1 was found in E12.5 postmitotic neurons in the DKO CP (III, Figure 4.19). Additionally, IF staining on P0 DKO brain sections showed that NeuroD1 was also up-regulated in the DKO hippocampal neurons, especially in the CA1 and CA2 regions of Ammon's horn (IV, Figure 4.19).
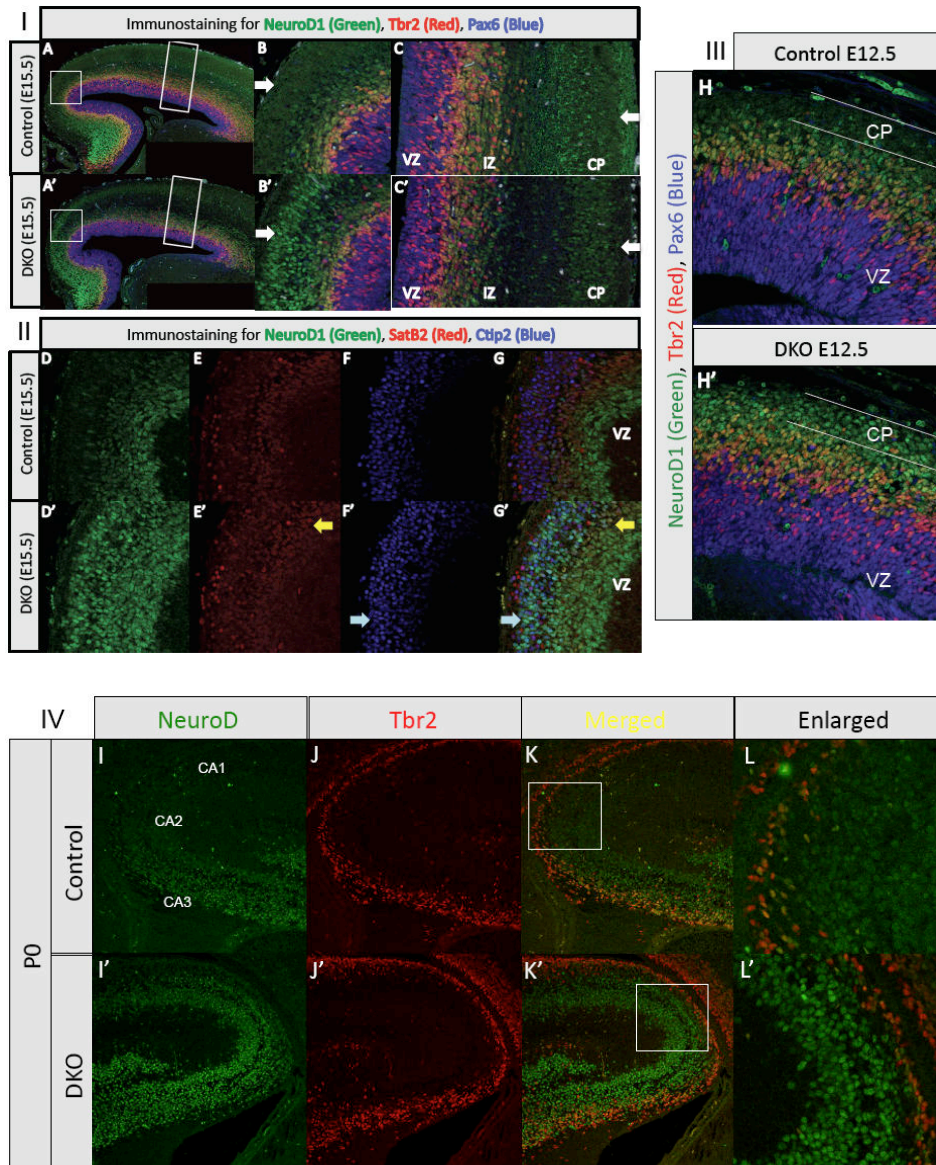
Figure 4.19: Ectopic NeuroD1 up-regulation in NeuroD2/6 DKO neocortex and hippocampus

(I) NeuroD1 is up-regulated in NeuroD2/6 DKO neocortex. **(A – A')** IF staining for NeuroD1 (green), Tbr2 (red) and Pax6 (blue). **(B – B')** Enlarged views of the areas in (A – A') square frames. **(C – C')** Enlarged views of the areas in (A – A') rectangular frames. **(II)** NeuroD1 is ectopically expressed in SatB2+ and Ctip2+ postmitotic neurons. **(D – D'**, **E – E' and F – F')** IF staining for NeuroD1 (D – D'), SatB2 (E – E') and Ctip2 (F – F'). **(G – G')** The overlay. The light blue and yellow arrowheads point to NeuroD1/Ctip2 and NeuroD1/SatB2 double positive neurons, respectively. IF staining in (I) and (II) was performed on the sections of E15.5 littermate control and DKO brains. **(III, H – H')** IF staining for NeuroD1 (green), Tbr2 (red) and Pax6 (blue) on the sections of E12.5 littermate control and DKO brains. **(IV)** NeuroD1 is up-regulated in NeuroD2/6 DKO hippocampus. **(I – I' and J – J')** IF staining for NeuroD1 (I – I') and Tbr2 (J – J') on the sections of P0 littermate control and DKO brains. **(K – K')** The overlay. **(L – L')** Enlarged views of the areas in (K – K') square frames. CA1, CA2 and CA3 denote the subareas of Ammon's horn.

4.20 NeuroD2/6 inactivation affects the ratio of UL and DL neurons

To examine if NeuroD2/6 were involved in cell specification during cortical development, I performed IF staining for the signature markers of different neuron subpopulations at E15.5. SatB2 and Ctip2 label CPNs (majorly situated in UL) and subcerebral projection neurons (majorly situated in DL), respectively[17]. It was showed that SatB2+ cells were visibly expanded in the NeuroD2/6 DKO neocortex when compared to the controls (A – A' and D – D', Figure 4.20), while Ctip2+ cells were reduced at E15.5 (B – B' and E – E', Figure 4.20). To confirm this, I also performed IF staining for Brn2 and Tbr1 for E15.5 control and DKO brains. Similarly, Brn2+ UL neurons were increased while Tbr1+ DL neurons were decreased in the NeuroD2/6 DKO brains (II, Figure 4.20). A detailed quantification for different neuron subpopulations will be carried out in the future.
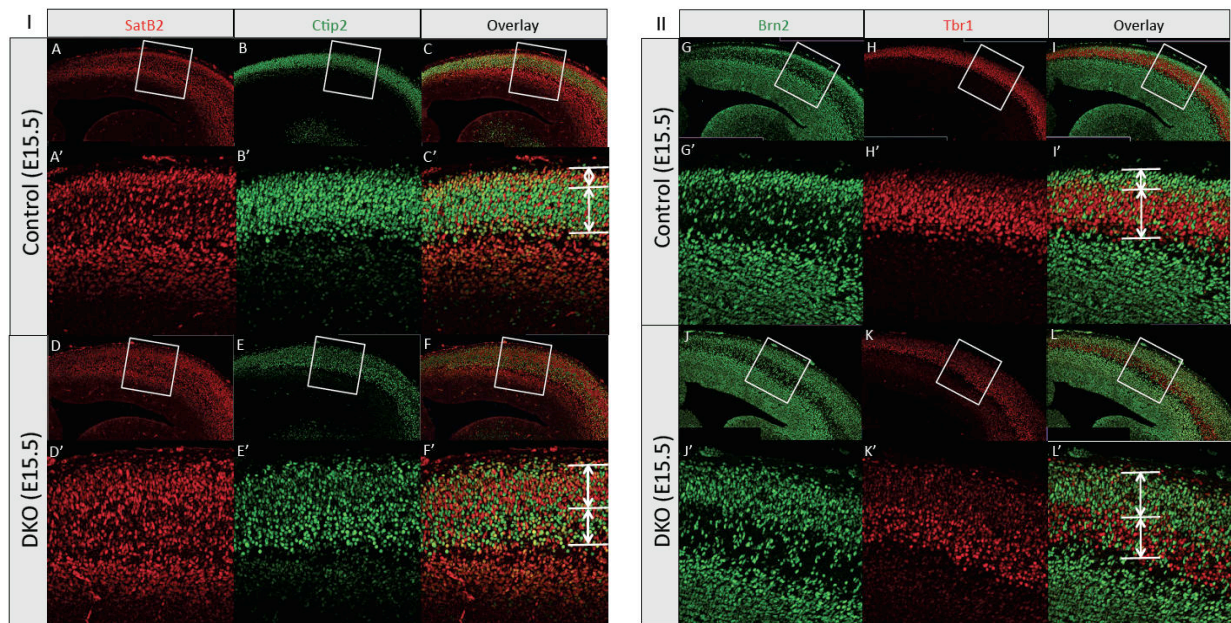
Figure 4.20: NeuroD2/6 DKO neocortex displays increased UL and decreased DL neurons
(I) Increased SatB2+ cells and reduced Ctip2+ cells in the E15.5 DKO brains. IF staining for SatB2 **(A – A' and D – D')** and Ctip2 **(B – B' and E – E'),** respectively. **(C – C' and F – F')** the overlays. **(A' – F')** Enlarged views of the areas in (A – F) square frames. **(II)** Increased Brn2+ cells and reduced Tbr1+ cells in the E15.5 DKO brains. IF staining for Brn2 **(G – G' and J – J')** and Tbr1 **(H – H' and K – K'),** respectively. **(I – I' and L – L')** the overlays. **(G' – L')** Enlarged views of the areas in (G – L) square frames. All IF staining experiments were performed on E15.5 littermate control and DKO brain sections.

4.21 Neurons in DL are selectively reduced in NeuroD2/6 DKO brains

Sox5 is a key regulator for the sequential specification of corticofugal projection

neurons[121]. Foxp2 is known to promote the neurogenesis of a subset of DL neurons[122]. Tbr1 is essential for the specification of layer VI neurons and patterning of cortico-thalamic axon projection[12]. To find out which subpopulations of DL neurons were reduced in NeuroD2/6 DKO brains, I performed IF staining for these markers on the sections of E18.5 control and DKO brains. The Foxp2+ subpopulation was significantly reduced in the DKO embryos (C – C' and yellow cells in D – D', Figure 4.21), while Sox5+ and Ctip2+ subpopulations were not considerably affected (A – A' to B – B', Figure 4.21 and D, Figure 4.2). This finding indicated that the reduction of Sox5+ cells in DKO brains (D, Figure 4.2) was most likely to be due to loss of Foxp2+ cells. In addition, Tbr1+ neurons were also markedly reduced in DKO brains (E – E', Figure 4.21). The quantification for Foxp2+ and Tbr1+ cells will also be carried out in the future.
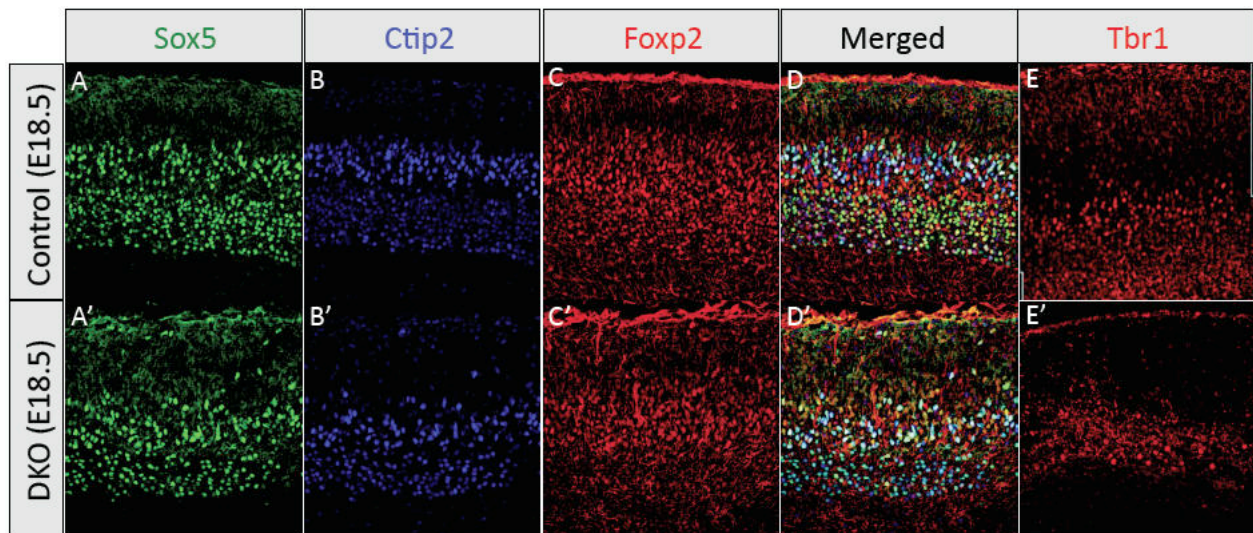
Figure 4.21: Foxp2+ and Tbr1+ DL neurons were reduced in E18.5 NeuroD2/6 DKO brains
(A – C and A' – C') IF staining for Sox5 (A – A'), Ctip2 (B – B') and Foxp2 (C – C'). **(D – D')** the overlays for (A – C) and (A' – C'), respectively. **(E – E')** IF staining for Tbr1. All IF staining experiments were performed on the sections of E18.5 littermate control and DKO brains.

4.22 Defective differentiation of Tbr2+ basal progenitors in NeuroD2/6 DKO brains

Tbr2 is a fate-determinant gene as well as a molecular marker for basal progenitors (BPs) in the developing cortex[11]. To investigate the roles of NeuroD2/6 in differentiation of BPs, I performed IF staining for Tbr2 on the sections of control and DKO brains at three developmental stages: E15.5, E17.5 and P0. There was not significant difference

in Tbr2 expression in the E15.5 DKO brains in comparison to the littermate controls (A – A', Figure 4.22). However, Tbr2+ cells were ectopically increased at E17.5 and P0, resulting in massive accumulation in perinatal DKO mice (B – B' and C – C', Figure 4.22). The expansion of Tbr2+ cells in the DKO brains was also confirmed by ISH (D – D', Figure 4.22).
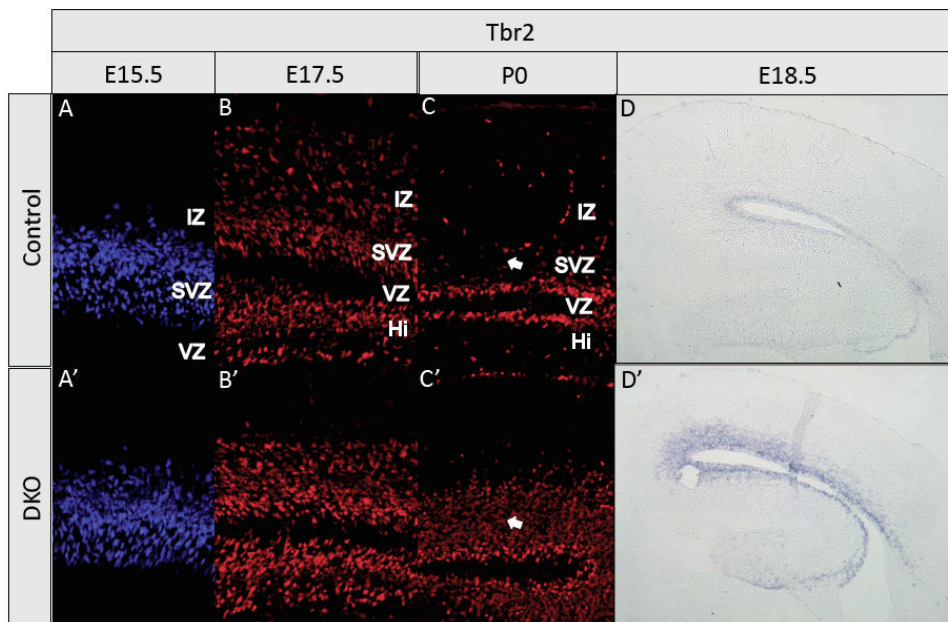
Figure 4.22: Tbr2+ basal progenitors were aberrantly increased in NeuroD2/6 DKO mice
(A – C and A' – C') IF staining for Tbr2 on the sections of E15.5 (A – A'), E17.5 (B – B') and P0 (C – C') littermate control and DKO brains. **(D – D')** ISH for Tbr2 on the sections of E18.5 littermate control and DKO brains.

4.23 Birthdating analysis of ectopic Tbr2+ cells in NeuroD2/6 DKO embryos

To determine when the ectopic Tbr2+ cells were produced, Bromodeoxyuridine (BrdU) pulse-chase was employed to analyze their birthdates. BrdU is a thymidine analogue, which can be incorporated into DNA during the S-phase of mitotic cells. The excessive BrdU can be quickly eliminated from the body (within ~15 min in rodent species). BrdU injection allows the selective labelling of cells in division at a particular time point *in vivo*[123]. I injected BrdU at the fixed time point (15:00 ± 0.5 hour) of serial embryonic days (E14.5 – E17.5) and analyze the P0 DKO mice by co-IF staining for Tbr2 and BrdU. I could rarely observe any Tbr2/BrdU double positive cells in the DKO mice with E14.5 BrdU injection (data not shown), which was in line with our finding that the

number of Tbr2+ cells was not increased until E15.5. The number of double positive cells increased slightly at E15.5 (A – C, Figure 4.23). The majority of double positive cells were found in the P0 DKO mice with BrdU injection at E16.5 (A' – C', Figure 4.23), the peak of UL neuron production from Tbr2+ BPs. The number of double positive cells was considerably decreased in the P0 DKO mice with E17.5 BrdU injection (A'' – C'', Figure 4.23). Combining the data of Figure 4.22 and 4.23, I concluded that the differentiation of Tbr2+ BPs was severely impaired in NeuroD2/6 DKO embryos.
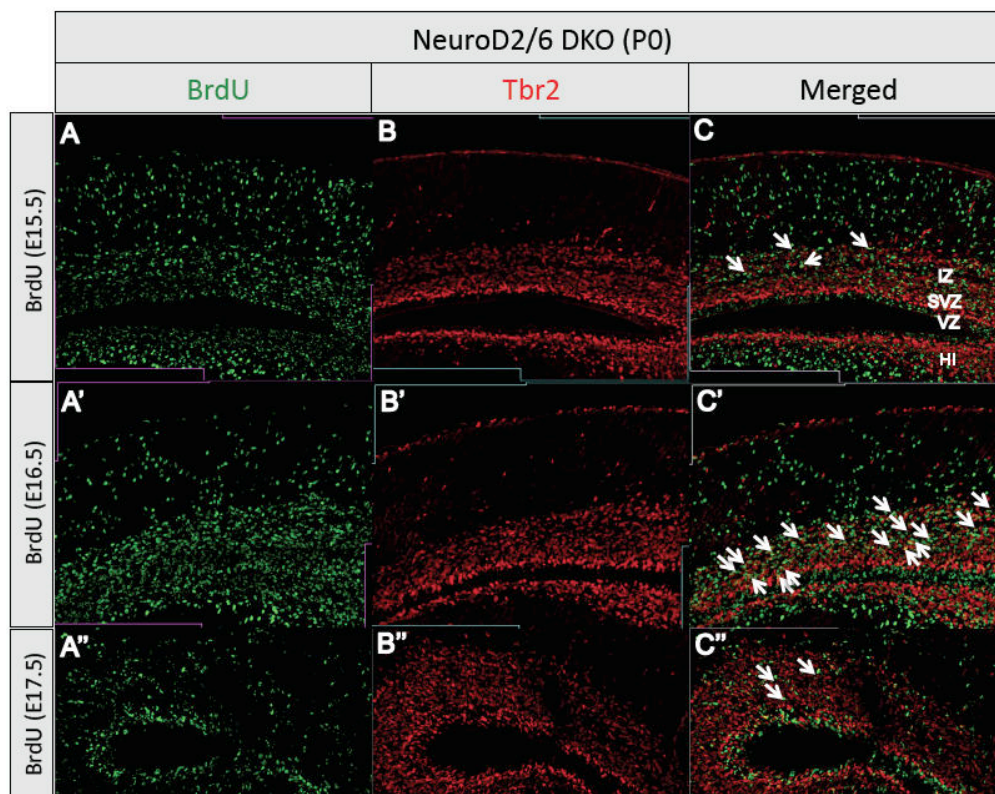
Figure 4.23: The majority of ectopic Tbr2+ cells were born at E16.5
(A – A'') IF staining for BrdU (green) injected on E15.5 (A), E16.5 (B) and E17.5 (C) on the sections of P0 NeuroD2/6 DKO brains. **(B – B'')** Co-IF staining for Tbr2 (red) on the same sections corresponding to (A – A''). **(C – C'')** the overlays. Each of the white arrowheads marks a Tbr2/BrdU double positive cell.

4.24 NeuroD6 is expressed in Tbr2+ cells in the SVZ/IZ

A key question in my study is whether NeuroD2/6 regulate cell differentiation cell intrinsically or via secreted signals (cell extrinsically). A prerequisite for cell intrinsic regulation is that NeuroD2/6 and Tbr2 are expressed in the same cell. Due to the lack of good NeuroD2/6 antibodies, IF staining for Cre (under the control of endogenous NeuroD6 promoter) was used to denote NeuroD6 expression in our NeuroD6-Cre mice.

I performed co-IF experiments for Tbr2 and Cre on the sections of E12.5 and E18.5 embryonic brains. At both stages, a population of Tbr2/Cre double positive cells had been observed in the SVZ or IZ of control embryos (A – C and G – I, Figure 4.24). In E18.5 DKO embryos, most ectopic Tbr2+ cells were also Cre positive, implying that these cells that failed to differentiate and instead accumulated in the SVZ/IZ were originally expressing NeuroD6 (G' – I', Figure 4.24). I also found that Cre expression was absent in Pax6+ APs in the VZ (D – F, Figure 4.24).
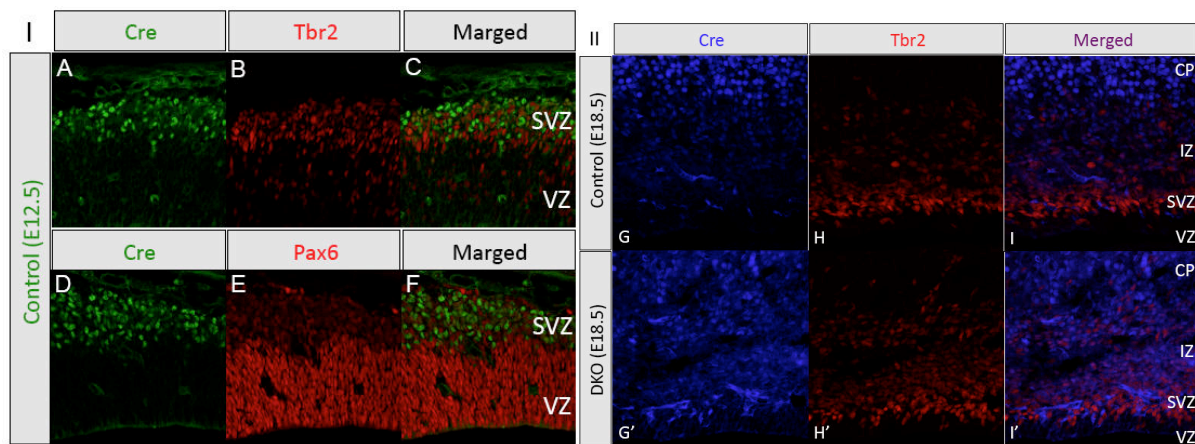
Figure 4.24 The Cre (NeuroD6) expression is detectable in Tbr2+ cells, but not in Pax6+ cells
(A – C) IF staining for Cre (A, green), Tbr2 (B, red) and the overlay (C). **(D – F)** IF staining for Cre (D, green), Pax6 (E, red) and the overlay (F). The IF staining experiments were performed on the sections of E12.5 control brains. **(G – G' to I – I')** IF staining for Cre (G – G', blue), Tbr2 (H – H', red) and the overlays (I – I') on the sections of E18.5 littermate control and DKO brains.

4.25 Over-expressed Neuro2/6 promote the differentiation of Tbr2+ progenitors

To further investigate the functions of NeuroD2/6 in neuronal differentiation, I electroporated the Cre-triggered expression constructs of NeuroD6 at E12.5 and NeuroD2 at E13.5 (as described in section 4.1), respectively, and analyzed the electroporated brains at E18.5. IF staining for Tbr2 showed that *in vivo* restoration of NeuroD2 or NeuroD6 in DKO brains enabled the conversion of Tbr2+ BPs into migrating neurons in the CP (C and I, Figure 4.25) in comparison to the unelectroporated hemisphere (A, B and H, Figure 4.25). Unexpectedly, over-expression of NeuroD2/6 also prematurely exhausted the pool of Pax6+ APs (F and K, Figure 4.25), in which NeuroD6 (Cre) is normally not expressed. DAPI staining on the neighboring brain section showed the presence of cells, albeit at lower density, in the

electroporation areas of SVZ/VZ (G, Figure 4.25). This finding argued that the absence of progenitors was not simply an electroporation artifact. The positive staining for Tuj1, an earliest marker for specified neurons, in the electroporation areas of VZ (M – P, Figure 4.25) implicated that cells in these areas might have undergone neuronal differentiation. Additionally, it is known that Notch signaling inhibits cell differentiation via its downstream effector Hes5 during corticogenesis[124,125]. ISH for Hes5 on the sections of NeuroD2/6 electroporated brains (E18.5) showed that Hes5 expression was dramatically down-regulated in the NeuroD2/6 over-expression areas (Q – S and Q' – S', Figure 4.25). Taken together, the over-expression of NeuroD2/6 facilitated the differentiation and migration of SVZ/VZ progenitors.
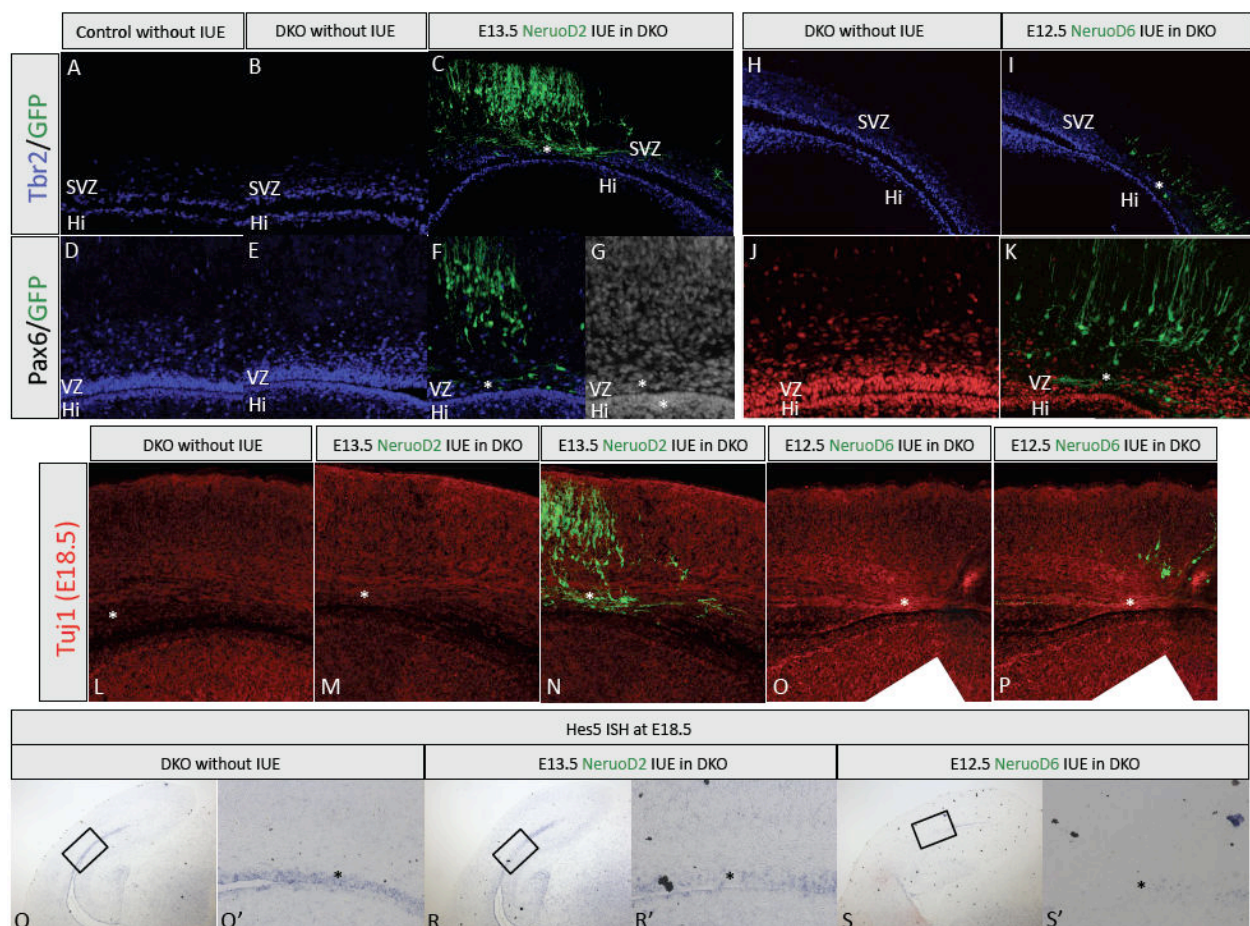
Figure 4.25: Over-expressed NeuroD2/6 in progenitors promote neuronal differentiation
(A – F) IF staining for Tbr2 (A) or Pax6 (D) on the sections of control brains, unelectroporated hemispheres of DKO brains (B or E) and co-IF for GFP (NeuroD2) with Tbr2 (C) or Pax6 (F) on the sections of E13.5 NeuroD2-electroporated hemispheres of DKO brains. **(G)** DAPI staining for the adjacent section of (F). **(H – K)** IF staining for Tbr2 (H) or Pax6 (J) on the sections of unelectroporated hemispheres of DKO brains and co-IF for GFP (NeuroD6) with Tbr2 (I) or Pax6 (K) on the sections of

E12.5 NeuroD6-electroporated hemispheres of DKO brains. **(L – P)** IF staining for Tuj1 on the sections of unelectroporated (L), E13.5 NeuroD2-electroporated (M) and E12.5 NeuroD6-electroporated (O) hemispheres of DKO brains, and co-IF for GFP and Tuj1 on the sections of E13.5 NeuroD2-electroporated (N) and E12.5 NeuroD6-electroporated (P) hemispheres of DKO brains. **(Q – S)** ISH for Hes5 on the sections of unelectroporated hemisphere (Q), E13.5 NeuroD2-electroporated (R) and E12.5 NeuroD6-electroporated (S) hemispheres of DKO brains. **(Q' – S')** Enlarged views of the areas in (Q – S) rectangular frames. All IF and ISH experiments were performed on E18.5 embryonic brains.

4.26 Olig2+ progenitors are increased in NeuroD2/6 DKO neocortex

To investigate possible effects of NeuroD2/6 on gliogenesis, I performed IF staining for the glial progenitor marker Olig2. Olig2 is mainly expressed in the progenitors that will differentiate into astrocytes and oligodendrocytes[40,126]. Surprisingly, I found that Olig2+ cells were substantially increased in E18.5, but not E16.5, DKO brains in comparison to the controls (A – A' and B' – B', Figure 4.26). I then quantified the total number of Olig2+ cells for 3 pairs of E18.5 littermate control and DKO brains (at similar coronal planes in each pair). The number of Olig2+ cells in the DKO was approximately doubled that in the control with statistic consistence [control: 234 ± 53; DKO: 456 ± 35; p = 0.0053] (C, Figure 4.26).
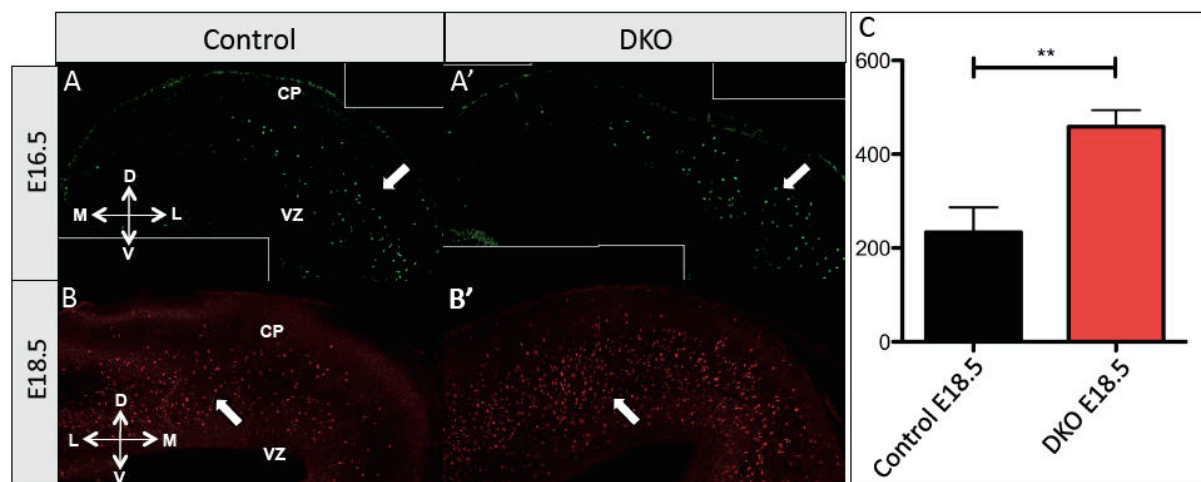
Figure 4.26: Increased number of Olig2+ cells in perinatal NeuroD2/6 DKO brains
(A – A' and B' – B') IF staining for Olig2 on the sections of E16.5 (A – A') and E18.5 (B – B') littermate control and DKO brains. **(C)** Quantification for Olig2+ cells in E18.5 control and DKO brains (n=3).

4.27 Expression of NeuroD6 and Olig2 is mutually exclusive

I also performed co-IF staining for Cre (NeuroD6) and Olig2 to examine their co-localization. The expression of Cre and Olig2 did not overlap at all in the neocortex of E18.5 control or DKO brains, regardless of the increase of Olig2+ cells in the DKO (A – C and A' – C', Figure 4.27). I then analyzed the E18.5 DKO brains, which had been electroporated with NeuroD2 at E13.5 and injected with BrdU at E14.5, by co-IF staining for GFP, BrdU and Olig2. Intriguingly, GFP+ (NeuroD2+) and Olig2+ cells displayed mutually exclusive distribution in the electroporated DKO brain hemisphere (D, F and G, Figure 4.27). The BrdU labeled cells in the NeuroD2 electroporated area migrated properly into the UL (E, Figure 4.27), arguing that the decrease of Olig2+ cells was not caused by defective cell migration. But another possibility still exits that the abnormal production of Olig2+ cells in the electroporated area may be a secondary effect caused by the premature differentiation of SVZ/VZ progenitors forced by NeuroD2 over-expression. More experiments are required to confirm these findings and to identify the downstream mechanisms for Neurod2/6 regulated lineage selection.
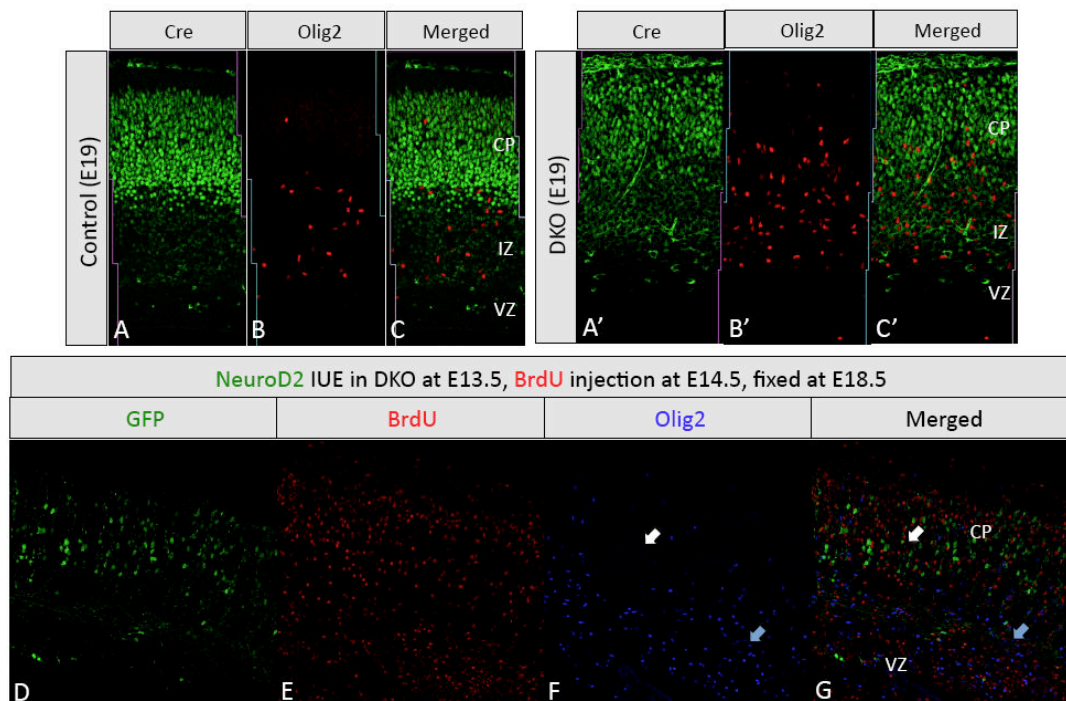
Figure 4.27: NeuroD2/6 and Olig2 show mutually exclusive expression in the cerebral cortex
(A – C and A' – C') IF staining for Cre (A and A') and Olig2 (B and B') on the sections of E18.5 littermate control and DKO brains and the overlays (C and C'). **(D – G)** IF staining for GFP (D), BrdU (E) and Olig2 (F) on sections of E13.5 NeuroD2-electroporated hemisphere of DKO brain (E18.5) and the overlay (G).

4.28 ISH based expression screen and more about potential NeuroD2/6 downstream targets
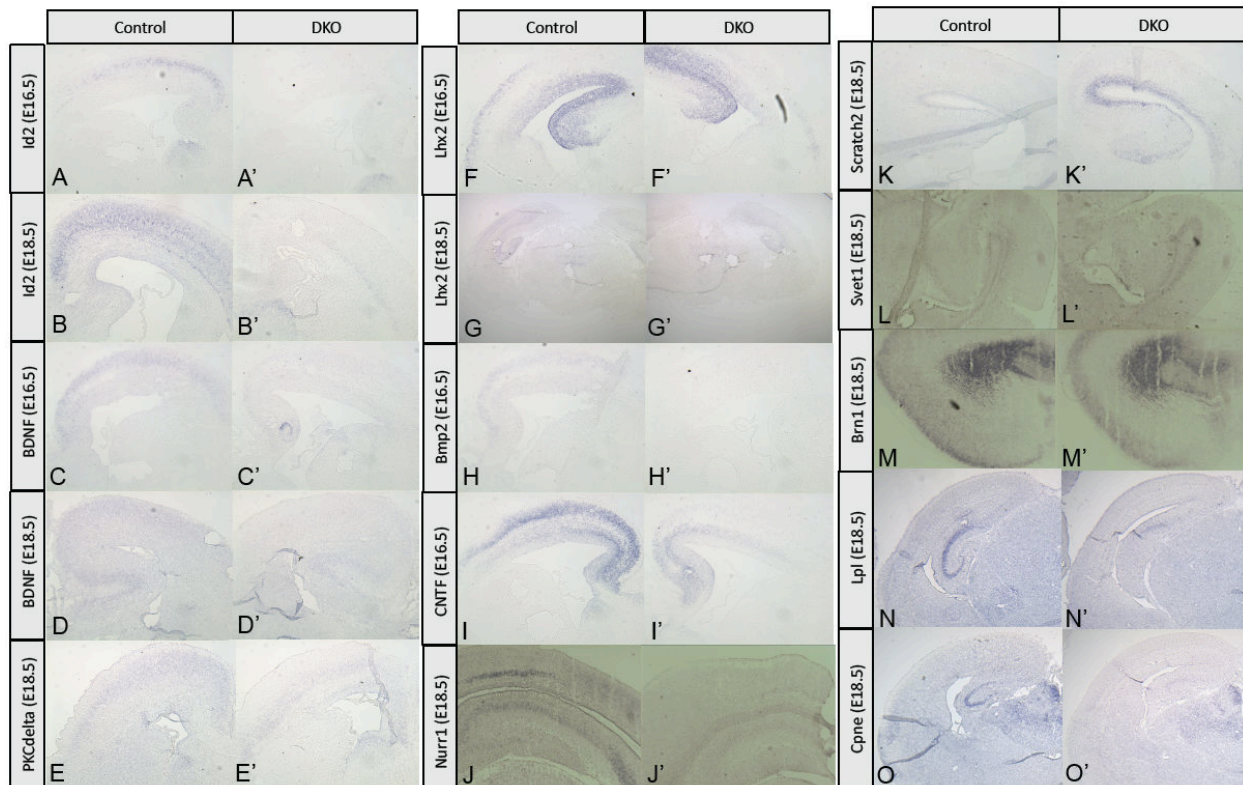
Figure 4.28: Genes with altered expression patterns in NeuroD2/6 DKO brains
(A – A' to B – B') ISH for Id2 at E16.5 (A – A') and E18.5 (B – B'). **(C – C' to D – D')** ISH for BDNF at E16.5 (C – C') and E18.5 (D – D'). **(F – F' to G – G')** ISH for Lhx2 at E16.5 (F – F') and E18.5 (G – G'). **(H – H' to I – I')** ISH for Bmp2 (H – H') and CNTF (I – I') at E16.5. **(J – J' to O – O' and E – E')** ISH for Nurr1 (J – J'), Scratch2 (K – K'), Svet1 (L – L'), Brn1 (M – M'), Lpl (N – N'), Cpne (O – O') and PKCdelta (E – E') at E18.5. All ISH experiments were done on the sections of littermate control and DKO brains.

One of the main aims in my study is to identify the downstream molecular mechanisms that are responsible for the developmental defects caused by genetic deletion of NeuroD2/6. To address this issue, I performed an extensive ISH based gene expression screen using E16.5 and/or E18.5 control and DKO brain tissues. I have subcloned the transcript fragments for approximately 300 different genes (including cell skeleton proteins, transcriptional factors, adhesion molecules, intracellular kinases and so on) for in-vitro synthesis of digoxigenin labeled ISH anti-sense RNA probes. I have performed ISH experiments for many, but not yet all of those probes. Most tested genes showed

normal expression pattern in NeuroD2/6 DKO brains, but some were robustly regulated in the DKO cerebral cortex. I have summarized the gene expression patterns of interesting candidates in control and DKO brains in this section. The expression alteration of some genes in the DKO brains was observed only once, so more experiments would be required for confirmation in the future.

The down-regulated genes in NeuroD2/6 DKO brains:

Id2 gene codes a HLH protein that lacks a basic DNA binding domain but is still able to interact with E-box proteins. Id2 is thus considered as a dominant negative repressor for class II bHLH TFs[127]. The Id2 expression was dramatically reduced in the CP of E16.5 and E18.5 DKO embryos (A – A' and B – B', Figure 4.28). Id2 might be downstream of NeuroD2/6 to serve as a regulator of NeuroD2/6 function by negative feedback loop. It would be interesting to study the mechanisms how NeuroD factors regulate the expression of Id2 and other potential antagonists.

BDNF (C – C' and D – D', Figure 4.28) and **Lhx2** (F – F' and G – G', Figure 4.28) were also down-regulated in the CP of DKO brains at E16.5 and E18.5.

PKCdelta (protein kinase C delta isoform) showed decreased expression in E18.5 DKO visual cortex (E – E', Figure 4.28).

Bmp2 (H – H', Figure 4.28) and **CNTF** (I – I', Figure 4.28), both cytokines, were also reduced in the postmitotic compartment of E16.5 DKO neocortex.

Nurr1 expression was entirely absent in the DKO subplate cells (J – J', Figure 4.28).

Lpl and **Cpne** (hippocampal pyramidal neuron markers) were specifically down-regulated in CA2 and CA3 neurons of Ammon's horn (N–N' and O–O', Figure 4.28).

The up-regulated genes in NeuroD2/6 DKO brains:

Scratch2 is a zinc-finger TF, which might be involved in neuron differentiation[128]. Its expression was increased in the SVZ of E18.5 DKO brains (K–K', Figure 4.28).

Svet1 is a long intergenic non-coding RNA, which was previously reported in our lab as a UL marker[129]. Svet1 was also selectively up-regulated in the SVZ of E18.5 DKO brains (L – L', Figure 4.28).

Brn1 expression was increased in the CP of E18.5 DKO embryos (M – M', Figure 4.28), which was in line with my finding that UL were expanded in the DKO brains in comparison to the controls.

Due to the large number of tested probes, I summarized my data of ISH based expression screen on the control and DKO brains in the table below (Table 4.1) for three situations: 1) I had not yet tested the probes in the DKO brains till the moment of dissertation completion (Not tested); 2) the expression was not changed in the cortical areas of control and DKO embryonic brains (Not changed); 3) the expression differences between control and DKO mice had not been surely detected due to tissue damage or failed ISH experiments (inconclusive).

Table 4.1: The summary for expression patterns of tested genes in control and DKO brains

Number	Gene Name	Stage	Expression in Control	Expression in DKO
1	DCC	E15.5	DEC, SVZ, Sp	Not tested
2	DCC	E18.5	HP, DG, PC	Not changed
3	Unc5a	E15.5	DEC, Sp	Not tested
4	Unc5a	P0	DEC, PC	Not tested
5	Unc5b	E15.5	DEC, Sp	Not tested
6	Unc5c	E15.5	DEC, Sp, IZ	Not tested
7	Unc5c	P0	UL	Not tested
8	Unc5d	E15.5	Sp, IZ	Not tested
9	Unc5d	P0	Sp, PC, UL	Not tested
10	FoxO1	E16.5	SVZ, DEC, BG	Not tested
11	FoxO1	P0	BG	Not tested
12	FoxO4	E16.5	VZ	Not tested
13	FoxO6	E16.5	CP, HP, DG, BG	Not tested
14	Ddah1	E16.5	VZ, HT, DL	Not tested
15	Ddah2	E16.5	SVZ, VZ, CP	Not tested
16	Oct6	E16.5	UL, HP, BG	Not tested
17	Ngn2	E16.5	VZ, HT	Not changed
18	Nrp1	E16.5	IZ, HP	Not tested
19	Nrp2	E16.5	PC, HP, TVZ	Not tested
20	Robo2	E16.5	IZ, HP, BG, Th	Not tested
21	Slit1	E16.5	CP, BGE	Not tested
22	GAP43	E16.5	CP, Sup, Sp, BG	Not changed
23	Svet1	E16.5	SVZ	Not changed
24	Emx1	P0	CP	Inconclusive
25	EphB3	P0	HP	Not changed
26	Ryk	P0	DEC, BG	Inconclusive
27	Celsr3	E18.5	CP, HP, PC, DG, BG	Not changed
28	Fzd3	E18.5	CP, HP	Inconclusive

29	PlxnA1	E16.5	CP, HP, Sup, VZ, Th	Inconclusive
30	PlxnA1	E18.5	CP, HP, Sup, VZ	Not changed
31	Rac1	E14.5	VZ, CP	Inconclusive
32	Rac1	E16.5	CP, Sup, HP, VZ	Inconclusive
33	Rac1	E18.5	CP, HP, VZ, Th	Inconclusive
34	Rac3	E18.5	CP, HP, Th	Inconclusive
35	Bmp2K	E16.5	CP, VZ	Inconclusive
36	Bmp2K	P0	DL, SVZ, Sp	Inconclusive
37	GLAST	E16.5	VZ	Inconclusive
38	GLAST	P0	VZ	Not changed
39	Fgf9	E16.5	CP, VZ	Not changed
40	Fgf9	P0	UL	Inconclusive
41	Gsk3beta	E16.5	CP, VZ, HP, BG, Th	Not changed
42	Gsk3beta	P0	CP, VZ	Inconclusive
43	Hes5	E16.5	VZ	Not changed
44	Hes5	P0	VZ	Not changed
45	Lis1	P0	CP, Sp, VZ	Not changed
46	NeuroD4	P0	No expression	Inconclusive
47	NT-3	E15.5	UL	Inconclusive
48	NT-3	P0	CP	Inconclusive
49	Hes1	E16.5	VZ	Not changed
50	EphB6	P0	CP, BG	Not tested
51	PlxnB1	E16.5	CP, HP	Not tested
52	PlxnC1	E16.5	UL, DEC, VZ	Not tested
53	Sema5A	E18.5	VZ, DG	Not changed
54	Sema5B	E16.5	VZ	Not tested
55	Sema6A	E16.5	CP, HP, Th	Not tested
56	Sema6D	E16.5	IZ, BGE	Not tested
57	Sema7A	E16.5	CP, HP, Th	Not tested
58	Slit3	E16.5	UL, HP	Not tested
59	Sema3C	E18.5	DL, HP	Inconclusive
60	EphA7	E16.5	CP, Sup, Sp, BG	Inconclusive
61	EphA8	E16.5	HP, BG	Not changed
62	Hbp3	E16.5	PC, HP, AG	Inconclusive
63	Nectin3	E16.5	UL, HP, AG	Inconclusive
64	PlxnD1	E16.5	PC, HP	Not changed
65	Bcl6	E18.5	CP	Inconclusive
66	Cdh8	E15.5	SVZ	Not changed
67	Cdh8	E18.5	CP, SVZ, HP, BG	Not changed
68	Crym	E18.5	CP, HP	Inconclusive
69	Odz3	E18.5	CP	Not changed
70	Tcf3	E18.5	CP, SVZ, VZ	Not changed
71	Tcf4	E18.5	CP, SVZ, VZ	Inconclusive
72	Tcf12	E18.5	CP, SVZ, VZ	Not changed
73	Fyn	E16.5	DEC, VZ	Inconclusive
74	Lhx9	E16.5	VZ	Not changed
75	Ngef	E16.5	PC, BG	Inconclusive
76	RhoA	E16.5	VZ	Not changed
77	TLX	E16.5	VZ	Not changed
78	Dab1	E18.5	CP, PC, HP, DG	Not changed
79	FAK	E18.5	CP, HP	Not changed

80	Fyn	E18.5	CP, HP	Inconclusive
81	IlK	E18.5	VZ	Not changed
82	Itgb1	E18.5	HP, VZ	Not changed
83	Lix1	E18.5	CP, HP, DG	Not changed
84	Mdga1	E18.5	UL, HP	Not changed
85	NomaGAP	E18.5	CP, HP, Th	Not changed
86	p35	E18.5	Cp, HP, PC, AG	Not changed
87	p39	E18.5	CP, HP, Th	Inconclusive
88	PAK1	E18.5	CP, HP, Th	Inconclusive
89	PAK2	E18.5	CP, HP, AG, Th	Inconclusive
90	Rnd2	E18.5	SVZ	Not changed
91	Rnd3	E18.5	CP, VZ, Th	Not changed
92	Bmp7	E16.5	ChP	Not changed
93	Etv5	E15.5	SVZ	Not changed
94	COUP-TF	E15.5	caudal SVZ	Not changed
95	Tcf3	E15.5	SVZ, BG, BGE	Not changed
96	Tcf12	E15.5	SVZ, BG, BGE	Not changed
97	PlxnA4	E15.5	SVZ, Th	Not changed

DEC: developing entorhinal cortex; **Sup**: subplate; **Sp**: septum; **SVZ**: subventricular zone; **VZ**: ventricular zone; **IZ**: immediate zone; **HP**: hippocampal pyramidal neurons; **DG**: dentate gyrus; **PC**: piriform cortex; **UL**: neocortical upper layers; **DL**: neocortical deeper layers; **CP**: cortical plate; **BG**: basal ganglia; **BGE**: basal ganglia eminences; **Th**: thalamus; **HT**: hypothalamus; **TVZ**: thalamic ventricular zone; **ChP**: choroid plexus; **AG**: amygdala. **Not tested**: The probes had not been tested on the DKO cortical tissues. **Not changed**: the genes did not display obvious alterations in expression patterns on the tested control and DKO brains. **Inconclusive**: Differential expression could not be surely evaluated on the tested DKO tissues.

5. Discussion:

The formation of commissural connectivity is fundamental for normal brain development and higher cognitive functions. Excitatory neurons in the UL of cerebral neocortex form thick axonal fascicles that grow medially and ultimately constitute the CC as major commissural fiber tract. Callosal agenesis has been found in a number of genetic mouse mutants, where CC formation is impaired at different developmental stages. The CPNs in SatB2 null mutant mice are converted into subcerebrally projecting neurons as a result of ectopic Ctip2 expression[18]. Sip1 promotes callosal axon growth by regulating expression of the cytoskeleton associated molecule - ninein. In Sip1 deficient mice, callosal axon growth is not fully lost but dramatically retarded due to reduced cytoskeleton stability[130]. Genetic inactivation of NfiA or NfiB impedes the formation of midline glial structures and thus results in failure of callosal axons to cross the midline[119,120]. Genetic silence of many axon guidance molecules (such as netrin-1, DCC, Robo1/2, slits, EfnB1, sema3c) in mice leads to abnormal CC formation or callosal agenesis caused by disrupted ligand-receptor interaction between callosal axons and midline glia cells[26-33]. Naturally, distinctive genes control important processes at different stages of callosal axogenesis. Critical disturbances prior to midline crossing may result in complete agenesis of the CC.

NeuroD2/6 DKO mice lack AC and CC, so the two cerebral hemispheres are not directly interconnected. The newborn DKO mice display grossly normal UL neuron fate specification, initial axon outgrowth and development of midline glial structures[50]. However, callosal axons defasciculate prior to midline interaction and aberrantly invade the ipsilateral CP. These characteristics make NeuroD2/6 DKO mice a novel and unique model to study callosal axon fasciculation and pathfinding at a stage before midline interaction.

5.1 NeuroD2/6 control callosal axon growth cell intrinsically

During cortical development, CPN fate specification is determined by SatB2[18]. When young SatB2+ CPNs migrate radially in IZ, they polarize and initiate medial axon outgrowth. These callosal axons carry various cell adhesion molecules that allow them to contact each other and adhere homophilically. As a result, similar axons fasciculate

and form compact fiber tracts to jointly follow the inter-hemispheric path under the influence of external signaling cues. The restoration of SatB2 expression in SatB2 deficient mice only results in partial rescue of CC formation, indicating that SatB2 instructs CC formation both cell intrinsically and extrinsically[33]. In NeuroD2/6 DKO mice, CPNs express SatB2 and grow medially oriented axon. However, these fibers defasciculate before reaching the cingulate cortex and project astray to the ipsilateral CP[50]. My first question was whether NeuroD2/6 regulate callosal axon growth mainly through cell intrinsic or extrinsic mechanisms.

I combined Cre mediated recombination under control of the endogenous NeuroD6 promoter (in NeuroD6-Cre mice) with IUE of conditional expression vectors into the embryonic brain to specifically drive gene expression in postmitotic neurons of the cerebral cortex *in vivo*. The restoration of NeuroD2/6 expression in only a small population of neocortical pyramidal neurons with minimal modification of the environment was expected to segregate cell intrinsic from cell extrinsic effects. Indeed, focal electroporation of NeuroD6 at E12.5 or NeuroD2 at E13.5 was sufficient to rescue callosal axon growth of electroporated neurons in the DKO cortex. Alterations of environmental clues in the medial cortex (that may be caused by the inactivation of NeuroD2/6) can thus not be the primary reason for CC agenesis. The primary effect of NeuroD2/6 inactivation on callosal axon guidance is thus cell intrinsic. This is also confirmed by showing that EfnA4 expression also affects callosal axon growth in a cell autonomous way, and that over-expression of a secreted EfnA4 variant has not such comparable effect in DKO mice. The cell intrinsic regulation of NeuroD2/6 in CC formation allows for convenient investigation of the underlying mechanisms by IUE of potential targeted genes.

5.2 NeuroD2/6 modulate gene expression in UL neurons without modifying cell identities and cortical lamination

Nestin is an intermediate filament protein that specifically labels RG cells and their processes. Pax6 is a fundamental coordinator for the proliferation and differentiation of APs, and thus regulates cortical size, regionalization and neuron identities[110]. Phosphorylated ERK1/2 follow a latero-medially progressive expression in the VZ during corticogenesis and reach the maximal peak at E15.5[21], which correlates with pyramidal neuron commitment. Actually, impaired UL neuron production and precocious

gliogenesis are observed in ERK1/2 mutant mice, suggesting their involvement in the timing of cortical cell differentiation[112,131]. IF staining for all these markers shows little difference in control and DKO mice. In addition, Cre (NeuroD6) expression cannot be detected in Pax6+ VZ APs. Taken together, NeuroD2/6 do not directly regulate the neurogenic differentiation of APs.

Brn1/2 are critical for the generation and positioning for UL neurons[15]. Brn2 is normally expressed in SVZ progenitors, differentiating UL neurons and particularly enriched in upper CP. Over-expression of Brn2 is able to prematurely induce the expression of SatB2[132]. Relatively normal expression levels of Brn2 and SatB2 in the NeuroD2/6 DKO CP suggest that the principal molecular identity of most UL neurons is not considerably disturbed in the DKO brains, although the migration of UL neurons may be marginally affected indicated by the disperse distribution of SatB2+ cells. In addition, Sox5 is a master regulator for the sequential specification and migration of distinct corticofugal neuron subtypes located in DL[121]. Ctip2 is another essential player in DL neurons that is required for the differentiation of Layer V neurons and patterning of their subcerebral projections[14]. In NeuroD2/6 DKO mice, both Sox5+ and Ctip2+ DL cells appear to be normally specified and laminated within the CP. In a word, the expression patterns of typical markers in the neocortex of NeuroD2/6 DKO mice suggest that the differentiation and migration of most UL and DL neurons do not critically depend on NeuroD2/6 (or compensated by ectopic NeuroD1), although the ratio of UL versus DL neurons was increased at E15.5 in the DKO mice.

Ptn is a secreted growth factor that is widely expressed in various organs, such as lung, kidney, gut and bone marrow. In the nervous system, Ptn was predicted to stimulate neurite outgrowth in rat and was originally termed neurite growth-promoting factor 1[133]. Limch1 is a microfilament associated molecule with so far unknown functions. Ptn and Limch1 are normally expressed in neocortical UL neurons and were previously used to mark distinct CPN subsets[114]. In NeuroD2/6 DKO mice, the expression levels of both factors are dramatically reduced. Additionally, the expression of Cux1, another frequently used UL marker, is also decreased in DKO brains. All these results conclusively suggest that NeuroD2/6 play vital roles in patterning expression profiles of UL neurons. The absence of Cux1 in NeuroD2/6 null neurons can be completely rescued by *in vivo* restoration of NeuroD2 expression, suggesting that Cux1 may be a

direct downstream target of NeuroD2/6. Strikingly, Cux1 plays an important role in glutamatergic synapse formation[134], which is impeded in NeuroD2/6 DKO mice[50]. Whether NeuroD factors and Cux1 regulate synaptic plasticity in the same genetic axis will be explored in the future. The maintenance of Brn2 expression and the loss of Cux1 expression in the same UL neurons of DKO mice show that Cux1 is indeed transcriptionally down-regulated (but not simply caused by the death, mis-specification or mis-migration of UL neurons).

5.3 NeuroD family transcription factors redundantly regulate cell differentiation in genetically linked pathways

The stages of neuronal differentiation in the mammalian telencephalon are defined by sequential but overlapping expression of some neuronal bHLH proteins. Ngn1 and Ngn2 are expressed in proliferating neuronal progenitors that reside in the VZ or SVZ. Ngn1/2 synergize as earliest neuronal specific determinants and facilitate the initial phase of radial migration away from the neurogenic territory[38,135,136]. Neuronally specified cells start to transiently express NeuroD1 as they are migrating in SVZ/IZ, which suggests a function in neuronal differentiation and delineates a border between precursor and postmitotic compartments. Serial expression of Ngn1/2 and NeuroD1 is conserved and also found in VZ of the developing spinal cord of frogs and rats[137]. The onset of NeuroD2/6 expression follows that of NeuroD1, and robust NeuroD2/6 expression is mostly confined to postmitotic neurons that migrate in the IZ and CP. The switch from NeuroD1 to NeuroD2/6 expression thus marks the maturation of pyramidal neurons. In contrast to Ngn1/2 deficient mice where neuronal specification was disrupted[135], NeuroD2/6 DKO mice exhibited mainly defects in later neuronal functions: impaired commissural tract formation, disorganized dendritic morphology and reduction of glutamatergic synapses[50]. Ngn1/2, NeuroD1 and NeuroD2/6 thus coordinate the sequential phases of pyramidal neuron development in the neocortex: determination, differentiation and maturation (Figure 5.1).

Neocortical neurogenesis is much more severely affected in Ngn1/2 DKO mice than either of the single mutant mice, suggesting that they share largely redundant functions[38]. Likewise, only the genetic inactivation of both NeuroD2 and NeuroD6 results in callosal agenesis and obvious abnormalities in the developing cerebral cortex[50]. In my PhD project, I have confirmed the functional redundancy of NeuroD2

and NeuroD6 by showing that single restoration of either NeuroD2 or NeuroD6 expression *in vivo* was sufficient to rescue pyramidal neuron differentiation and callosal axon growth in the NeuroD2/6 DKO mice.
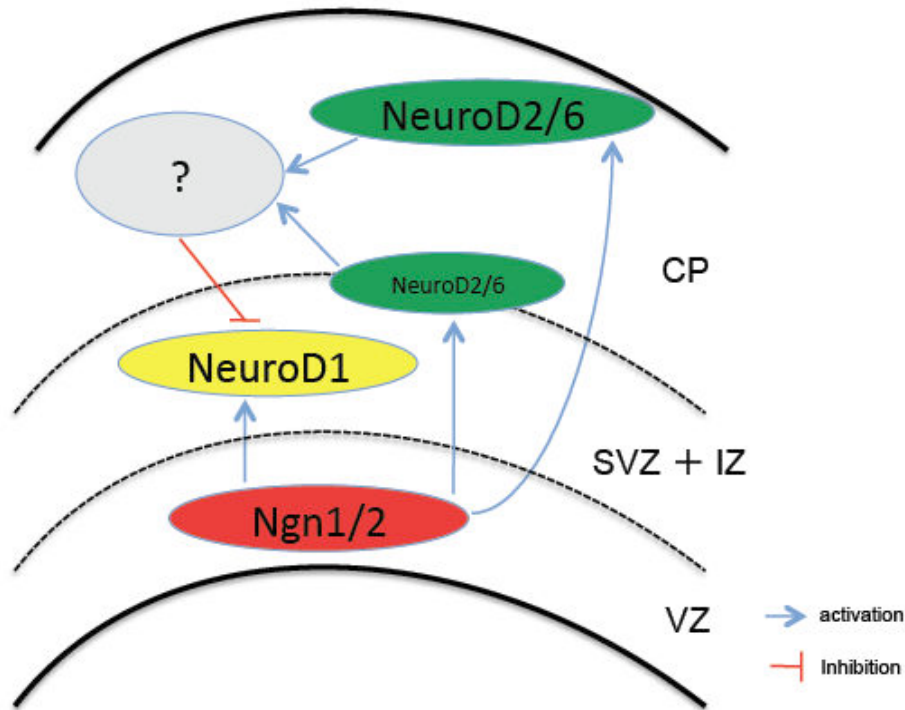

Figure 5.1: Sequential expression of proneural bHLH transcriptional factors in neocortex
Ngn1/2, NeuroD1 and NeuroD2/6 are ventro-dorsally differentially expressed in developing cerebral cortex. Ngn1/2 can promote expression of later bHLH transcriptional factors[135], however, genetic interaction between NeuroD1 and NeuroD2/6 remains still elusive.

NeuroD family TFs have long been assumed to promote neuronal survival and differentiation. Genetic deletion of NeuroD1 leads to nearly complete loss of the hippocampal dentate gyrus as a result of activated Bax-dependent apoptosis of immature granule neurons[138,139]. NeuroD2 single deficient mice show increased programmed cell death in the cerebellum and dentate gyrus[140]. Ectopic NeuroD1 expression in the CP of NeuroD2/6 DKO embryos may contribute to the rescue of NeuroD2/6 deficiency and protect NeuroD2/6 null pyramidal neurons from apoptosis and mis-differentiation. Indeed, NeuroD1/2/6 triple deficient mice, which have been generated in our lab, display massive cell death and more severe defects in neuron migration and differentiation (unpublished data, by personal communication with my colleague Olga Grishina). Nevertheless, missing expression of UL and hippocampal markers indicates merely partial substitution of NeuroD1 for NeuroD2/6. The survival of

most UL and DL pyramidal neurons, in spite of defective inter-hemispheric connectivity, in NeuroD2/6 DKO mice suggests that excitatory pyramidal neurons do not depend on extrinsic trophic factors secreted by innervated contralateral axons, unlike cerebellar granule cells[140]. Instead, the survival of cortical pyramidal neurons may largely depend on intrinsic regulation or locally diffusible signals.

Complementarily or sequentially expressed bHLH TFs can regulate cellular behaviors in a genetically related fashion. For instance, Ngn1/2 and Mash1 are mainly expressed in dorsal and ventral subpopulations of telencephalic progenitors, respectively[38]. Their reciprocally graded expression contributes to patterning neocortical regionalization, supported by the finding that Mash1 is aberrantly expressed in the dorsal lineage and activates normally ventrally specific markers in Ngn1/2 double mutant embryos[38]. In addition, over-expression of Ngn2 *in vivo* can induce later bHLH TFs, such as NeuroD1 and NeuroD2, suggesting that Ngn2 acts upstream of NeuroD1/2 to instruct neuron differentiation[135]. This idea has also been concreted by another finding that NeuroD1 expression was disrupted in Ngn2/Mash1 double mutant[38]. However, little attention has been paid to genetic relationship between NeuroD1 and NeuroD2/6 to date. In wild type brains, migrating pyramidal neurons immediately loose NeuroD1 expression as soon as they reach the CP. In my studies, I have shown that NeuroD1 is ectopically up-regulated in NeuroD2/6 null UL and DL neurons, indicating that NeuroD2/6 may regulate NeuroD1 expression *in vivo*. Considering that NeuroD2/6 serve frequently as transcription activators, it can be speculated that NeuroD2/6 induce other immediate transcription regulator(s) that in turn repress NeuroD1 expression (Figure 5.1). The hypothesized repressor(s) is/are not yet confirmed or identified, but we are recently working on the screening of potential candidates by mRNA deep sequencing.

5.4 EfnA4 restoration facilitates partial and specific rescue of callosal agenesis
The altered expression of several ephrin ligands and Eph receptors in DKO embryonic brains suggests that NeuroD2/6 are key regulators to shape expression patterns of Eph-ephrin members in cerebral neocortex. In particular, EfnA4 is most significantly decreased and directly regulated by NeuroD2/6, confirmed by *in vitro* luciferase assay. E-box motifs (CANNTG) are relatively short and unspecific consensus sequences that are universally enriched in the promoter regions of many genes. Binding preferences to a certain E-box motif are not yet clearly conclusive, but vary with different subsets of

class II bHLH TFs, dimerization partners and tissue contexts. One report has shown that heterodimers of NeuroD1 and Tcf3 preferentially bind to the motif 'CATCTG' to promote insulin gene expression in pancreas[37]. A number of potential E-box motifs cluster in six compact genomic fragments in the 5 kbp upstream of EfnA4 coding region. Our luciferase assay conclusively suggests that the EC1, which lies closest to EfnA4 transcription initiation site, contains the functional motif to promote EfnA4 expression.

Eph-ephrin family members are critically devoted to axon guidance. It is natural to speculate that defective callosal axogenesis in NeuroD2/6 DKO mice may result from altered Eph-ephrin signaling. Indeed, the restoration of EfnA4 enabled NeuroD2/6 deficient callosal axons to grow in a compact fascicle along the normal callosal trajectory. Interestingly, some of the other down-regulated ephrins seem not to be primarily involved in NeuroD2/6 dependent CC formation, suggested by the finding that the restoration of EfnA1/A3/B1 expression had little positive effect on the disturbed callosal axon growth. Therefore, I conclude that EfnA4 modulates callosal axogenesis in a relatively specific manner. Nevertheless, the observations that not all of EfnA4 restored fibers re-fasciculate in the SVZ/IZ, and that the restored fibers could reach but hardly cross the midline, indicate that EfnA4 can only partially rescue the CC agenesis in the DKO mice. This point has also been justified by fasciculation quantification. The incomplete rescue of EfnA4 suggests that there are other responsible pathways downstream of NeuroD2/6 that contribute to CC formation. Cntn2 and NfiA/B were found robustly regulated by NeuroD2/6 during my PhD project but were unfortunately ruled out, because *in vivo* gain-of-function analysis revealed no rescue in DKO brains. In our preliminary experiments, I have identified some more promising downstream candidates, including members in semaphorin – plexin signalling and Robo – slit signalling. Sema3C has been known as an important guidance cue for midline crossing of callosal projecting fibers via interaction with neuropilin receptors[34], but the roles of semaphorin – plexin interplay in CC formation are still largely unknown. So it would be a logical axis for further studies.

The simultaneous expression of Eph-ephrin members in the developing neocortex and the high promiscuity of ligand-receptor interactions prompt a question whether different receptors or ligands can actually evoke specific biological effects. Of note, EfnB1 reverse signalling functions specifically to regulate CC formation as the deletion of

EfnB1 leads to misguidance of callosal axons into the septum[62], despite of strong EfnB2 expression in UL neurons of the developing neocortex, as is shown in my ISH and others' published data (Allen Brain Institute). This suggests that EfnB2 cannot compensate for the loss of EfnB1 to regulate the interaction between callosal axons and midline glia cells. Another well-studied example for inter-areal wring is the establishment of cortico-thalamic topography, during which EfnA5 with regional and graded expression pattern acts as a unique instructor for EphA receptor positive axons[67]. Other ephrinA ligands, such as EfnA1 and EfnA2, are universally distributed in the neocortex and seem incapable to influence the targeted migration of these axons. Additionally, Prof. Pasko Rakic's group have reported that the interaction of EphA receptors and ephrinA ligands is crucial for radial columnar integration of glutamatergic excitatory neurons in the neocortex by demonstrating that over-expression of EphA7 in mouse neocortex induced abnormal clonal columnar aggregation[141]. I observed the similar phenomena when I electroporated EfnA1 and EfnB1, but not EfnA3 or EfnA4, in my studies. This finding implies that some ephrin ligands can regulate neuronal columnar organization in neocortex via activating EphA7 forward signaling while the others cannot. In a word, Eph-ephrin family members may have interactive and functional specificity in different *in vivo* scenarios, though the biochemical basis of their distinction still requires more investigation. Given that EfnA4 is phylogenetically more divergent than any other A subclass ligands[56], the specificity of EfnA4 mediated rescue is not supposed to be a surprise.

Regarding to EphA receptors, gain-of-function analysis for EphA3/A4 and the ectopic up-regulation of EphA2 jointly imply that EphA forward signaling are not critically involved in CC formation downstream of NeuroD2/6. The increased EphA2 expression in DKO brains may compensate for the reduction of EphA3/A4 receptors. Considering the universal importance of EphA forward signaling during embryogenesis, genetic redundancy via responsive backup circuits can be hypothesized for these receptors. The issue whether ectopic EphA2 expression in the DKO brains is due to up-regulation of NeuroD1 will be addressed using NeuroD1/2/6 triple deficient mice as a tool in the near future.

5.5 EfnA4/Ntrk2 reverse signaling promotes callosal axon fasciculation and guidance

Ctip2 can facilitate the fasciculation of subcerebral projection axons, which is supported by the finding that axonal bundling is acutely disturbed in internal capsule in Ctip2 mutant mice[142]. Neocortical Ctip2 expression is strongest in subcerebrally projecting pyramidal neurons in layer V and is repressed by SatB2 in UL CPNs[18]. Axonal fasciculation of CPNs must thus be controlled by other factors than Ctip2. SatB2 is an obvious candidate, but in SatB2 deficient mice, callosal axons do not defasciculate in the ipsilateral cortex but instead project subcerebrally[17]. We have recently showed that NeuroD2/6 are essential for axon guidance and fasciculation of callosal, but not subcerebral, projection axons[50]. Here, I identified reverse signaling from Eph receptors to EfnA4/Ntrk2 as underlying mechanism.

It has long been known that ephrinAs are classic ligands to activate EphA forward signaling on the receptor side. As ephrinAs are GPI-anchored and lack any intracellular domain, it was a surprise to many, when ephrinAs were reported to also mediate reverse signaling via interactions with other transmembrane co-receptors on the ligand side. My initial observation that EfnA4 was normally expressed in the CP of developing neocortex but nearly entirely lost in NeuroD2/6 DKO mice did not provide any information on which signaling mode of EfnA4 is involved in CC formation. The forward signaling (activated by EfnA4) in the ipsilateral neocortex could in principle influence the patterning of cingulate cortical neurons, midline glia cells and in turn callosal axon projection. EfnA4 reverse signaling could also influence outgrowing axons of CPNs cell autonomously. To study the functional mode of EfnA4 in callosal axon growth, I adopted a modified variant of EfnA4, which was experimentally verified to be detached from the cell membrane and secreted into the extracellular space. The secreted EfnA4 variant (with intact ephrin domain) is supposed to still interact with Eph receptors but has no means to initiate reverse signaling in the host cells. I used IUE to over-express the secreted EfnA4 variant in the developing neocortex of NeuroD2/6 DKO mice. In contrast to WT EfnA4, the secreted variant was not able to rescue targeted callosal axon growth. This suggests that EfnA4 does directly modulate the behaviors of callosal growth cones via reverse signaling, rather than influence the environment of the CT via activating forward signaling.

For functional reverse signaling, EfnA4 needs to pair with membrane associated co-receptors. Co-localization of EfnA4 and the potential co-receptor(s) is an apparent prerequisite for their *cis* interaction. Among the known co-receptors of ephrinAs, p75 and Ret were excluded as they were not co-expressed with EfnA4 in the neocortex of control or DKO mice. In cultured retinal ganglion neurons, EfnA5 and EfnA6 can interact with Ntrk receptors and promote axonal branching whereas this effect can be antagonized by environmental EphA7-Fc[115]. However, the biological relevance of EfnAs/Ntrks reverse signaling *in vivo* remains still ambiguous. In my studies, the interaction of EfnA4 and Ntrk2/3 was verified by co-IP using transfected HEK293 cells. Subsequently, I confirmed that EfnA4 mediated reverse signaling was Ntrk2 dependent, by showing that co-expressed kinase-dead Ntrk2, but not WT Ntrk2, abolished the positive effect promoted by EfnA4 in the callosal axons of NeuroD2/6 DKO embryos. This suggests that Ntrk2 might be a relevant EfnA4 co-receptor to promote the guidance and fasciculation of callosal fibers. Besides, fasciculation quantification was also supportive to this idea. The EfnA4/Ntrk2 functional specificity was again underlined by the observation that co-expression of kinase-dead Ntrk3 with EfnA4 did not interfere with EfnA4 mediated fasciculation. These data have provided the first evidence, to my knowledge, that EfnA4 and Ntrk2 can functionally interact *in vivo* and influence callosal axonal behaviors via reverse signaling. In favour of this point, the thickness of CC has been found substantially reduced in Ntrk2 deficient mice, implicating that Ntrk2 signaling indeed plays vital roles in CC development[143].

While Ntrk2 and Ntrk3 share similar molecular structures, they frequently play distinctive roles during the development of nervous system. This is firstly supported by differential roles that their high-affinity ligands play in the same biological context. For instance, in cultured cerebellar granule cells, BDNF contributes to the promotion of neurite outgrowth, but NT-3 tends to pattern neurite morphology[144]. Using the genetically modified mouse model, where the coding sequence of BDNF was substituted by that of NT-3, Patrik Ernfors' lab argued that BDNF and NT-3 preferentially induced different groups of neuro-peptides and calcium binding proteins, and thus diverse neuro-physiological properties in the brain[145]. Surprisingly, BDNF and NT-3 act antagonistically in neocortical pyramidal neurons. BDNF can inhibit the dendritic growth encouraged by NT-3 in layer VI neurons, and vice versa in layer IV neurons in the neocortex[146]. The functional inequivalence of Ntrk2 and Ntrk3 is also reflected by the

phenotypic differences of Ntrk2 and Ntrk3 deficient mice. Genetic inactivation of Ntrk2 results in apoptotic loss of trigeminal, nodose and petrosal sensory ganglion cells and facial motor nuclei[147], while genetic deletion of Ntrk3 mainly affects axon myelination and thus leads to severe loss of functional innervation of Ia muscle afferents[148]. So Ntrk2 and Ntrk3 normally regulate different biological processes despite of their widely overlapping expression in nervous system. However, compensatory mechanisms may exist in Ntrk2 dependent callosal axon growth, as some callosal fibers can still make inter-hemispheric connection in Ntrk2 deficient mice[149].

5.6 EfnA4/Ntrk2 interaction modulates the intracellular cascades of Ntrk2 *in vitro* and *in vivo*

Interaction with ephrinAs can help the co-receptors selectively activate distinct downstream pathway(s). For example, EfnA2/5 interact with p75NTR receptor and predominantly activate Fyn kinase to steer retinocollicular axon projection instead of the more often employed signaling cascades, such as c-Jun N-terminal kinase and nuclear factor-kappaB[117]. Ntrk1 activation, by recruitment of EfnA5, up-regulates the phosphorylation of pAKT S473 up to three folds, but not of pERK1/2 or pPLCγ1, to regulate axon branching[115]. To study the biological consequences of EfnA4/Ntrk2 interaction, I firstly compared phosphorylation levels of pAKT, pERK1/2 and pPLCγ1 in HEK293 cells that were transiently transfected with Ntrk2 alone or co-transfected with EfnA4/Ntrk2. Relatively quantification (normalized to α tubulin or total homogeneous protein level) indicates the proportional changes of the phosphorylated targets in total cellular proteins and homotypic proteins, respectively. It turned out that introduction of EfnA4 in Ntrk2 expressing cells could enhance the phosphorylation of AKT at T308 and S473 up to approximately 2 folds and 1.5 folds, respectively. These data are in agreement with the above-mentioned findings that EfnA5 increases pAKT S473 to promote axon branching[115], and that EfnA4 reverse signaling induces stronger phosphorylation of AKT in Jurkat TAg cell line[75]. In contrast, the phosphorylation level of pPLCγ1 was substantially reduced in the presence of EfnA4 regardless of BDNF stimuli. Phosphorylated ERK1/2 levels were mildly down-regulated in EfnA4 positive cells when not exposed to extra BDNF. Taken together, EfnA4/Ntrk2 interplay appears to bias Ntrk2 towards pAKT signaling at expenses of the other targets *in vitro*. Interestingly, down-regulation of pPLCγ1 and pERK1/2 was not found in retinal PC12 cell line

employed in the research of Prof. Uwe Dresher's group[115]. This may possibly due to different cellular contexts and methodologies.

When I verified the kinased-dead Ntrk2/3 variants, I also found that WT Ntrk2/3 could be moderately activated in cultured HEK293 cells in serum free DMEM media. This might result from some unknown activating tropic factor(s) in the media or from uncanonical activation of these receptors. A recent piece of work has showed that epidermal growth factor (EGF) mediated Src kinases are able to trans-activate Ntrk2/3 in the absence of cognate ligands[150]. Under such circumstance, application of extra ligands *in vitro* could lead to Ntrk2/3 hyper-activation. This might be an explanation why the short pulse of BDNF up-regulated pERK1/2 extraordinarily in both Ntrk2 alone or EfnA4/Ntrk2 transfected cells to the comparable levels. Stronger endogenous AKT phosphorylation might mask similar effects of BDNF stimulation on pAKT levels.

As EfnA4 expression is significantly reduced in the neocortex of NeuroD2/6 DKO embryos, it was anticipated that the phosphorylation levels of Ntrk2 downstream effectors might display contrary alterations to those in HEK293 cells. Indeed, it is true for AKT signaling, by showing that pAKT phosphorylation levels were reproducibly reduced by approximately 25% at T308 and 20% at S473. Nonetheless, pPLCγ1 was also dramatically reduced in E18.5 DKO cortex in contrast to the *in vitro* data. This discordance may imply that other regulators of PLCγ1 expression or phosphorylation are dys-regulated by genetic deletion of NeuroD2/6. Phosphorylated ERK1/2 are predominantly expressed in the VZ according to my results. Considering that NeuroD family TFs mainly regulate the functions of postmitotic neurons, and that EfnA4 expression is unchanged in the VZ, it is hardly likely that pERK1/2 are regulated through NeuroD2/6-EfnA4 axis in the cortical plate. Collectively, the most plausible mechanism is that EfnA4/Ntrk2 regulate callosal axon fasciculation and guidance via activation of pAKT signaling *in vivo*.

5.7 EfnA4/Ntrk2 functional reverse signaling depends on SHC-binding tyrosine
To further investigate which intracellular cascade is actually functional in callosal axon growth, I generated the Ntrk2 variants carrying binding-site specific mutations (Y515F and Y816F). These mutant variants of Ntrk2 are supposed to interfere with the docking and activation of SHC (Y515F) and PLCγ1 (Y816F), respectively. *In vivo* functional

interference indicates that disruption of SHC binding, but not PLCγ1 binding, specifically abolished EfnA4/Ntrk2 mediated rescue. This finding and fasciculation quantification data jointly suggest that SHC-binding tyrosine is necessary for fasciculate callosal axon growth, which in turn highlights our speculation that pAKT cascades are effective for CC formation.

AKT signaling cascades have been reported to regulate different aspects of axonal morphogenesis, including distal branching to enlarge growth cone areas, lengthening and resistance to growth cone collapses[86,88,90,151]. Moreover, several research groups have found that PI3K-pAKT signaling is locally activated in axon growth cones and contributes to remodelling of cytoskeletal components[152–154], which is a requisite for axonal guidance. Most of mentioned studies, nonetheless, are based on cultured neurons. Here, I suggest that Ntrk2-pAKT signaling *in vivo* promotes the fasciculation and guidance of callosal projection axons. In fact, AKT isoforms have been reported to be potentially associated with CC agenesis in human patients[155,156].

5.8 A hypothesized working model: EphA/EfnA4/Ntrk2 form a protein complex to modulate callosal axon guidance

A central issue for a migrating growth cone exposed to various guidance cues is how to coordinate different responses into coalescent information. Researchers have once claimed that one advantage of ephrinA/co-receptor complexes may be the integration of short- and long-range signals[77]. To extend our understanding of EfnA4/Ntrk2 interplay in this aspect, a mutated variant of EfnA4 (EfnA4^{E126K}), which was unable to interact with EphA receptors, was generated and characterized in my project. Here, I have reported that EphA/EfnA4/Ntrk2 interact in the same protein complex with EfnA4 as an intermediary, by showing that Ntrk2 could be precipitated by EphA4-Fc-6His via EfnA4, but not EfnA4^{E126K}. Combining the pull-down assay and gain-of-function analysis of EfnA4^{E126K}, dual roles of EfnA4 may be suggested in callosal axon growth: firstly, a regulator for Ntrk2 signaling to promote axonal fasciculation and growth; secondly, a sensor for EphA expression to guide axons turning ventrally away from the cingulate cortex towards the midline. Therefore, EphA/EfnA4/Ntrk2 complex synergizes diffusible (BDNF, NT-4 or EGF) and local (EphAs) signals in the developing cerebral cortex. More evidence may still be needed to confirm my hypothesis.

In embryonic control brains, EphA4 and EphA5 are robustly expressed in VZ and CP in cerebral cortex, delineating a cell sparse channel in the SVZ/IZ where callosal axons normally navigate. In the NeuroD2/6 DKO brains, EphA2 is ectopically expressed in the VZ and CP, highlighting the necessity of bilateral expression patterns of EphA receptors. Given that EphAs/ephrinAs interactions more frequently promote repulsive axon migration *in vivo*, I assume that the expression of EphA receptors may form a permissive corridor to confine EfnA4 positive callosal fibers to the typical callosal path. Thus, I have proposed a functional model for EphA/EfnA4/Ntrk2 regulation (Figure 5.2). Currently, the experiments to examine whether callosal axons carrying EfnA4 truly migrate repulsively in response to EphA expression are ongoing.
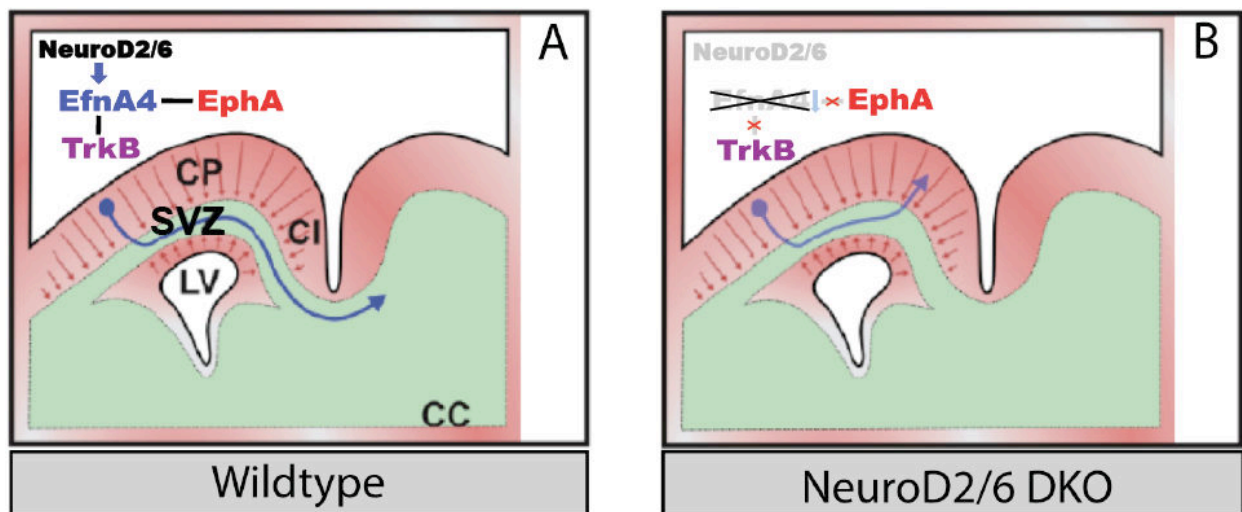

Figure 5.2: A functional model for Eph/EfnA4/Ntrk2 interaction in callosal axon growth
(A and B) The expression of EphA4 receptors (red) creates a permissive corridor in the SVZ/IZ for medially projecting and EfnA4/Ntrk2 (TrkB) expressing callosal axons in WT brains. Molecularly, EfnA4 (regulated by NeuroD2/6) interacts with Ntrk2 and EphA receptors simultaneously to promote fasciculate callosal axon growth along the cingulate cortex towards the midline (A). However, the proper guidance is disrupted in the NeuroD2/6 DKO brains due to loss of EfnA4, the intermediary of Ntrk2 and EphA receptors (B).

5.9 Dynamic balance of forward and reverse signals may count

My ISH data have demonstrated that both Eph receptors and ephrin ligands are expressed in cortical projection neurons. They may simultaneously transduce forward and reverse signaling in the same cells. The intake information may be conflicting, prompting a principal question how an axon eventually decides where to go. It has been suggested that high level of ephrin ligands can sequester Eph receptors from *trans*

activation via *cis* interaction[72]. Another elegant piece of work has demonstrated that the receptors and ligands are segregated in different sub-compartments on plasma membrane of growth cones to mediate binary signaling: EphA forward signaling tends to trigger growth cone collapse while ephrinA reverse signaling promotes growth cone survival using cultured motor neurons as a model[69]. The authors suggest that the eventual decision on growth cone collapse/survival rather relies on the relative levels of signal input from receptors and ligands as well as their subcellular localization. Given that the expression of ephrin ligands decreases while EphA2 expression increases in NeuroD2/6 DKO brains, the biological equilibrium of forward and reverse signaling may have been shifted towards the growth restricting effects of EphAs, as therefore contributes to defective axon growth.

5.10 NeuroD2/6 regulate cell differentiation via both intrinsic and extrinsic mechanisms

The corticogenesis is a highly spatio-temporally regulated process: neurogenesis (first DL neuron production followed by UL neuron production) and gliogenesis occurred sequentially. The progressive cell specification and differentiation are controlled by orchestrated efforts of intrinsic TF regulation and extrinsic feedback signals[7]. Double positive IF staining for Cre (NeuroD6) and Tbr2 (but not Pax6) can be detected in E12.5 and E18.5 control brains, and particularly in ectopically accumulative Tbr2+ cells in E18.5 DKO brains. These data imply that NeuroD6 is constantly expressed in a subset of Tbr2+ BPs. In addition, *in vivo* over-expression of NeuroD2/6 directly converted Tbr2+ progenitors into postmitotic neurons and markedly down-regulated the expression of Hes5, a differentiation inhibitor. Taken together, my results conclusively suggest that NeuroD2/6 positively regulate neuronal differentiation of Tbr2+ progenitors in a cell intrinsic manner during cortical development. Surprisingly, Pax6+ APs were also prematurely exhausted by NeuroD2/6 over-expression. The Cre dependent recombination (under control of the endogenous NeuroD6 promoter) does not happen in Pax6+ progenitors, as is confirmed by the finding that Cre protein was hardly detectable in these cells by IF staining. So the Cre-activatable restoration of NeuroD2/6 was not expected in Pax6+ APs. Whether the absence of Pax6+ APs in the NeuroD2/6 electroporation areas was simply an experimental artifact remains to be a question. However, another attractive hypothesis should not be disregarded: an extrinsic feedback signaling from Tbr2+ to Pax6+ cells might exist to regulate the apical-to-basal

progenitor conversion, which was locally affected by the premature differentiation of Tbr2+ progenitors in the NeuroD2/6 electroporation areas. More experiments will be performed in the future to address this issue.

During early neurogenesis (E12.5 – E14.5), NeuroD2/6 may play an important role in establishment of neuron identities, indicated by increased UL and decreased DL in the E15.5 DKO brains. However, whether the mechanism(s) is/are intrinsic or extrinsic remains still inconclusive. During late neurogenesis (E15.5 – E17.5), NeuroD2/6 can promote the differentiation of Tbr2+ progenitors, most likely into UL neurons, based on the observation that the majority of ectopic Tbr2+ cells were produced at E15.5 and E16.5. This finding also provides us an explanation for the paradox - the Satb2+ UL neurons appear to be increased in the E15.5 DKO neocortex (A' and D', Figure 4.20) but eventually reduced at E18.5 (D, Figure 4.2). The total number of Satb2+ cells in E18.5 DKO neocortex may be a combined consequence of earlier and later UL neuron production. Gliogenesis normally arises along with the ending of neurogenesis. It is surprising to find that the number of Olig2+ glial progenitors in E18.5 DKO brains is significantly increased. Considering the mutually exclusive expression of Cre (NeuroD6) and Olig2, the phenotype must be caused by diffusible environmental factors (cell extrinsically). In one word, NeuroD2/6 may regulate cell specification and differentiation of different progenitor populations at different developmental stages via either intrinsic or extrinsic mechanisms.

6. References:

1. Fishell, G. & Hanashima, C. Pyramidal Neurons Grow Up and Change Their Mind. *Neuron* **57,** 333–338 (2008).
2. Götz, M. & Huttner, W. B. The cell biology of neurogenesis. *Nat. Rev. Mol. Cell Biol.* **6,** 777–788 (2005).
3. Noctor, S. C., Martinez-Cerdeno, V., Ivic, L. & Kriegstein, A. R. Cortical neurons arise in symmetric and asymmetric division zones and migrate through specific phases. *Nat Neurosci* **7,** 136–144 (2004).
4. Anthony, T. E., Klein, C., Fishell, G. & Heintz, N. Radial Glia Serve as Neuronal Progenitors in All Regions of the Central Nervous System. *Neuron* **41,** 881–890 (2004).
5. Tabata, H., Kanatani, S. & Nakajima, K. Differences of Migratory Behavior between Direct Progeny of Apical Progenitors and Basal Progenitors in the Developing. *Cereb. Cortex* **19,** 2092–2105 (2009).
6. Kowalczyk, T. *et al.* Intermediate Neuronal Progenitors (Basal Progenitors) Produce Pyramidal–Projection Neurons for All Layers of Cerebral Cortex. *Cereb. Cortex N. Y. NY* **19,** 2439–2450 (2009).
7. Greig, L. C., Woodworth, M. B., Galazo, M. J., Padmanabhan, H. & Macklis, J. D. Molecular logic of neocortical projection neuron specification, development and diversity. *Nat. Rev. Neurosci.* **14,** 755–769 (2013).
8. Molyneaux, B. J., Arlotta, P., Menezes, J. R. L. & Macklis, J. D. Neuronal subtype specification in the cerebral cortex. *Nat Rev Neurosci* **8,** 427–437 (2007).
9. Bayatti, N. *et al.* Progressive loss of PAX6, TBR2, NEUROD and TBR1 mRNA gradients correlates with translocation of EMX2 to the cortical plate during human cortical development. *Eur. J. Neurosci.* **28,** 1449–1456 (2008).
10. Muzio, L. & Mallamaci, A. Emx1, emx2 and pax6 in specification, regionalization and arealization of the cerebral cortex. *Cereb. Cortex N. Y. N 1991* **13,** 641–647 (2003).
11. Sessa, A., Mao, C., Hadjantonakis, A.-K., Klein, W. H. & Broccoli, V. Tbr2 Directs Conversion of Radial Glia into Basal Precursors and Guides Neuronal Amplification by Indirect Neurogenesis in the Developing Neocortex. *Neuron* **60,** 56–69 (2008).
12. Bedogni, F. *et al.* Tbr1 regulates regional and laminar identity of postmitotic neurons in developing neocortex. *Proc. Natl. Acad. Sci.* **107,** 13129–13134 (2010).
13. Han, W. *et al.* TBR1 directly represses Fezf2 to control the laminar origin and development of the corticospinal tract. *Proc. Natl. Acad. Sci.* **108,** 3041–3046 (2011).
14. Chen, B. *et al.* The Fezf2–Ctip2 genetic pathway regulates the fate choice of subcortical projection neurons in the developing cerebral cortex. *Proc. Natl. Acad. Sci.* **105,** 11382–11387 (2008).
15. Sugitani, Y. *et al.* Brn-1 and Brn-2 share crucial roles in the production and positioning of mouse neocortical neurons. *Genes Dev.* **16,** 1760–1765 (2002).
16. Franco, S. J. *et al.* Fate-Restricted Neural Progenitors in the Mammalian Cerebral Cortex. *Science* **337,** 746–749 (2012).
17. Britanova, O. *et al.* Satb2 Is a Postmitotic Determinant for Upper-Layer Neuron Specification in the Neocortex. *Neuron* **57,** 378–392 (2008).
18. Alcamo, E. A. *et al.* Satb2 regulates callosal projection neuron identity in the developing cerebral cortex. *Neuron* **57,** 364–377 (2008).
19. D'Arcangelo, G. Reelin mouse mutants as models of cortical development disorders. *Epilepsy Behav. EB* **8,** 81–90 (2006).
20. Assadi, A. H. *et al.* Interaction of reelin signaling and Lis1 in brain development. *Nat. Genet.* **35,** 270–276 (2003).

21.   Seuntjens, E. *et al.* Sip1 regulates sequential fate decisions by feedback signaling from postmitotic neurons to progenitors. *Nat. Neurosci.* **12,** 1373–1380 (2009).

22.   Shimogori, T., Banuchi, V., Ng, H. Y., Strauss, J. B. & Grove, E. A. Embryonic signaling centers expressing BMP, WNT and FGF proteins interact to pattern the cerebral cortex. *Dev. Camb. Engl.* **131,** 5639–5647 (2004).

23.   Fukuchi-Shimogori, T. & Grove, E. A. Neocortex patterning by the secreted signaling molecule FGF8. *Science* **294,** 1071–1074 (2001).

24.   Paul, L. K. *et al.* Agenesis of the corpus callosum: genetic, developmental and functional aspects of connectivity. *Nat. Rev. Neurosci.* **8,** 287–299 (2007).

25.   Richards, L. J., Plachez, C. & Ren, T. Mechanisms regulating the development of the corpus callosum and its agenesis in mouse and human. *Clin. Genet.* **66,** 276–289 (2004).

26.   Robichaux, M. A. *et al.* EphB1 and EphB2 intracellular domains regulate the formation of the corpus callosum and anterior commissure. *Dev. Neurobiol.* n/a-n/a (2015). doi:10.1002/dneu.22323

27.   Hu, Z. *et al.* Corpus Callosum Deficiency in Transgenic Mice Expressing a Truncated Ephrin-A Receptor. *J. Neurosci.* **23,** 10963–10970 (2003).

28.   Nishikimi, M., Oishi, K., Tabata, H., Torii, K. & Nakajima, K. Segregation and Pathfinding of Callosal Axons through EphA3 Signaling. *J. Neurosci.* **31,** 16251–16260 (2011).

29.   Andrews, W. *et al.* Robo1 regulates the development of major axon tracts and interneuron migration in the forebrain. *Development* **133,** 2243–2252 (2006).

30.   López-Bendito, G. *et al.* Robo1 and Robo2 Cooperate to Control the Guidance of Major Axonal Tracts in the Mammalian Forebrain. *J. Neurosci.* **27,** 3395–3407 (2007).

31.   Unni, D. K. *et al.* Multiple Slits regulate the development of midline glial populations and the corpus callosum. *Dev. Biol.* **365,** 36–49 (2012).

32.   Keeble, T. R. *et al.* The Wnt Receptor Ryk Is Required for Wnt5a-Mediated Axon Guidance on the Contralateral Side of the Corpus Callosum. *J. Neurosci.* **26,** 5840–5848 (2006).

33.   Srivatsa, S. *et al.* Unc5C and DCC act downstream of Ctip2 and Satb2 and contribute to corpus callosum formation. *Nat. Commun.* **5,** (2014).

34.   Niquille, M. *et al.* Transient Neuronal Populations Are Required to Guide Callosal Axons: A Role for Semaphorin 3C. *PLoS Biol* **7,** e1000230 (2009).

35.   Piper, M. *et al.* Neuropilin 1-Sema Signaling Regulates Crossing of Cingulate Pioneering Axons during Development of the Corpus Callosum. *Cereb. Cortex* **19,** i11–i21 (2009).

36.   Giger, R. J. *et al.* Neuropilin-2 Is Required In Vivo for Selective Axon Guidance Responses to Secreted Semaphorins. *Neuron* **25,** 29–41 (2000).

37.   Longo, A., Guanga, G. P. & Rose, R. B. Crystal Structure of E47−NeuroD1/Beta2 bHLH Domain−DNA Complex: Heterodimer Selectivity and DNA Recognition†,‡. *Biochemistry (Mosc.)* **47,** 218–229 (2008).

38.   Fode, C. *et al.* A role for neural determination genes in specifying the dorsoventral identity of telencephalic neurons. *Genes Dev.* **14,** 67–80 (2000).

39.   Castro, D. S. *et al.* Proneural bHLH and Brn Proteins Coregulate a Neurogenic Program through Cooperative Binding to a Conserved DNA Motif. *Dev. Cell* **11,** 831–844 (2006).

40.   Ono, K., Takebayashi, H. & Ikenaka, K. Olig2 transcription factor in the developing and injured forebrain; cell lineage and glial development. *Mol. Cells* **27,** 397–401 (2009).

41.   Wegener, A. *et al.* Gain of Olig2 function in oligodendrocyte progenitors promotes remyelination. *Brain* **138,** 120–135 (2015).

42.   Bermingham, N. A. *et al.* Math1: An Essential Gene for the Generation of Inner Ear Hair Cells. *Science* **284,** 1837–1841 (1999).

43. Helms, A. W. & Johnson, J. E. Progenitors of dorsal commissural interneurons are defined by MATH1 expression. *Development* **125,** 919–928 (1998).

44. Bermingham, N. A. *et al.* Proprioceptor pathway development is dependent on Math1. *Neuron* **30,** 411–422 (2001).

45. Ledent, V., Paquet, O. & Vervoort, M. Phylogenetic analysis of the human basic helix-loop-helix proteins. *Genome Biol.* **3,** research0030.1-research0030.18 (2002).

46. Lee, J. E. *et al.* Conversion of Xenopus ectoderm into neurons by NeuroD, a basic helix-loop-helix protein. *Science* **268,** 836–844 (1995).

47. Liu, M. *et al.* Loss of BETA2/NeuroD leads to malformation of the dentate gyrus and epilepsy. *Proc. Natl. Acad. Sci. U. S. A.* **97,** 865–870 (2000).

48. Miyata, T., Maeda, T. & Lee, J. E. NeuroD is required for differentiation of the granule cells in the cerebellum and hippocampus. *Genes Dev.* **13,** 1647–1652 (1999).

49. Ince-Dunn, G. *et al.* Regulation of Thalamocortical Patterning and Synaptic Maturation by NeuroD2. *Neuron* **49,** 683–695 (2006).

50. Bormuth, I. *et al.* Neuronal Basic Helix–Loop–Helix Proteins Neurod2/6 Regulate Cortical Commissure Formation before Midline Interactions. *J. Neurosci.* **33,** 641–651 (2013).

51. Cherry, T. J. *et al.* NeuroD Factors Regulate Cell Fate and Neurite Stratification in the Developing Retina. *J. Neurosci.* **31,** 7365–7379 (2011).

52. Ravanpay, A. C. & Olson, J. M. E protein dosage influences brain development more than family member identity. *J. Neurosci. Res.* **86,** 1472–1481 (2008).

53. Wu, S.-X. *et al.* Pyramidal neurons of upper cortical layers generated by NEX-positive progenitor cells in the subventricular zone. *Proc. Natl. Acad. Sci. U. S. A.* **102,** 17172–17177 (2005).

54. Klein, R. Eph/ephrin signalling during. *Development* **139,** 4105–4109 (2012).

55. Kullander, K. & Klein, R. Mechanisms and functions of eph and ephrin signalling. *Nat. Rev. Mol. Cell Biol.* **3,** 475–486 (2002).

56. Pasquale, E. B. Eph–ephrin promiscuity is now crystal clear. *Nat. Neurosci.* **7,** 417–418 (2004).

57. Himanen, J.-P. *et al.* Repelling class discrimination: ephrin-A5 binds to and activates EphB2 receptor signaling. *Nat. Neurosci.* **7,** 501–509 (2004).

58. Shamah, S. M. *et al.* EphA receptors regulate growth cone dynamics through the novel guanine nucleotide exchange factor ephexin. *Cell* **105,** 233–244 (2001).

59. Xu, N.-J. & Henkemeyer, M. Ephrin-B3 reverse signaling through Grb4 and cytoskeletal regulators mediates axon pruning. *Nat Neurosci* **12,** 268–276 (2009).

60. Galian, C., Bjorkholm, P., Bulleid, N. & von Heijne, G. Efficient Glycosylphosphatidylinositol (GPI) Modification of Membrane Proteins Requires a C-terminal Anchoring Signal of Marginal Hydrophobicity. *J. Biol. Chem.* **287,** 16399–16409 (2012).

61. Janes, P. W. *et al.* Adam Meets Eph: An ADAM Substrate Recognition Module Acts as a Molecular Switch for Ephrin Cleavage In trans. *Cell* **123,** 291–304 (2005).

62. Bush, J. O. & Soriano, P. Ephrin-B1 regulates axon guidance by reverse signaling through a PDZ-dependent mechanism. *Genes Dev.* **23,** 1586–1599 (2009).

63. Henkemeyer, M. *et al.* Nuk Controls Pathfinding of Commissural Axons in the Mammalian Central Nervous System. *Cell* **86,** 35–46 (1996).

64. Orioli, D., Henkemeyer, M., Lemke, G., Klein, R. & Pawson, T. Sek4 and Nuk receptors cooperate in guidance of commissural axons and in palate formation. *EMBO J.* **15,** 6035–6049 (1996).

65. Kullander, K. *et al.* Kinase-Dependent and Kinase-Independent Functions of EphA4 Receptors in Major Axon Tract Formation In Vivo. *Neuron* **29,** 73–84 (2001).

66.   Klein, R. Eph/ephrin signaling in morphogenesis, neural development and plasticity. *Curr. Opin. Cell Biol.* **16,** 580–589 (2004).

67.   Torii, M. & Levitt, P. Dissociation of Corticothalamic and Thalamocortical Axon Targeting by an EphA7-Mediated Mechanism. *Neuron* **48,** 563–575 (2005).

68.   Drescher, U. w. e. & Knoell, B. Axon guidance processes in the retinotectal and vomeronasal projection are controlled by Eph receptor tyrosine kinases and ephrins1. *Zoology* **104,** 228–231 (2001).

69.   Marquardt, T. *et al.* Coexpressed EphA Receptors and Ephrin-A Ligands Mediate Opposing Actions on Growth Cone Navigation from Distinct Membrane Domains. *Cell* **121,** 127–139 (2005).

70.   Holmberg, J. & Frisén, J. Ephrins are not only unattractive. *Trends Neurosci.* **25,** 239–243 (2002).

71.   Davy, A. *et al.* Compartmentalized signaling by GPI-anchored ephrin-A5 requires the Fyn tyrosine kinase to regulate cellular adhesion. *Genes Dev.* **13,** 3125–3135 (1999).

72.   Carvalho, R. F. *et al.* Silencing of EphA3 through a cis interaction with ephrinA5. *Nat. Neurosci.* **9,** 322–330 (2006).

73.   Hornberger, M. R. *et al.* Modulation of EphA Receptor Function by Coexpressed EphrinA Ligands on Retinal Ganglion Cell Axons. *Neuron* **22,** 731–742 (1999).

74.   Konstantinova, I. *et al.* EphA-Ephrin-A-Mediated β Cell Communication Regulates Insulin Secretion from Pancreatic Islets. *Cell* **129,** 359–370 (2007).

75.   Holen, H. L. *et al.* Signaling through ephrin-A ligand leads to activation of Src-family kinases, Akt phosphorylation, and inhibition of antigen receptor-induced apoptosis. *J. Leukoc. Biol.* **84,** 1183–1191 (2008).

76.   Holmberg, J. *et al.* Ephrin-A2 reverse signaling negatively regulates neural progenitor proliferation and neurogenesis. *Genes Dev.* **19,** 462–471 (2005).

77.   Bonanomi, D. *et al.* Ret Is a Multifunctional Coreceptor that Integrates Diffusible- and Contact-Axon Guidance Signals. *Cell* **148,** 568–582 (2012).

78.   Knoll, B., Zarbalis, K., Wurst, W. & Drescher, U. A role for the EphA family in the topographic targeting of vomeronasal axons. *Development* **128,** 895–906 (2001).

79.   Klein, R. *et al.* The trkB tyrosine protein kinase is a receptor for brain-derived neurotrophic factor and neurotrophin-3. *Cell* **66,** 395–403 (1991).

80.   Barbacid, M. Structural and Functional Properties of the TRK Family of Neurotrophin Receptors. *Ann. N. Y. Acad. Sci.* **766,** 442–458 (1995).

81.   Minichiello, L. TrkB signalling pathways in LTP and learning. *Nat. Rev. Neurosci.* **10,** 850–860 (2009).

82.   Huang, E. J. & Reichardt, L. F. NEUROTROPHINS: Roles in Neuronal Development and Function1. *Annu. Rev. Neurosci.* **24,** 677–736 (2001).

83.   Reichardt, L. F. Neurotrophin-regulated signalling pathways. *Philos. Trans. R. Soc. Lond. B Biol. Sci.* **361,** 1545–1564 (2006).

84.   Roskoski Jr., R. ERK1/2 MAP kinases: Structure, function, and regulation. *Pharmacol. Res.* **66,** 105–143 (2012).

85.   Avruch, J. MAP kinase pathways: The first twenty years. *Biochim. Biophys. Acta BBA - Mol. Cell Res.* **1773,** 1150–1160 (2007).

86.   Dajas-Bailador, F., Bantounas, I., Jones, E. V. & Whitmarsh, A. J. Regulation of axon growth by the JIP1–AKT axis. *J. Cell Sci.* **127,** 230–239 (2014).

87.   Meli, R., Weisová, P. & Propst, F. Repulsive Axon Guidance by Draxin Is Mediated by Protein Kinase B (Akt), Glycogen Synthase Kinase-3β (GSK-3β) and Microtubule-Associated Protein 1B. *PLoS ONE* **10,** e0119524 (2015).

88. Atwal, J. K., Massie, B., Miller, F. D. & Kaplan, D. R. The TrkB-Shc Site Signals Neuronal Survival and Local Axon Growth via MEK and PI3-Kinase. *Neuron* **27,** 265–277 (2000).

89. Miyamoto, Y. *et al.* Akt and PP2A Reciprocally Regulate the Guanine Nucleotide Exchange Factor Dock6 to Control Axon Growth of Sensory Neurons. *Sci. Signal.* **6,** ra15-ra15 (2013).

90. Diez, H., Garrido, J. J. & Wandosell, F. Specific Roles of Akt iso Forms in Apoptosis and Axon Growth Regulation in Neurons. *PLoS ONE* **7,** e32715 (2012).

91. Martin-Zanca, D., Barbacid, M. & Parada, L. F. Expression of the trk proto-oncogene is restricted to the sensory cranial and spinal ganglia of neural crest origin in mouse development. *Genes Dev.* **4,** 683–694 (1990).

92. Mu, X., Silos-Santiago, I., Carroll, S. L. & Snider, W. D. Neurotrophin receptor genes are expressed in distinct patterns in developing dorsal root ganglia. *J. Neurosci.* **13,** 4029–4041 (1993).

93. Lamballe, F., Klein, R. & Barbacid, M. trkC, a new member of the trk family of tyrosine protein kinases, is a receptor for neurotrophin-3. *Cell* **66,** 967–979 (1991).

94. Gruart, A., Sciarretta, C., Valenzuela-Harrington, M., Delgado-García, J. M. & Minichiello, L. Mutation at the TrkB PLCγ-docking site affects hippocampal LTP and associative learning in conscious mice. *Learn. Mem.* **14,** 54–62 (2007).

95. Bartkowska, K., Paquin, A., Gauthier, A. S., Kaplan, D. R. & Miller, F. D. Trk signaling regulates neural precursor cell proliferation and differentiation during cortical. *Development* **134,** 4369–4380 (2007).

96. Nikoletopoulou, V. *et al.* Neurotrophin receptors TrkA and TrkC cause neuronal death whereas TrkB does not. *Nature* **467,** 59–63 (2010).

97. McAllister, A. K., Lo, D. C. & Katz, L. C. Neurotrophins regulate dendritic growth in developing visual cortex. *Neuron* **15,** 791–803 (1995).

98. Gorski, J. A., Zeiler, S. R., Tamowski, S. & Jones, K. R. Brain-Derived Neurotrophic Factor Is Required for the Maintenance of Cortical Dendrites. *J. Neurosci.* **23,** 6856–6865 (2003).

99. Wilson Horch, H., Krüttgen, A., Portbury, S. D. & Katz, L. C. Destabilization of Cortical Dendrites and Spines by BDNF. *Neuron* **23,** 353–364 (1999).

100. Wirth, M. J., Brün, A., Grabert, J., Patz, S. & Wahle, P. Accelerated dendritic development of rat cortical pyramidal cells and interneurons after biolistic transfection with BDNF and NT4/5. *Development* **130,** 5827–5838 (2003).

101. Zheng, W.-H., Kar, S. & Quirion, R. FKHRL1 and its homologs are new targets of nerve growth factor Trk receptor signaling. *J. Neurochem.* **80,** 1049–1061 (2002).

102. Eide, F. F. *et al.* Naturally Occurring Truncated trkB Receptors Have Dominant Inhibitory Effects on Brain-Derived Neurotrophic Factor Signaling. *J. Neurosci. Off. J. Soc. Neurosci.* **16,** 3123–3129 (1996).

103. Wit, J. D., Eggers, R., Evers, R., Castrén, E. & Verhaagen, J. Long-Term Adeno-Associated Viral Vector-Mediated Expression of Truncated TrkB in the Adult Rat Facial Nucleus Results in Motor Neuron Degeneration. *J. Neurosci.* **26,** 1516–1530 (2006).

104. Ohira, K., Shimizu, K. & Hayashi, M. TrkB dimerization during development of the prefrontal cortex of the macaque. *J. Neurosci. Res.* **65,** 463–469 (2001).

105. Haapasalo, A. *et al.* Regulation of TRKB Surface Expression by Brain-derived Neurotrophic Factor and Truncated TRKB Isoforms. *J. Biol. Chem.* **277,** 43160–43167 (2002).

106. Du, J. *et al.* Regulation of TrkB receptor tyrosine kinase and its internalization by neuronal activity and Ca2+ influx. *J. Cell Biol.* **163,** 385–395 (2003).

107. Heerssen, H. M., Pazyra, M. F. & Segal, R. A. Dynein motors transport activated Trks to promote survival of target-dependent neurons. *Nat. Neurosci.* **7,** 596–604 (2004).

108. Götz, R. & Sendtner, M. Cooperation of Tyrosine Kinase Receptor TrkB and Epidermal Growth Factor Receptor Signaling Enhances Migration and Dispersal of Lung Tumor Cells. *PLoS ONE* **9,** e100944 (2014).

109. Subramanian, L. *et al.* Transcription factor Lhx2 is necessary and sufficient to suppress astrogliogenesis and promote neurogenesis in the developing hippocampus. *Proc. Natl. Acad. Sci. U. S. A.* **108,** E265–E274 (2011).

110. Walcher, T. *et al.* Functional dissection of the paired domain of Pax6 reveals molecular mechanisms of coordinating neurogenesis and proliferation. *Development* **140,** 1123–1136 (2013).

111. Tuoc, T. C. *et al.* Selective cortical layering abnormalities and behavioral deficits in cortex-specific Pax6 knock-out mice. *J. Neurosci. Off. J. Soc. Neurosci.* **29,** 8335–8349 (2009).

112. Samuels, I. S. *et al.* Deletion of ERK2 Mitogen-Activated Protein Kinase Identifies Its Key Roles in Cortical Neurogenesis and Cognitive Function. *J. Neurosci. Off. J. Soc. Neurosci.* **28,** 6983–6995 (2008).

113. Faedo, A. *et al.* COUP-TFI Coordinates Cortical Patterning, Neurogenesis, and Laminar Fate and Modulates MAPK/ERK, AKT, and ß-Catenin Signaling. *Cereb. Cortex N. Y. NY* **18,** 2117–2131 (2008).

114. Molyneaux, B. J. *et al.* Novel subtype-specific genes identify distinct subpopulations of callosal projection neurons. *J. Neurosci. Off. J. Soc. Neurosci.* **29,** 12343–12354 (2009).

115. Marler, K. J. M. *et al.* A TrkB/EphrinA Interaction Controls Retinal Axon Branching and Synaptogenesis. *J. Neurosci.* **28,** 12700–12712 (2008).

116. Poopalasundaram, S., Marler, K. J. M. & Drescher, U. EphrinA6 on chick retinal axons is a key component for p75NTR-dependent axon repulsion and TrkB-dependent axon branching. *Mol. Cell. Neurosci.* **47,** 131–136 (2011).

117. Lim, Y.-S. *et al.* p75NTR Mediates Ephrin-A Reverse Signaling Required for Axon Repulsion and Mapping. *Neuron* **59,** 746–758 (2008).

118. Felsenfeld, D. P., Hynes, M. A., Skoler, K. M., Furley, A. J. & Jessell, T. M. TAG-1 can mediate homophilic binding, but neurite outgrowth on TAG-1 requires an L1-like molecule and β1 integrins. *Neuron* **12,** 675–690 (1994).

119. das Neves, L. *et al.* Disruption of the murine nuclear factor I-A gene (Nfia) results in perinatal lethality, hydrocephalus, and agenesis of the corpus callosum. *Proc. Natl. Acad. Sci. U. S. A.* **96,** 11946–11951 (1999).

120. Steele-Perkins, G. *et al.* The Transcription Factor Gene Nfib Is Essential for both Lung Maturation and Brain Development. *Mol. Cell. Biol.* **25,** 685–698 (2005).

121. Lai, T. *et al.* SOX5 Controls the Sequential Generation of Distinct Corticofugal Neuron Subtypes. *Neuron* **57,** 232–247 (2008).

122. Tsui, D., Vessey, J. P., Tomita, H., Kaplan, D. R. & Miller, F. D. FoxP2 Regulates Neurogenesis during Embryonic Cortical Development. *J. Neurosci.* **33,** 244–258 (2013).

123. Wojtowicz, J. M. & Kee, N. BrdU assay for neurogenesis in rodents. *Nat. Protoc.* **1,** 1399–1405 (2006).

124. Gaiano, N. & Fishell, G. THE ROLE OF NOTCH IN PROMOTING GLIAL AND NEURAL STEM CELL FATES. *Annu. Rev. Neurosci.* **25,** 471–490 (2002).

125. Kageyama, R. & Ohtsuka, T. The Notch-Hes pathway in mammalian neural development. *Cell Res.* **9,** 179–188 (1999).

126. Marshall, C. A. G., Novitch, B. G. & Goldman, J. E. Olig2 Directs Astrocyte and Oligodendrocyte Formation in Postnatal Subventricular Zone Cells. *J. Neurosci.* **25,** 7289–7298 (2005).

127. Iavarone, A., Garg, P., Lasorella, A., Hsu, J. & Israel, M. A. The helix-loop-helix protein Id-2 enhances cell proliferation and binds to the retinoblastoma protein. *Genes Dev.* **8,** 1270–1284 (1994).

128. Paul, V. *et al.* Scratch2 Modulates Neurogenesis and Cell Migration Through Antagonism of bHLH Proteins in the Developing Neocortex. *Cereb. Cortex* (2012). doi:10.1093/cercor/bhs356

129. Tarabykin, V., Stoykova, A., Usman, N. & Gruss, P. Cortical upper layer neurons derive from the subventricular zone as indicated by Svet1 gene expression. *Development* **128,** 1983–1993 (2001).

130. Srivatsa, S., Parthasarathy, S., Molnár, Z. & Tarabykin, V. Sip1 Downstream Effector ninein Controls Neocortical Axonal Growth, Ipsilateral Branching, and Microtubule Growth and Stability. *Neuron* **85,** 998–1012 (2015).

131. Ortega, J. A. & Alcántara, S. BDNF/MAPK/ERK–Induced BMP7 Expression in the Developing Cerebral Cortex Induces Premature Radial Glia Differentiation and Impairs Neuronal Migration. *Cereb. Cortex* **20,** 2132–2144 (2010).

132. Dominguez, M. H., Ayoub, A. E. & Rakic, P. POU-III Transcription Factors (Brn1, Brn2, and Oct6) Influence Neurogenesis, Molecular Identity, and Migratory Destination of Upper-Layer Cells of the Cerebral Cortex. *Cereb. Cortex N. Y. NY* **23,** 2632–2643 (2013).

133. Garcia-Gutierrez, P. & Garcia-Dominguez, M. Pleiotrophin fights Brd2 for neuronal differentiation. *Neural Regen. Res.* **10,** 544–546 (2015).

134. Cubelos, B. *et al.* Cux1 and Cux2 Regulate Dendritic Branching, Spine Morphology, and Synapses of the Upper Layer Neurons of the Cortex. *Neuron* **66,** 523–535 (2010).

135. Mattar, P. *et al.* Basic Helix-Loop-Helix Transcription Factors Cooperate To Specify a Cortical Projection Neuron Identity. *Mol. Cell. Biol.* **28,** 1456–1469 (2008).

136. Lee, S., Lee, B., Lee, J. W. & Lee, S.-K. Retinoid signaling and neurogenin2 function are coupled for the specification of spinal motor neurons through a chromatin modifier CBP. *Neuron* **62,** 641–654 (2009).

137. Ma, Q., Fode, C., Guillemot, F. & Anderson, D. J. NEUROGENIN1 and NEUROGENIN2 control two distinct waves of neurogenesis in developing dorsal root ganglia. *Genes Dev.* **13,** 1717–1728 (1999).

138. Kim, W.-Y. NeuroD Regulates Neuronal Migration. *Mol. Cells* **35,** 444–449 (2013).

139. Schwab, M. H. *et al.* Neuronal Basic Helix-Loop-Helix Proteins (NEX and BETA2/Neuro D) Regulate Terminal Granule Cell Differentiation in the Hippocampus. *J. Neurosci.* **20,** 3714–3724 (2000).

140. Olson, J. M. *et al.* NeuroD2 Is Necessary for Development and Survival of Central Nervous System Neurons. *Dev. Biol.* **234,** 174–187 (2001).

141. Torii, M., Hashimoto-Torii, K., Levitt, P. & Rakic, P. Integration of neuronal clones in the radial cortical columns by EphA and ephrin-A signalling. *Nature* **461,** 524–528 (2009).

142. Arlotta, P. *et al.* Neuronal Subtype-Specific Genes that Control Corticospinal Motor Neuron Development In Vivo. *Neuron* **45,** 207–221 (2005).

143. Medina, D. L. *et al.* TrkB regulates neocortex formation through the Shc/PLCγ-mediated control of neuronal migration. *EMBO J.* **23,** 3803–3814 (2004).

144. Segal, R. A., Pomeroy, S. L. & Stiles, C. D. Axonal growth and fasciculation linked to differential expression of BDNF and NT3 receptors in developing cerebellar granule cells. *J. Neurosci.* **15,** 4970–4981 (1995).

145. Linnarsson, S., Willson, C. A. & Ernfors, P. Cell death in regenerating populations of neurons in BDNF mutant mice. *Mol. Brain Res.* **75,** 61–69 (2000).

146. McAllister, A. K., Katz, L. C. & Lo, D. C. Opposing Roles for Endogenous BDNF and NT-3 in Regulating Cortical Dendritic Growth. *Neuron* **18,** 767–778 (1997).

147.   Conover, J. C. *et al.* Neuronal deficits, not involving motor neurons, in mice lacking BDNF and/or NT4. *Nature* **375,** 235–238 (1995).

148.   Klein, R. *et al.* Disruption of the neurotrophin-3 receptor gene trkC eliminates la muscle afferents and results in abnormal movements. *Nature* **368,** 249–251 (1994).

149.   Gates, M. A., Tai, C. C. & Macklis, J. D. Neocortical neurons lacking the protein-tyrosine kinase B receptor display abnormal differentiation and process elongation in vitro and in vivo. *Neuroscience* **98,** 437–447 (2000).

150.   Puehringer, D. *et al.* EGF transactivation of Trk receptors regulates the migration of newborn cortical neurons. *Nat. Neurosci.* **16,** 407–415 (2013).

151.   Markus, A., Zhong, J. & Snider, W. D. Raf and Akt Mediate Distinct Aspects of Sensory Axon Growth. *Neuron* **35,** 65–76 (2002).

152.   Chadborn, N. H. *et al.* PTEN couples Sema3A signalling to growth cone collapse. *J. Cell Sci.* **119,** 951–957 (2006).

153.   Piper, M. *et al.* Differential requirement of F-actin and microtubule cytoskeleton in cue-induced local protein synthesis in axonal growth cones. *Neural Develop.* **10,** 3 (2015).

154.   Varea, O., Escoll, M., Diez, H., Garrido, J. J. & Wandosell, F. Oestradiol signalling through the Akt–mTORC1–S6K1. *Biochim. Biophys. Acta BBA - Mol. Cell Res.* **1833,** 1052–1064 (2013).

155.   Poot, M., Kroes, H. Y. & Hochstenbach, R. AKT3 as a candidate gene for corpus callosum anomalies in patients with 1q44 deletions. *Eur. J. Med. Genet.* **51,** 689–690 (2008).

156.   Boland, E. *et al.* Mapping of Deletion and Translocation Breakpoints in 1q44 Implicates the Serine/Threonine Kinase AKT3 in Postnatal Microcephaly and Agenesis of the Corpus Callosum. *Am. J. Hum. Genet.* **81,** 292–303 (2007).

7. Affidavit

"I, Kuo Yan, certify under penalty of perjury by my own signature that I have submitted the thesis on the topic [**NeuroD Family Transcription Factors Regulate Corpus Callosum Formation and Cell Differentiation during Cerebral Cortical Development**]. I wrote this thesis independently and without assistance from third parties, I used no other aids than the listed sources and resources.

All points based literally or in spirit on publications or presentations of other authors are, as such, in proper citations (see "uniform requirements for manuscripts (URM)" the ICMJE www.icmje.org) indicated. The sections on methodology (in particular practical work, laboratory requirements, statistical processing) and results (in particular images, graphics and tables) correspond to the URM (s.o) and are answered by me. My interest in any publications to this dissertation correspond to those that are specified in the following joint declaration with the responsible person and supervisor. All publications resulting from this thesis and which I am author correspond to the URM (see above) and I am solely responsible.

The importance of this affidavit and the criminal consequences of a false affidavit (section 156,161 of the Criminal Code) are known to me and I understand the rights and responsibilities stated therein.

Date   Signature

<u>Declaration of any eventual publications</u>

Kuo Yan had the following share in the following publications:

1. Bormuth I,* <u>Yan K</u>,* Yonemasu T, Gummert M, Zhang M, Wichert S, Grishina O, Pieper A, Zhang W, Goebbels S, Tarabykin V, Nave KA, Schwab MH. Neuronal basic helix-loop-helix proteins Neurod2/6 regulate cortical commissure formation before midline interactions. *Journal of Neuroscience, 2013, 9;33(2):641-51.*
- *equally contributing first authors*

Contribution: Kuo Yan performed the experiments (immunostaining and *in situ* hybridization) required for the figures in the paper and contributed to screening the downstream targets of NeuroD2/6.

2. Patzig J, Jahn O, Tenzer S, Wichert SP, de Monasterio-Schrader P, Rosfa S, Kuharev J, <u>Yan K</u>, Bormuth I, Bremer J, Aguzzi A, Orfaniotou F, Hesse D, Schwab MH, Möbius W, Nave KA, Werner HB. Quantitative and integrative proteome analysis of peripheral nerve myelin identifies novel myelin proteins and candidate neuropathy loci. *Journal of Neuroscience, 2011, 9;31(45):16369-86.*

Contribution: Kuo Yan verified the mRNA presence of targeted genes in myelin by *in situ* hybridization.

*3. **Tashiro K, Teissier A, Kobayashi N, Nakanishi A, Sasaki T, <u>Yan K</u>, Tarabykin V, Vigier L, Sumiyama K, Hirakawa M, Nishihara H, Pierani A, Okada N.*** A mammalian conserved element derived from SINE displays enhancer properties recapitulating Satb2 expression in early-born callosal projection neurons.
Plos one, 2011, 6(12):e28497.

Contribution: Kuo Yan contributed to the entire figure 3 and supplementary figure 3 by analyzing neocortical expression patterns of genes located on AS021 loci on mouse chromosome 1, including SatB2.

Signature, date and stamp of the supervising University teacher

_____

Signature of the doctoral candidate

_____

8. Curriculum Vitae

My curriculum vitae does not appear in the electronic version of my dissertation for reasons of data protection.

9. Publication List:

*1. Bormuth I,** **Yan K,*** *Yonemasu T, Gummert M, Zhang M, Wichert S, Grishina O, Pieper A, Zhang W, Goebbels S, Tarabykin V, Nave KA, Schwab MH.* **Neuronal basic helix-loop-helix proteins Neurod2/6 regulate cortical commissure formation before midline interactions.** *Journal of Neuroscience, 2013, 9;33(2):641-51.*
* equally contributing first authors

2. Yan K, Grishina O, Camarero G, Bessa E, Günther U, Parthasarathy S, Wunderlich R, Bormuth I, Tarabykin V. **Ephrin class A reverse signaling guides callosal axon growth via Efna4-Ntrk2 receptor complex downstream of Neurod2/6.** *In preparation.*

3. Patzig J, Jahn O, Tenzer S, Wichert SP, de Monasterio-Schrader P, Rosfa S, Kuharev J, **Yan K,** *Bormuth I, Bremer J, Aguzzi A, Orfaniotou F, Hesse D, Schwab MH, Möbius W, Nave KA, Werner HB.* **Quantitative and integrative proteome analysis of peripheral nerve myelin identifies novel myelin proteins and candidate neuropathy loci.** *Journal of Neuroscience, 2011, 9;31(45):16369-86.*

4. Tashiro K, Teissier A, Kobayashi N, Nakanishi A, Sasaki T, **Yan K,** *Tarabykin V, Vigier L, Sumiyama K, Hirakawa M, Nishihara H, Pierani A, Okada N.* **A mammalian conserved element derived from SINE displays enhancer properties recapitulating Satb2 expression in early-born callosal projection neurons.** *Plos one, 2011, 6(12):e28497.*

10. Acknowledgements:

Here are my extra thanks for the staff working for International Graduate Program Medical Neuroscience, such as Chen, Ralf, Julia, Benedict and Lutz. You guys assisted me to organize the courses, calculate the credit points and answer all my ridiculous questions about the graduation. It is no doubt of big help! Besides, I also want to strongly thank NeuroCure Cluster of Excellence, who generously offered me the 18-month PhD fellowship for as well as a comfortable working environment.

I am also ready to take this chance to thank my dissertation reviewers in advance, although I do not have an idea about you guys yet at this moment. Hopefully, just hopefully, the reviewing can be finished as soon as possible. Help me out, bitte!

Last but not least, my most important partner - my wife, *Cookie Kang*, counts so much for me! Being with you, I could feel everywhere home and everyday with hope and love. You fed confidence when the experiments failed, you gave smiles when the life was not easy, you took so good care of me so that I want to say, 'the biggest success of mine in the last six years is not the acquisition of a PhD, but marrying you!'